Characterization of *Arabidopsis* Myotubularins AtMTM1and AtMTM2: from Development to Stress Adaptation

Dissertation

zur

Erlangung des Doktorgrades (Dr. rer. nat.)

der

Mathematisch-Naturwissenschaftlichen Fakultät

der

Rheinischen Friedrich-Wilhelms-Universität Bonn

vorgelegt von

Akanksha Nagpal

aus

Indien

Bonn 2014

Angefertigt mit Genehmigung der Mathematisch-Naturwissenschaftlichen Fakultät der Rheinischen Friedrich-Wilhelms-Universität Bonn

1. Referent: PD Dr. Frantisek Baluska
2. Referent: Prof. Dr. Diedrik Menzel

Tag der Promotion: 27.08.2014

Diese Dissertation ist auf dem Hochschulschriftenserver der ULB Bonn http://hss.ulb.uni-bonn.de/diss-online elektronisch publiziert.

Erscheinungsjahr: 2014

Table of Contents

List of Figures

List of Tables

Abbreviations

LIST OF FIGURES

LIST OF TABLES

Abbreviations

ABA	Abscisic Acid
AOTFs	Acousto-optic tunable filters
ATX	*Arabidopsis* homolog of Trithorax
AUX1	AUXIN RESISTANT1
BFA	Brefeldin A
CC	Coiled coil
CLSM	Confocal laser scanning microscopy
Col-0	*Arabidopsis thaliana* ecotype Columbia 0
COR	C-terminal of Roc
CMT	Charcot-Marie-Tooth disease
DENN	Differentially expressed in normal versus neoplastic
DFC-DA	2',7'Dichlorofluorescin diacetate
DMSO	Dimethyl sulfoxide
DNA	Desoxyribonucleic acid
DSP	Dual-specificity serine–threonine phosphatase
DKO	Double Knock-out (AtMTM1 and AtMTM2 Knock-out)
DsRed	*Discosoma spec.* red fluorescent protein
DW	Dry weight of leaf
EDTA	Ethylenediamine tetraacetic acid
EEA1	Early-endosomal antigen 1
EGTA	Ethylene glycol tetraacetic acid
ER	Endoplasmatic reticulum
FM1-43	N-(3-triethylammoniumpropyl)-4-(4-(diethylamino)styryl)pyridinium dibromide
FM4-64	N-(3-triethylammoniumpropyl)-4-(6-(4-(diethylamino)phenyl)hexatrienyl)pyridinium dibromide
FW	Fresh weight of leaf
FYVE	Fab1p/YOTB/Vac1p/EEA1
GFP	Green fluorescent protein
GRAM	Glucosyl transferase, Rab-like GTPase activator and myotubularins
GUS	ß-Glucoronidase

HPLC	High performance liquid chromatography
K_m	Michaelis constant (moles per litre of solution)
LB	Luria Bertani
LRR	Leucine rich repeat
M1KO	AtMTM1 Knock-out
M2KO	AtMTM2 Knock-out
M1OX	AtMTM1 Over-expression
MES	2-(N-morpholine)-ethanesulphonic acid
MS	Murashige and Skoog
MTM	Myotubularin
MTMR2	Myotubularin-Related-Protein-2
NF-L	Neurofilament light
OD	Optical density
PAP	Phosphatase adapter protein
PH	Pleckstrin Homology
PHD	Plant homedomain
PI3Ks	Phosphoinositide 3-kinases
PIN2	PIN-FORMED auxin efflux carrier
PIs	Phosphoinositide
PLD1	Phospholipase D1
PtdIns	Phosphatidylinositol
PtdIns3P	Phosphatidylinositol 3-phosphate
PtdIns(3,4)P$_2$	Phosphatidylinositol-3,4-bisphosphate
PtdIns(3,5)P$_2$	Phosphatidylinositol-3,5-bisphosphate
PtdIns(4,5)P$_2$	Phosphatidylinositol-4,5-bisphosphate
PtdIns5P	Phosphatidylinositol 5-phosphate
PTP	Protein tyrosine phosphatases
PX	Phox homology
RFP	Red fluorescent protein
RID	Rac1-induced localization domain
RNA	Ribonucleic acid
ROC	Ras like GTPase domain
ROS	Reactive oxygen species
RWC	Relative water content

SBF	Set-Binding-Factor
SER	Sarco/endoplasmic reticulum
SET	Suvar3-9, Enhancer-of-zeste, Trithorax
SID	SET motif-interacting domain
SR	Serine-rich
TCR	T-cell receptor
TGN	Trans-Golgi network
TRIS	2-Amino-2-(hydroxymethyl)-1,3-propandiol
TW	Rehydrated weight of leaf
V_{max}	Limiting velocity
XLMTM	X-linked myotubular myopathy
YEB	Yeast Extract Broth
YFP	Yellow fluorescent protein

1.   INTRODUCTION

1.1.   DISCOVERY OF MYOTUBULARIN

Myotubularin is a lipid phosphatase that was initially identified by Dr. A. Spiro (a New York neurologist) who reported on myotubular myopathy, a severe congenital muscle disorder characterized by defective muscle cell development via abnormal positioning of nuclei of muscle myotubes (Spiro et al., 1966). Several years later, this disease was linked to a recessive genetic disorder which caused muscle weakness in infants, sometimes even leading to the infant's death (Fardeau, 1992; Wallgren-Pettersson et al., 1996). Muscle biopsy of patients showed centrally located nuclei in small, rounded muscle cells looking like fetal myotubes (myotubular / centronuclear appearance) (Heckmatt et al., 1985; Laporte et al., 1996; Sewry, 1998; Manta et al., 2006). The gene segment was termed as MTM1 and protein encoded by MTM1 was named "myotubularin" (MTM).

The D-3 position of phosphatidylinositol 3-phosphate (PtdIns3P) and phosphatidylinositol 3,5-bisphosphate (PtdIns(3,5)P$_2$), is dephosphorylated by MTMs, generating phosphatidylinositol (PtdIns) and phosphatidylinositol 5-phosphate (PtdIns5P) respectively (Blondeau et al., 2000; Walker et al., 2001; Berger et al., 2002; Begley et al., 2003; Schaletzky et al., 2003). These proteins are found in all eukaryotes; e.g. 14 myotubularins in human, 2 in *Arabidopsis thaliana*, 19 in *Entamoeba histolytica* etc. In human, these lipid phosphatase are required for the regulation of vesicular trafficking, membrane transport (Corvera et al., 1999; Odorizzi et al., 2000), autophagy and cell proliferation. MTMs share similar substrate specificity in-vitro but biochemical and genetic evidence has shown that they have unique functions, as depletion of one myotubularin leads to specific disease phenotypes. For example, mutation in MTM1 leads to X-linked myotubular myopathy (XLMTM) (Laporte et al., 1996), while mutation in Myotubularin-Related-Protein-2 (MTMR2) and MTMR13/Set-Binding-Factor-2 (SBF2) cause Charcot-Marie-Tooth disease type (CMT) 4B1 and 4B2, respectively (Bolino, 2000; Kim et al., 2002; Azzedine et al., 2003; Senderek et al., 2003). Little is known about the functions of plant MTMs. All that is known about their role in plants is that the deletion of AtMTM1 elevates plant's tolerance to dehydration stress in *Arabidopsis thaliana* (Ding et al., 2009; Ding et al., 2012).

1.2. STRUCTURE AND FUNCTIONS OF MYOTUBULARIN DOMAINS

These PI phosphatases are extremely conserved through evolution, which consists of a number of catalytically active and inactive proteins (Begley et al., 2006). They belong to a unique subgroup of a large family of dual-specificity serine–threonine phosphatases (DSP), which are able to dephosphorylate serine/threonine as well as tyrosine residues (Denu and Dixon, 1998), termed Class I Cys-based protein tyrosine phosphatases (PTPs) (Ding et al., 2012). PTPs constitute a large enzyme family characterized by a Cys-X_5-Arg active site motif within a catalytic domain (amino acids 200-300), where X is any residue, the conserved cysteine residue is needed for catalysis, substituting as a nucleophile in the catalytic mechanism, which confines the phosphate of the substrate by a thioester bridge, while catalyzing the enzymatic reaction and the arginine is essential in synchronizing the substrate phosphate group. Within the catalytic domain, the PTPs share greater than 30% sequence identity (Denu and Dixon, 1998). Despite this similarity, myotubularin phosphatases have poor activity towards phosphoprotein substrates in-vitro. Now, it has been proved that myotubularins utilize phosphoinositide lipids (PIs), instead of phosphoproteins, as physiological substrates (Blondeau et al., 2000; Taylor et al., 2000; Zhao et al., 2001; Walker et al., 2001; Kim et al., 2002; Berger et al., 2002). They have conserved domains that include a GRAM (Glucosyl transferase, Rab-like GTPase activator and myotubularins), a RID (Rac1-induced localization domain) (Laporte et al., 2002a), a PTP/DSP active site homology, a phosphatase domain containing the conserved active site required for phosphatase activity (Laporte et al., 2001; Wishart et al., 2001), a SET motif-interacting domain (SID), a part of the protein phosphatase domain and a coiled coil domain (CC) (Begley et al., 2006) (Figure 1).

Figure 1: A schematic depiction of the distribution of protein domains in myotubularins.

An N-terminal GRAM domain, is found in a number of proteins and could mediate function in intracellular lipid/protein binding interactions (Doerks et al., 2000) by binding to phosphoinositides, mainly to PtdIns3P and PtdIns(3,5)P_2, which are also the major substrates of MTMRs (Schaletzky et al., 2003; Berger et al., 2003; Tsujita et al., 2004; Lorenzo et al., 2005). It represents a divergent PH (Pleckstrin Homology) domain which sustains the implications of myotubularins in PIs regulation (Wishart and Dixon, 2002; Schaletzky et al., 2003). Mutations in the GRAM domain of MTM1 lead to XLMTM, underscoring the significance of the GRAM domain for cellular function (de Gouyon et al., 1997; Laporte et al.,

1998). The phosphatase domain is sandwiched between N-terminal RID and C-terminal SID motif. (Begley et al., 2003; Robinson et al., 2006). The RID domain is a membrane- targeting motif necessary for myotubularin recruitment to the plasma membrane ruffles induced by constitutively activated Rac GTPase (Laporte et al., 2002a; Laporte et al., 2002b). It is also reported that the RID domain mediates protein interaction with neurofilament light chain (NF-L) in the case of hMTMR2 (Previtali et al., 2003). The SID is present in all active and inactive members of this family (Cui et al., 1998; Nandurkar et al., 2003). It binds with the SET (Suvar3-9, Enhancer-of-zeste, Trithorax) (Stassen et al., 1995) domain of the Trithorax family which alters chromatin on the histone tails by methylating specific lysines (Rea et al., 2000). Mutations in the SID, result in abnormal growth and differentiation as it hinders its binding to SET (Cui et al., 1998; Firestein et al., 2000). It is also reported that the SID mediates protein-protein interactions (Laporte et al., 2002a) e.g in hMTMR1 for interaction with MTMR12/3-PAP (3-phosphatase adapter protein) (Nandurkar et al., 2003). The Coiled Coil (CC) domain lies to the downstream of the phosphatase domain at the C-terminal of nearly all myotubularins except for a few sequences, found in Amoebozoa, which have N-terminal coiled-coil domain. This domain mediates homodimerisation of myotubularins e.g in MTMR2 (Berger et al., 2003) as well as heterodimer formation e.g in MTMR2 / MTMR5 (Kim et al., 2003), MTMR7 / MTMR9 (Mochizuki and Majerus, 2003) and MTM1 / MTMR12 (3-PAP) (Nandurkar et al., 2003).

Other protein or lipid interacting modules apart from the above domains have been found in some myotubularins like PSD-95/Dlg/ZO-1 binding domain (PDZ-BD), differentially expressed in normal versus neoplastic (DENN), pleckstrin homology (PH), Fab1p/YOTB/Vac1p/EEA1 (FYVE) and Serine-rich domain (SR). The Serine-rich domain, which is present upstream of the GRAM domain in hMTMR2, regulates endosomal targeting of hMTMR2 (Franklin et al., 2011). The PDZ-BD is usually a short stretch of 3-7 amino acids at the C-terminus of human proteins of the MTM1 and MTMR5 subgroups (Fabre et al., 2000), which mediates protein-protein interactions (Previtali et al., 2003). Some homologs of myotubularin also contain a FYVE-finger domain (Laporte et al., 2001; Wishart et al., 2001), is known to bind specifically to PtdIns3P in proteins such as the early-endosomal antigen 1 (EEA1) (Gaullier et al., 1998). It plays an important role in the endocytic pathway as PtdIns3P localizes mainly to the endosomes, where it interacts with FYVE-finger proteins (Gillooly et al., 2000). MTMR13/SBF2 and MTMR5/SBF1 contain an N-terminal DENN domain (Robinson and Dixon, 2005). MTMR5 and MTMR13 may play an important role in Rab regulation (Yoshimura et al., 2010) as DENN domain is found in several Rab GTPase

(Levivier et al., 2001), which are important effectors of membrane trafficking exchange factors. Loss of the dDENN domain (one of the three subdomains of the DENN domain) in MTMR13/SBF2 results in CMT4B2 disease (Senderek et al., 2003). Additionally, MTMR13/SBF2 contains a classical PtdIns(3,4,5)P$_3$ binding PH-domain (Berger et al., 2006). In the case of MTMR5/SBF1, it is shown to have regulatory function on cell growth (Firestein et al., 2001).

1.3.   PHYLOGENY AND EVOLUTION OF MYOTUBULARINS

Myotubularins are widely distributed in all eukaryotes, from the simple unicellular to the multicellular plants and animals except obligate intracellular parasites (*Encephalitozoon cuniculi, Plasmodium falciparum*) and eukaryotic algae (*Cyanidioschyzon merolae*). Myotubularin functions were analyzed in an evolutionary context tracing phylogentic relationship between different domains of myotubularins of thirty different species spanning four eukaryotic supergroups counted different complements of myotubularins ranging from zero in *Chlamydomonas reinhardtii* to 19 in *Entamoeba histolytica* (Kerk and Moorhead, 2010).

The PH–GRAM domain exists across a broad range of organisms except myotubularin sequence of *Giardia* (GL50803-112811), *Leishmania* (LmjF12.0320) and *Trypanosoma* (Tb927.6.870). They do not have a PH-GRAM domain which suggests that this domain architecture was established early in eukaryotic evolution. The catalytic domain (Cys-X$_5$–Arg) is consistently found in all myotubularin sequences which suggests that all myotubularins share a common local active site architecture and catalytic mechanism. One of the most remarkable features of the myotubularin family is the presence of enzymatically inactive myotubularins which contain conserved mutations in the amino acids in the catalytic site. Inactive MTMs also found in *Giardia lamblia* which lack cysteine and arginine residues in the catalytic site; *Leishmania* and *Trypanosoma* both have cysteine and arginine, but histidine is missing from the catalytic loop region. This suggests that inactive MTMs also arose early in eukaryotic evolution. Inactive myotubularins without the PH-GRAM domain as found in *Giardia*, *Leishmania* and *Trypanosoma* has been termed as inactive excavate myotubularins by Kerk and Moorhead (Kerk and Moorhead, 2010). In human, half of the family members were found to be inactive due to lack of the conserved cysteine residue from the catalytic loop which is required for the activity. Various heteromeric interactions between inactive and active myotubularins have been reported in human, e.g. active phosphatase MTM1 or MTMR2 interacts with inactive MTMR12/3-PAP (Nandurkar et al., 2003); inactive MTMR5/SBF1 also interacts with active MTMR2 (Kim et al., 2003); inactive

MTMR9/STYX interacts with active MTMR6 (Zou et al., 2009); active MTMR7 (Mochizuki and Majerus, 2003) or active MTMR8 (Lorenzo et al., 2006); inactive MTMR10 with the active members MTM1 or MTMR2 (Lorenzo et al., 2006). Despite lacking enzymatic functions, these inactive MTMs play an important role in the regulation of active enzymes (Begley and Dixon, 2005). These inactive myotubularins increase the 3-phosphatase activity of the catalytically active phosphatases, e.g., inactive hMTMR9 increases the 3-phosphatase activity of MTMR6 up to 6-fold, activity of hMTMR2 towards PtdIns3P and PtdIns(3,5)P$_2$ increases by over 10 and 25 fold amounts with the interaction of inactive hMTMR13 (Kim et al., 2003; Nandurkar et al., 2003; Mochizuki and Majerus, 2003; Berger et al., 2006; Zou et al., 2009). They change the subcellular localization of active phosphatase (Nandurkar et al., 2003; Kim et al., 2003; Lorenzo et al., 2006) and also modify the substrate specificity (Nandurkar et al., 2001).

Previously, the family of myotubularins of *Homo sapiens*, *Drosophila melanogaster* and *Caenorhabditis elegans* was split into six subgroups, three consist of active phosphatases and three comprising inactive ones (Nandurkar et al., 2001,Wishart et al., 2001). In 2010, Kerk and Moorhead added myotubularin homologues of the cindaria phyla (*Nematostella*), the placozoan phylum (*Trichoplax*) and the unicellular choanoflagellate (*Monosiga*) to the above classification, which suggested that gene diversification into subgroups had been done at the origin of metazoan. In Amoebozoan (*Entamoeba histolytica* and *Dictyostelium discoideum*), there are found unique inactive myotubularins along with a LRR (leucine rich repeat) domain, a ROCO domain, a supradomain (Bosgraaf and Van Haastert, 2003) containing a ROC (Ras like GTPase domain) and COR (C-terminal of Roc), and a protein kinase domain. The inactive myotubularins/LRR/ROCO/kinase architecture has been named as IMLRK domain. In plants, until now no inactive myotubularin has been discovered. Detailed phylogeny of the plant myotubularins will be discussed in the next section (Section 1.4).

1.4.   PLANT MYOTUBULARINS

There is no myotubularin gene found in algae e.g *Ostreococcus sp.,* and *Chlamydomonas reinhardtii,* which share a common ancestor with land plants (Merchant et al., 2007; Herron et al., 2009). There are two myotubularin genes found in *Physcomitrella patens,* which show similar structures to the metazoan except C-terminal regions of the moss proteins belonging to the Flagellar family of proteins existing in paraflagellar rod component proteins of eukaryotes (Ding et al., 2012). Single myotubularin has been found in mono- and dicotyledonous plants except *Arabidopsis thaliana*. When the genome of *Arabidopsis* was searched for myotubularin-like genes with similarity to the amino acid sequence of the hMTMR2, two

myotubularin (AtMTM) homologs encoded by the At3g10550 and At5g04540 genes which are present on chromosomes 3 and 5, respectively (referred here as AtMTM1 and AtMTM2, respectively), were identified (Ding et al., 2009). It has been reported that these two genes are evolved by a segmental chromosomal duplication as 3'-phosphatidylinositol phosphate-dependent kinase is conserved on both chromosomes. At3g10540 gene is present adjacent to AtMTM1, while At5g04510 gene is located two genes downstream of AtMTM2 (as shown in Figure 2). It seems that these two genes may have developed through different paths to accommodate for different behavior.
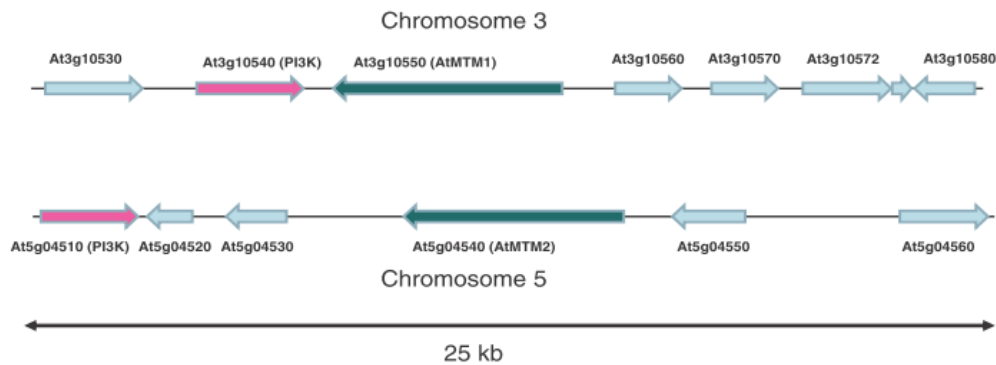
Figure 2: Positions of the At3g10550 and At5g04540 genes on chromosomes 3 and 5, respectively which encode conserved 3'-PIP- dependent kinases (pink).

Green areas on the two chromosomes represent conserved DNA sequences. On chromosome 5, the two genes between AtMTM2 and the 3'-PtdInsP-dependent kinase (At5g04530 and At5g04520) encode a KCS19 (3-ketoacyl-CoA synthase19) and a hypothetical protein respectively. (Ding et al., 2012).

These two proteins are highly related to each other showing 77% identical, 85% similarity to each other. These proteins are 34% identical, 49% similar, 4×10^{-81} to the hMTMR2. Majority of the amino acids essential for the enzyme activity of the human myotubularins (Begley et al., 2005; Begley et al., 2006) are conserved in the plant myotubularins. Both proteins also contain a conserved PH-GRAM domain, a RID, a CC domain as well as the catalytic domain along with the SID like hMTMR2 (Laporte et al., 2002a; Begley et al., 2003). Both have conserved biochemically active catalytic sites and both are ubiquitously expressed in plant. Despite these similarities, these proteins behave in different manner, AtMTM1 has shown different affinity towards PtdIns3P and PtdIns(3,5)P_2 (K_m = 146 μM and V_{max} = 142.6 pmol min^{-1}mg^{-1} for Ptdins(3,5)P_2 ; K_m = 201.7 μM and V_{max} = 94.3 pmol min^{-1}mg^{-1} for Ptdins3P) (Ding et al., 2009). PtdIns(3,5)P_2 is preferably chosen as substrate than PtdIns3P by AtMTM1. Similarly, AtMTM2 prefers PtdIns(3,5)P_2 as substarte (K_m = 158.2 μM and V_{max} = 28.4 pmol min^{-1}mg^{-1} for Ptdins(3,5)P_2; K_m = 216.5 μM and V_{max} = 15.4 pmol min^{-1}mg^{-1} for Ptdins3P)

(Ding et al., 2012). But AtMTM2 showed lower phosphatase activity as compared to AtMTM1. It has been observed that in drought stress condition, there is an elevation in the expression of AtMTM1 as well as an increment in PtdIns5P level in AtMTM2 knock out as compared to AtMTM1 Knock out mutants. RFP tagged AtMTM1 shows different localization (large number of vesicles) as compared to GFP tagged AtMTM2 (dense patches around the epidermal cells) in *Nicotiana benthamiana,* which suggests that these two genes are functionally divergent (Ding et al., 2012).

1.5.   PHOSPHOINOSITIDES

Phosphatidylinositol (PtdIns), are an integral part of the cell lipid pool that can travel between and within cells by passing through a bilayer membrane of all eukaryotic cells (Stevenson et al., 2000). It belongs to the glycerophospholipids composed of two fatty acid tails, which are linked via a glycerol backbone and an inorganic phosphate, to the polar inositol head group. They play an important role as intracellular and intercellular messengers in various processes, which help in plant development (cell proliferation and differentiation), cytoskeletal dynamics and cellular signaling process (Wang, 2004). Phosphorylated products of phosphatidylinositol are named as phosphoinositides (PIs), which comprise less than 10% of the total lipids existing in eukaryotic cell membranes. Seven distinct phosphoinositides are highly water-insoluble, which are generated by phosphorylating the inositol headgroup at different positions (i.e. D-3, -4, -5 positions) via distinct lipid kinases of phosphatidylinositols (PtdIns). They are the key regulators of a variety of cellular processes – including signal transduction that regulates cell growth, survival and proliferation (Katso et al., 2001), cellular compartmentalization through actin remodelling, cytoskeletal reorganization, glucose metabolism and regulation of various membrane trafficking events, which enables the subcellular coordination of the stress responses (Di Paolo et al., 2006; Samaj et al., 2004). Myotubularins use phosphatidylinositol monophosphate (PtdIns3P) and phosphatidylinositol bisphosphate (PtdIns(3,5)P$_2$) as substrates and generates PtdIns and phosphatidylinositol monophosphate (PtdIns5P) respectively. For maintaining cellular homeostasis (Michell et al., 2006), it is essential to have rapid interconversion of these PIs during vesicle trafficking between cell compartments.

1.5.1. PTDINS3P

One of the seven phosphorylated derivatives of phosphatidylinositol is phosphatidylinositol 3-phosphate (PtdIns3P), formed by phosphorylation of inositol at the D3-position by phosphoinositide 3-kinases (PI3Ks). In mammals, three classes of PI3Ks (Classes I–III) have

been classified based on their substrate specificity and organization of subunits (Vanhaesebroeck et al., 2001), like enzymes of Class I PI3Ks use PtdIns, PtdIns4P and PtdIns(4,5)P$_2$ (preferred substrate), Class II PI3Ks use PtdIns and PtdIns4P as substarte,while class III PI3Ks use only PtdIns as a substrate to form PtdIns3P (Vanhaesebroeck et al., 2001). In yeast and plants, there is only one class of PI3Kinase i.e class III PI3Ks which is known. In plants, PtdIns3P is present in very low amount (2–15 % of the total PtdIns) (Brearley and Hanke, 1992; Boss and Im, 2012). PtdIns3P and PI3K play a crucial role in membrane trafficking processes, which involve autophagy, retromer pathway (recycling from endosomes to the trans-Golgi network (TGN)) and vacuolar trafficking of the Golgi-derived vesicles (Backer, 2008; Vermeer and Munnik, 2010). These processes also suggest the localization of PtdIns3P in the cell like endosomes, TGN, multivesicular bodies, vacuolar membrane and autophagosomes (Kim et al., 2001; Kihara et al., 2001; Obara et al., 2008; Gillooly et al., 2001). Earlier it was known that PtdIns3P only binds with those proteins which contain FYVE domain. In the past few years, PtdIns3P is found to bind with various other domains e.g. pleckstrin homology (PH) domain along with C- terminal domain (CTD) of *Arabidopsis* dynamin like protein (ADL6) enhances lipid binding affinity towards PtdIns3P by 4 times (Lee et al., 2002); C2 domain of a pollen-specific C2 domain-containing protein (NaPCCP) binds with PtdIns3P in a Ca^{2+} independent fashion (Lee et al., 2009); highly conserved epsin N-terminal homology (ENTH) domain of Epsin-related proteins (EpsinR2) in *Arabidopsis* interacts with PtdIns3P (Lee et al., 2007).

Like in animal cell, PtdIns3P plays an important role in vesicular trafficking and membrane transport in plant cell too. Severe growth defects like short shoots, unelongated petiole and poor quality of seeds that affect the rate of germination have been noticed due to the expression of an antisense AtVPS 34 in *A. thaliana* (Welters et al., 1994). Inhibition of PI3K activity by wortmannin (Arcaro and Wymann, 1993; Stephens et al., 1994) decreases uptake of FM1-43 dye into tobacco cells (Emans et al., 2002) as well as in *Arabidopsis* root cells after treatment with salt stress (Leshem et al., 2007). Like other Phosphoinositides, activity of PtdIns3P is also affected by different environmental stresses. PtdIns3P activates NADPH oxidase, which results in the elevation of intracellular production of reactive oxygen species (ROS) after salt stress (Leshem et al., 2007) as well as after ABA exposure (Park et al., 2003). It is essential for root hair growth (Lee et al., 2008) as well as for proper functioning of guard cells (Jung et al., 2002) e.g. PI3K inhibitors decreased stomatal closing by reducing oscillations in the level of Ca^{2+} in response to ABA. PtdIns3P is associated with phototropin (phot1 and phot2) induced chloroplast accumulation (Aggarwal et al., 2013). Interaction of

actin binding protein profilin with PI3K type III establishes a link between membrane trafficking by PtdIns3P and actin cytoskeletal network (Aparicio-Fabre et al., 2006).

1.5.2. PTDINS(3,5)P₂

In 1989, Auger suggested the presence of PtdIns(3,5)P_2 as a lipid (Auger et al., 1989) but it was formally discovered in yeast and mouse a decade later (Dove et al., 1997; Whiteford et al., 1997). PtdIns(3,5)P_2 is synthesized from PtdIns3P by Fab1p (loss of Fab1p leads to formation of aploid and binucleate cells) in yeast and PIKfyve (a FYVE finger-containing phosphoinositide kinase) in mammals (Yamamoto et al., 1995; Boronenkov and Anderson, 1995; Michell et al., 2006). Both active PtdIns3P 5-kinases have N-terminal FYVE domain for binding PtdIns3P, followed by a central Cpn60-TCP1(CCT) like chaperone domain, which is linked to the C-terminal lipid kinase domain by a unique sequence, rich in histidine and cysteine residues (Michell et al., 2006; Whitley et al., 2009). Like other phosphoinositides, PtdIns(3,5)P_2 has multiple functions in eukaryote cell. This lipid regulates the fragmentation of endo-lysosomal sub-compartments, maintains vacuole/lysosome homeostasis during membrane trafficking (Cooke et al., 1998; Dove et al., 2009) and actuates the endolysosomal calcium channel TRPML1 (transient receptor potential cation channel, mucolipin subfamily, member 1) (Dong et al., 2010). Mutation in human PIPkIII (hPIPkIII) causes Francois–Neetens fleck corneal dystrophy, in which refractile flecks are present in the cells of the corneal stroma (Li et al., 2005). Mostly mutation in CCT domain causes disregulation in PtdIns(3,5)P_2 level. In *Arabidopsis*, there are four PIKfyve/Fab1p homologs encoded by various genes like At4g33240 (FAB1A), At3g14270 (FAB1B), At1g71010 (FAB1C), and At1g34260 (FAB1D). Out of four only two FAB1A and FAB1B have FYVE domain located near the N-terminus (Mueller-Roeber and Pical, 2002), which shows that they act as PtdIns3P 5-kinases in plants (Whitley et al., 2009). They localized to the endosomes in *Arabidopsis* root cells (Hirano et al., 2011a).

Many environmental stresses cause changes in PtdIns phosphorylation in plants (Meijer et al., 2001; Mikami et al., 1998). Likewise, hyperosmotic stress increases the level of PtdIns(3,5)P_2 e.g. elevation up to 20-fold in both *S. cerevisiae* and *S. pombe* (Dove et al., 1997; Morishita et al., 2002), 2–6-fold in somatic cells and pollen tubes of plants (Meijer et al., 1999; Meijer and Munnik, 2003; Zonia et al., 2004) and 10 fold in differentiated 3T3 L1 adipocytes of animal cells (Sbrissa and Shisheva, 2005). In *Arabidopsis*, fab1a and fab1b mutants have shown leaf curl phenotype after 4 weeks of post-germination, which is the typical phenotype exhibited by the auxin-resistant mutants including aux1 (Marchant et al., 1999) and axr4 (Hobbie and Estelle, 1995; Dharmasiri et al., 2006). In 2011, Hirano and Sato hypothesized that these two

proteins, FAB1A / FAB1B, might help in the regulation of auxin flow by recycling auxin carriers like AUX1, PIN2 (Swarup et al., 2004; Hirano and Sato, 2011b). FAB1A/B play an important role in the development of viable pollen as double knock of fab1a/fab1b has shown defect in male gametogenesis (abnormal vacuolar phenotype at tricellular stage).

Imbalanced expression of PtdIns(3,5)P$_2$ in knockdown of fab1a/b mutant leads to various development abnormalities like inhibition of root growth, hyposensitivity to exogenous auxin (NAA) and disturbance of root gravitropism (Hirano et al., 2011a). PtdIns(3,5)P$_2$ might play a crucial role in a variety of cellular processes, including endocytosis, protein sorting and maintenance of intracellular pH (Yamashiro et al., 1990) as reduced expression of FAB1A/B hinders endomembrane homeostasis including endocytosis and vacuolar acidification.

1.5.3. PTDINS5P

The study of Phosphatidylinositol 5-phosphate (PtdIns5P) started after its discovery in mammalian fibroblasts, which was found out to be the source of PtdIns(4,5)P2 (phosphatidylinositol (4,5)-bisphosphate) by type II PtdInsP kinases (Rameh et al., 1997). But later on, it was discovered that PtdIns5P is regulated by phosphatase like human PtdIns(4,5)P$_2$ 4-phosphatase types I and II rather than a kinase (Roberts et al., 2005; Ungewickell et al., 2005). Still, it is not clear whether this monophosphorylated phosphoinositide (PtdIns5P) can only be generated by phosphatases or whether a PtdIns-specific 5-kinase exists. However, it is produced by the dephosphorylation of PtdIns(4,5)P$_2$ or PtdIns(3,5)P$_2$ by lipid phosphatase, like myotubularins in plants (Wendy and Yang, 2012). It was the least-characterized member of the PI family and present as a minor fraction (~3-8%) of the total PtdInsP pool in *Chlamydomonas,* while the percentage is higher for vetch and tomato (~18%) (Meijer et al., 2001). Environmental stresses affect the cellular level of PtdIns5P e.g. increment in PtdIns5P concentration has been observed in *Chlamydomonas* (Meijer et al., 2001), yeast (Dove et al., 1997) and human (Sbrissa et al., 2002) cells after hyperosmotic stress.

Studies of PtdIns5P had been lagging behind due to low level of PtdIns5P in resting cells and inability to measure PtdIns5P using conventional high performance liquid chromatography (HPLC) due to overlapping peaks of Phosphatidylinositol 5-phosphate (PtdIns5P) and Phosphatidylinositol 4-phosphate (PtdIns4P). In 2010, Ndamukong et al. positively identified PtdIns5P in *Arabidopsis thaliana* by using radioactively labeled 4' position of PtdIns5P and PtdIns3P with type II phosphatidyl-inositol-4-phosphate 5-hydroxy kinases (PI4Kα) based on the fact that D-4 position of PtdIns5P and PtdIns3P can be phosphorylated by PI4Kα (Rameh et al., 1997) and then separated the PtdIns(4,5)P$_2$ from PtdIns(3,4)P$_2$ (phosphatidylinositol (3,4)-bisphosphate) by HPLC.

Despite its lower abundance, PtdIns5P emerged as a potential ligand in signal transduction pathway regulating many metabolic and cellular functions. The importance of PtdIns5P is underscored by the growing list of human genetic disorders caused by mutation in genes which encoded PtdIns5P regulatory proteins like centronuclear myopathy, an autosomal disorder, resulting from the sequence changes in hMTMR14 gene (Tosch et al., 2006). PtdIns5P emerges as a second messenger downstream of T-cell receptor (TCR) stimulation in the immune system as it regulates Dok proteins (Dok-1 and Dok-2) tyrosine phosphorylation in cells via binding to a pleckstrin homology (PH) domain of the Dok family (Guittard et al., 2009; Guittard et al., 2010). PtdIns5P binds with Phox homology (PX) domain of phospholipase D1 (PLD1) (Du et al., 2003). Interaction between PX domain and PtdIns3P stimulate amino acid of mammalian target of rapamycin (mTOR) complex (mTORC1) pathway (Yoon et al., 2011). Several pathological stimuli and situations alter phosphoinositide metabolism e.g. virulence factors IpgD from *Shigella flexneri* (Niebuhr et al., 2002) or SigD/SopB from *Salmonella* species (Mason et al., 2007) inject into the host cell by a type III secretion system (Van Gijsegem et al., 1993), where it acts as inositol 4-phosphatase and dephosphorylates PtdIns(4,5)P_2 into PtdIns5P. In mammalian cells, it results in membrane blebbing due to reduced membrane/cytoskeleton adhesion energy. Increased level of PtdIns5P caused by bacterial invasion induces Akt phosphorylation (Pendaries et al., 2005).

In 2008, Lecompte and collaborators have hypothesized that PtdIns5P plays an important role in regulating the flow of membrane material in mammalian cells from late endosomal compartments to the plasma membrane (Lecompte et al., 2008). Subcellular localization of PtdIns5P is still enigmatic as most of the PtdIns5P is found outside the nucleus like in the plasma membrane, the Golgi apparatus and SER (sarco/endoplasmic reticulum) (Sarkes and Rameh, 2010), but an increase in nuclear PtdIns5P pool has been observed during progression through the cell cycle e.g. elevation in nuclear PtdIns5P by 20-fold during G1 phase of cell cycle (Clarke et al., 2001). In the nucleus, PtdIns5P binds with ING2, a candidate tumor suppressor protein via a plant homedomain (PHD) finger. This interaction resulted in activation of p53 and p53-dependent apoptotic pathways (Gozani et al., 2003). Nuclear PtdIns5P also modifies ING2 localization under cellular stress (Jones et al., 2006). A large number of chromatin regulatory proteins have been reported, which contain the PHD finger, including the chromatin remodeling protein ACF, the ING1, a member of family of putative tumor suppressors and the *Arabidopsis* homolog of Trithorax (ATX1) (Feng et al., 2002; Fyodorov and Kadonaga, 2002; Alvarez-Venegas et al., 2006) and they bind with PtdIns5P. ATX1, a plant epigenetic regulator with histone H3K4 methyltransferase activity, which

controls floral organ development by maintaing homeotic gene expression (Alvarez-Venegas et al., 2003), binds specifically with PtdIns5P via a PHD and both co-regulate a shared set of genes (Alvarez-Venegas et al., 2006). Elevated level of PtdIns5P during dehydration and hypotonic stress affects the activity of ATX1 by restricting its access to the nucleus (Ndamukong et al., 2010). Detail will be discussed in the next section (Section1.6).

1.6.   RELATIONSHIP OF PtdIns5P WITH ATX1

The *Arabidopsis* Trihorax-like protein (ATX1), is a chromatin modifier involved in tri-methylating lysine 4 of histone H3 (H3K4me3). The idea ATX1 could bind lipid ligands like PtdIns5P came into highlight when it was found that the PHD finger of ING2 (a candidate tumor suppressor protein) interacts with PtdIns5P (Gozani et al., 2003). But further studies had been lagging behind due to low level of PtdIns5P and problem in separation by high performance liquid chromatography (HPLC), as peaks of PtdIns4P and PtdIns5P were overlapped. Cellular levels of PtdIns4P are much more abundant than putative PtdIns5P levels. In 2010, a quantitative determination of intracellular PtdIns5P in *Arabidopsis thaliana* is successfully done by radioactive mass assay (Ndamukong et al., 2010).

Earlier it was suggested that under dehydration stress and non stressed condition PtdIns5P and ATX1 in over-expressing AtMTM1 (OX-AtMTM1) regulate a common set of 140 target genes by microarray assays (Alvarez-Venegas, et al., 2006). Out of which 106 target genes were significantly down regulated under dehydration stress. It was shown that elevated PtdIns5P shifts ATX1 subcellular location from the nucleus to the cytoplasm. Cellular level of PtdIns5P is increased upon exposure of *Arabidopsis* to drought stress. The transcript level of plant-specific transcription factor WRKY70 is regulated by ATX1 (Alvarez-Venegas et al., 2007). Decreased level of WRKY70 is reported in homozygous ATX1 deleted (*atx1*) plants. The activity of ATX1 and the levels of tri-methylated histone 3 lysine4 (H3K4me3), a chromatin marker at the WRKY70 promoter is decreased in response to dehydration stress. WRKY70 transcript levels are diminished upon addition of exogenous PtdIns5P (Alvarez-Venegas, et al., 2006). As high PtdIns5P levels negatively influence ATX1 activity, both PtdIns5P and ATX1 regulate WRKY70. In drought stressed leaves of OX-AtMTM1, the levels of WRKY70 transcripts as well as H3K4me3 at the WRKY70 nucleosomes are significantly decreased as compared to wild-type Col-0 leaves. Increasing cellular PtdIns5P by OX-AtMTM1 shows diminution of ATX1 activity as well as retention of ATX1 in the cytoplasm. Changes in H3K4me3 and WRKY70 transcripts are correlated with the presence of ATX1 at the promoter nucleosomes. Thus, PtdIns5P establishes a link between chromatin modification and endogenous lipid-levels as well as ambient environmental stress.

1.7. MYOTUBULARINS AND DROUGHT STRESS

Despite sharing 85% similarity with each other (Ding et al., 2009), *Arabidopsis* myotubularins (AtMTM1 and AtMTM2) exhibit different transcriptional responses during dehydration stress, which is shown by different responsiveness towards dehydration (Ding et al., 2012). AtMTM1 gene during drought stress shows an increase in cellular PtdIns5P level as compared to AtMTM2 gene. GUS staining results have shown that there is an elevation in the expression of PAtMTM1::GUS after dehydration stress in hydathodes as compared to PAtMTM2::GUS. Even though there is 60% elevation in AtMTM1 transcripts under dehydration stress, as compared to AtMTM1 transcripts under watered conditions, no increase in AtMTM2 transcripts is observed under under both watered and dehydration stress conditions.

In soil, wild-type Col-0 and mutants of both myotubularins were given dehydration stress for 19 days. While on one hand, wild-type Col-0 and M2KO mutants were extremely dehydrated, on the other hand, the double knock-out (DKO mutants) and M1KO mutants demonstrated an increased resistance. Whole-genome expression analysis of *mtm1* and *mtm2* homozygous mutant plants are performed under watered as well as drought conditions by Affymetrix gene chips (Ding et al., 2012). 27 genes alter their expression in the *mtm1* background as compared to none in the *mtm2* background under watered conditions. After dehydration stress, 134 genes change expression, out of which 73 are up-regulated and 61 are down-regulated in the *mtm1* background. Most of the genes comprise biotic, abiotic and heat shock stress - response genes and transcription factors in which six belongs to the Myb family. Only four genes are downregulated in *mtm2* background, which includes ACS7 gene (At4g26200) involved in ethylene biosynthesis, At2g02060 gene encoding a transcription factor from the Myb family, and the At5g12030 gene encoding a cytosolic small heat shock protein and AtMTM2 gene, capturing the lost AtMTM2 transcripts in the SALK-147282 (Ding et al., 2012).

1.8. AIM OF THE THESIS

This thesis work aims to enhance understanding of the molecular mechanism of plant myotubularins in-vivo.

- The expression patterns of these two proteins will be studied with the help of β-glucuronidase (GUS) staining under different abiotic stress.

    Concentration of Phosphoinositides like PtdIns3P, PtdIns(3,5)P_2 and PtdIns5P alter after different abiotic stresses. Myotubularins are the enzymes which use

these phosphoinositides as substarte (PtdIns3P, PtdIns$(3,5)P_2$) and form products, PtdIns and PtdIns5P respectively.

- Effects of ABA will be checked on the mutants of myotubularins and also investigate the effect of myotubularins on the production of ROS.

    Loss of AtMTM1 alters the tolerance of the plant during drought stress, which is one of the major manifestation of abiotic stress in plants affecting the productivity of crop plants every year. Abscisic acid (ABA), is synthesized in response to drought stress (Schroeder et al., 2001). ABA plays an important role in regulating stomatal function during stress by coordinating events like changing ion fluxes within the guard cells, which in turn reduces transpirational water loss (Dodd, 2003; Levchenko et al., 2005; Vahisalu et al., 2008; Siegel et al., 2009) leading to production of activated oxygen species (Mori et al., 2001; Bright et al., 2006).

- The subcellular localization of myotubularins in *Nicotiana benthamiana* and function of two myotubularins in *Arabidopsis thaliana* roots, namely AtMTM1 and AtMTM2 will be investigated. Their possible roles in polarized exo/endocytosis are discussed.

- The subcellular localization of isoforms of AtMTM1 will be checked in tobacco leaves by infiltration method and to study the relationship of these isoforms with the PHD of ATX1 or ATX1.

    According to Franklin and coworkers (Franklin et al., 2011), the Serine-rich domain of hMTMR2 regulates its subcellular localization and phosphorylation of Ser[58] (a phosphorylation site within the Serine-rich domain) reduces hMTMR2 localization to endocytic structures. In plant myotubularins (AtMTM1), a Serine-rich domain is present upstream of the SID. In order to understand the importance of Serine and GRAM domain in AtMTM1, three different constructs were analyzed – GFP tagged AtAAF (isoform of AtMTM1 without Serine-rich domain present near SID), GFP tagged AtAAG (isoform of AtMTM1 without Serine-rich domain as well as without N-terminal sequences including the GRAM domain) and RFP tagged AtNP (isoform of AtMTM1 with Serine-rich domain but without N-terminal sequences including the GRAM domain). In 2010, it was shown that overexpression of RFP tagged Myotubularin (AtMTM1-RFP) relocates nuclear ATX1 from the nucleus to the cytoplasm via the PHD of ATX1 (Ndamukong et al., 2010). To find out effect of these domains in myotubularins, the isoforms will be co-expressed with the

GFP/ RFP tagged PHD (PHD-GFP/RFP) and GFP/ RFP tagged ATX1 (ATX1-GFP/ RFP).

In this study, *Arabidopsis thaliana* is used as the major experimental model system because of fully sequenced genome, easy to handle, rapid life cycle and availability of insertional mutants (Swarbreck et al., 2007).

2.   MATERIALS AND METHODS

2.1.   MATERIAL

2.1.1.   PLANT MATERIAL AND GROWTH CONDITIONS

Various mutants of myotubularin [SALK-147282:AtMTM2KO (M2KO), SALK-029185:AtMTM1KO (M1KO); Double Knock Out AtMTM1/AtMTM2 (DKO); Overexpression of AtMTM1: OX-AtMTM1 (M1OX)] along with AtMTM1prom::GUS and AtMTM1prom::GUS transformed *Arabidopsis* lines, gifted by Prof. Zoya Avramova, were used to study the myotubularins in plants. For control experiments, the ecotype Columbia (Col-0) of *A. thaliana* was used. Seeds were sterilized for 10 minutes using 6% sodium hypochlorite (NaClO) solution in 0.01% v/v Triton X-100. They were rinsed with sterile double-distilled (MilliQ) water for 5-6 times before dried on filter paper and stored at 4°C. The sterilized seeds were placed on one-half strength Murashige and Skoog (MS) medium including vitamins, 1% (w/v) sucrose and 0.4% (w/v) Phytagel (pH 5.6-5.8) (Murashige and Skoog, 1962) and were stratified at 4°C overnight to break dormancy before placing in the growth chamber maintained at 22°C temperature at a 16-h day/8-h night cycle. For different abiotic stresses, appropriate amount of different chemicals were added to the media. Seedlings were subjected to different abiotic stresses e.g. etiolated seedlings were kept on plates covered with aluminum foil after the initiation of germination by 2 hours illumination with white light at 22°C; for high temperature stress, 5 days old seedlings were kept at 37°C for 6 hours; for salt stress and ABA exposure, 4 days old seedlings were grown on different concentrations of salt and ABA respectively; for cold stress, 4 days old seedlings were kept at 4°C for 1 day. For germination statistics, radical emergence was used as criterion.

Commercially available peat moss based soil after treating with insecticide was used to grow the plants on soil in the growth chamber with 16 hours in the light at 23°C and 8 hours in the dark at 21°C, at a light irradiance of 150 $\mu E\ m^{-2}sec^{-1}$.

Nicotiana benthamiana was grown under a defined light and temperature regime, i.e., 16 hours in the light at a light irradiance of 200 $\mu E\ m^{-2}sec^{-1}$ and a temperature of 27°C and 8 hours in the dark at 24°C. After the seeds had germinated, they were allowed to grow over a period of two weeks, after which the individual plants were isolated and grown for another two weeks before being infiltrated with *Agrobacterium tumefaciens*.

2.1.2. FLUORESCENT MARKERS

Various fluorescent markers were used in order to identify the subcellular localization of myotubularins and isoforms of myotubularin.

2.1.3. MYOTUBULARINS AND ISOFORMS OF AtMTM1

For C-terminal GFP/RFP-fusion and expression in plants, the entry vector pDONR221 and expression vectors pB7FWG2,0 were used for cloning (gift from Prof. Zoya Avramova).

2.1.4. CHEMICALS

Various chemicals were purchased from the following companies: Amersham Bioscience, Appli Chem, Bio Rad, Boehringer Mannheim, Echelon Biosciences, Duchefa Biochemistry, Invitrogen, Merck, Molecular Probe, Roche, Roth and Sigma in order to perform various experiments. FM1-43 (N-(3-triethylammoniumpropyl)-4-(4-(diethylamino)styryl) pyridinium dibromide) and FM4-64 (N-(3-triethylammoniumpropyl)-4-(6-(4-(diethylamino) phenyl) hexatrienyl) pyridinium dibromide) (5 µM) dyes were used to label the plasma membrane and various endosome compartments, which showed green and red fluorescence respectively. Brefeldin A (35 µM) was used as an inhibitor of endocytosis in plant cells. Exogenous PtdIns5P (1.5 µM) was used to see the effect of Phosphoinositide on ROS signaling. 10 mM stock solution of 2',7'-Dichlorofluorescin diacetate (DFC-DA) dissolved in dimethyl sulfoxide (DMSO) was aliquoted to determine ROS in guard cells.

2.1.5. MEDIA AND SOLUTIONS

LB (Luria Bertani) (10g/l Tryptone, 5g/l Yeast extraction, 5g/l NaCl, pH 7.0) and YEB (Yeast Extract Broth) (1g/l Peptone, 1g/l yeast extraction, 5g/l beef extract, 5g/l sucrose, 2mM $MgCl_2$, pH 7.0) medium were used to grow *Escherichia coli* (DH10B) and *Agrobacterium tumefaciens* GV3101 (pMP90) respectively. To select specific resistances in the medium, specific antibiotics (Kanamycin or Spectinomycin) were included. Normally, plant materials were grown on one-half strength Murashige and Skoog medium along with Phytagel. For confocal studies, plant materials were grown on one-tenth strength Murashige and Skoog medium without Phytagel overnight prior use.

2.2. METHODS

2.2.1. PREPARATION OF COMPETENT *E. COLI*

The calcium chloride ($CaCl_2$) method was used to prepare Chemo-competent *E. coli* cells as divalent cations like calcium increases the ability of *E. coli* to take up foreign DNA into the

cell (Maniatis et al., 1982). A single colony was picked from a previously streaked plate with *E. coli* cells and inoculated in 3 ml of LB-medium for overnight at 37°C with shaking at 280 rpm. 1 ml of the pre-culture was added into a sterile Erlenmeyer flask containing primary culture of 100 ml LB medium. LB broth was incubated at 37°C on the shaker with gentle shaking until an OD_{600} of 0.5 was reached. The culture was divided in two pre-chilled 50 ml falcon tubes and was centrifuged for 10 minutes at 4,500 rpm at 4°C in order to spin down cell suspension. After discarding the supernatant, pellet was re-suspended into 2 ml of ice cold 0.1 M $CaCl_2$ solution in an ice bath for 30 minutes. After combining the contents of the two falcon tubes, the suspension was centrifuged at 4,500 g for 10 minutes at 4°C. Pellet was re-suspended gently in pre-cooled 2.5 ml solution containing 0.1 M $CaCl_2$ in 15% (v/v) glycerol. For long-term storage, 50 µl aliquots were dispensed in pre-chilled, sterile eppendorf tubes and frozen in liquid N_2. These aliquots were stored at -80°C, until used for transformation.

2.2.2. COMPETENT *E. COLI* TRANSFORMATION

The heat shock method was used to transform competent *E. coli* cells. The frozen aliquots of competent cells were thawed on ice and gently mixed with 5 µl plasmid DNA into eppendorf tubes. The whole mixture was incubated on ice for 20 minutes. The heat shock was carried out in a waterbath at 42°C for 45 seconds, then immediately transferred on ice again and incubated for 2 minutes. 500 µl of LB medium without antibiotics was added before incubating at 37ºC for 60 minutes on a shaker at 170 rpm. After 1 hour, the cell suspension was spread on LB agar plate with specific antibiotic for the selection of the inserted plasmid. The sealed plate was incubated for overnight at 37°C with agar side up.

2.2.3. PREPARATION OF ELECTRO-COMPETENT *AGROBACTERIUM TUMEFACIENS*

An *Agrobacterium tumefaciens* GV3101 colony was picked from a plate containing Gentamycin 15 µg/ml and inoculated in YEB medium (around 3 ml) without antibiotics at 28°C on the shaker at a speed of 200 rpm for overnight. 2 ml from overnight culture was added into 100 ml YEB medium in a sterile 500 ml flask and shaken vigorously at 28°C until culture attained an OD of 0.5 at 600nm. The culture was divided into pre-cooled falcon tubes and centrifuged for 15 minutes at 4000 rpm at 4°C. The pellet was re-suspended into 25 ml of cold 10 mM Tris / HCl buffer pH 7.5 and the content of two falcons were mixed together before centrifugation as above. After discarding the supernatant, the cells were gently re-suspended in 25 ml of 10% (v/v) glycerol. After a final centrifugation, the cells were re-suspended in 600 µl of 10% (v/v) glycerol. 50 µl of aliquots were dispensed into pre-chilled

eppendorf tube and frozen in liquid nitrogen. These electro-competent cells were stored at -80°C.

2.2.4. ISOLATION OF HIGH QUALITY PLASMID DNA FROM *E. COLI*

A single *E. coli* colony was picked up from the LB agar plate and inoculated in 2 ml liquid medium with an appropriate antibiotic at 37ºC on a shaker with speed of 180 rpm overnight. High copy plasmid DNA was isolated according to protocol given in the QIAGEN plasmid maxi kit (http://www.qiagen.com).

2.2.5. COMPETENT TRANSFORMATION OF *AGROBACTERIM TUMEFACIENS*

Transformation of competent *Agrobacterium tumefaciens* cells was carried out by high voltage electroporation (Shen and Forde, 1989). It is based on the principle that the permeability of the bacterial cell membrane is increased by applying an electric field, which helps in injecting plasmid DNA into the bacterium. An aliquot of frozen competent *A. tumefaciens* cells GV3101 was thawed on ice and transferred into a pre-chilled 1 mm electroporation cuvette (BioRad). 3-4 µl of plasmid DNA was gently mixed with competent cells on ice. The electroporation was carried out at a field strength of 1.8 kV/cm, a capacitance of 25 µF and resistors of 200 ohms. Immediately 500 µl of chilled YEB medium without antibiotics was added to the cuvette and gently mixed by pipetting and was transferred to a 2 ml eppendorf tube and incubated at 28°C for 2 hours with shaking at 200 rpm. Using a sterile spreader, 100 µl of this bacterial suspension was re-suspended on YEB agar containing an appropriate antibiotic under the sterile hood. Afterwards, the plate was sealed with parafilm and incubated at 28°C for two days in order to obtain visible colonies.

2.2.6. TRANSIENT TRANSFORMATION OF *N. BENTHAMIANA* PLANT

Transient expression of the fluorescent tagged proteins in *N. benthamiana* was carried out via the *A. tumefaciens* leaf infiltration method (Ron and Avni, 2004). An isolated colony of *Agrobacterium tumefaciens* containing the desired plasmid was inoculated in 3 ml of YEB medium containing the specific antibiotic against which the bacteria was resistant along with Rifampicin. After incubation over night at 28°C in a shaker at 200 rpm, the bacterial cells were centrifuged at 3500 rpm for 5 minutes at room temperature. The pellet was re-suspended in 1 ml of infiltration medium with freshly added 200 µM of Acetosyringone. Bacterial optical density was measured at 600 nm. The culture was diluted until an OD_{600} of 0.5 to 0.8 was attained and then incubated in a rotator for 1 hour. With the help of a needleless syringe, the bacterial suspension was injected into the abaxial surface of the leaf of 6 to 8 week old

tobacco plants. After 40 hours, the protein expression was observed under the confocal microscope using a 40x oil immersion lens (UPLAPO40XOI3, NA1.0).

2.2.7. PLANT TRANSFORMATION

Arabidopsis plants were transformed with different binary vectors to get stable transgenic plants using the floral-dip method as described by Clough and Bent, 1998. 25 ml of YEB medium containing appropriate antibiotics was inoculated with a transformed *Agrobacterium tumefaciens* colony at 28°C with gentle shaking for 2 days. 25 ml of pre-culture was mixed with 300 ml of fresh YEB medium in a sterile 2 liter flask for 16 hours at 28°C on a shaker until an OD_{600} of approximately 0.8 was reached. Well-watered *A. thaliana* plants containing many flower buds, which had their existing siliques removed, were used for transformation. 5 ml of 10% Tween 20 and 1 ml acetosyringone (100 mg /ml in chloroform) were added into the inoculation medium before dipping the plant. The entire aerial section of the plant was submerged and gently agitated for 5-10 seconds. The plant was covered with an autoclave bag to maintain high humidity and kept in dim light for 24 hours to allow it to recover from the inoculation procedure. After 1 day, the bag was removed and kept in the growth room at 23°C and 16 hours light / 8 hours night cycle for 2 months until harvest of seeds.

Transformed plants (T1) were selected on soil as survivors from spray treatments with the appropriate selection medium. For screening on a growth plates by visual inspection, a Leica MZ FL III fluorescence binocular, equipped with a GFP3 and RFP emission filters, was used for green and red fluorescent seedlings respectively.

2.2.8. MICROSCOPY

Imaging was performed using a FluoView FV 1000 confocal laser scanning microscope equipped with both an argon gas laser and laser diods, which are controlled by high-speed acousto-optic tunable filters (AOTFs), which allow a highly precise regulation of excitation intensity and wavelength. Different fluorophores were used in this study: The 488 nm argon laser line was used to excite GFP and the emission was detected between 490 and 530 nm. The 514 nm argon laser line was used to excite YFP and the emission was detected between 535 and 580 nm. At 561 nm, RFP was excited while its fluorescence was detected in the 570 to 630 nm range. For co-imaging of GFP or YFP with RFP, all images were acquired using sequential line scanning mode with rapid switching between the two exciting laser lines to avoid bleeding of fluorescence (Hutter, 2004). The transmitted light detector was used to acquire bright field-type images.

Seedlings stored vertically in sterile glass cuvettes for 24 hours prior to observation, were examined using a 10x (dry - UPLFLN10X U Plan Semi Apo, NA 0.4) and 40x (oil immersion - UPLAPO40XOI3, NA1.0) lens. *A. thaliana* samples were examined using the 40x oil immersion lens. In order to observe the transient expression in leaves of *N. benthamiana*, about 1 cm^2 piece was mounted between slide and cover slip in water with abaxial side up and examined using the 40x oil immersion lens. Time-lapse series were captured from single optical sections of tissues, which were acquired at defined time intervals. Serial confocal optical sections were acquired for Z-stack projections at different step sizes.

Various image processing software like Adobe Photoshop (Adobe Systems Inc.), Scion Image software package (Scion Corporation) and ImageJ were used to adjust contrast, projections of serial confocal sections and intensity for each image respectively. For growth measurement, seedlings were examined and photographed directly on the Petri dishes with the 10x lens mounted on an inverted Leica DMIRB microscope equipped with a CCD-camera. Microscopy of guard cells was done using a microscope fitted with 40x and 63x objectives.

2.2.9. FM4-64 / FM1-43 DYE STAINING

For FM4-64 dye staining of control and BFA-treated plants, 4 days old seedlings were transferred from 1/2 MS Plates to 1/10 MS Medium on sterile slides to recover from any stress for 1 day. Then, seedlings were stained with pre-cooled FM4-64 or FM1-43 solutions (5 µM in the 1/10 MS medium) at 4˚C for 5 minutes to slow down endocytosis. After a wash with the 1/10 MS medium for 2-3 minutes, the stained seedlings were treated by BFA solution (35 µM) in the dark for 1 hour before being examined under the confocal microscope using a 40x oil immersion lens.

ABA treatment or FM4-64 staining in transformed *N. benthamiana* leaves was either performed with excised leaf pieces or the dye solution (10 µM) was infiltrated into the abaxial side of transformed tobacco leaf using a needless syringe prior to excision (Bloch et al., 2005; Bolte et al., 2004). After that they were examined immediately under a laser-scanning confocal microscope using a 40x oil immersion lens for fluorescence. FM1-43 is excited at 488 nm and emission detected at ~590 nm. Image was scanned simultaneously for GFP and FM4-64 by using different emission detectors (490 – 530 nm and 667 – 746 nm, respectively), while being excited with the argon laser line at 488 nm.

2.2.10. DETECTION OF REACTIVE OXYGEN SPECIES (ROS)

For the observation of ROS in the guard cells, intact leaves were illuminated for 3 hours (120 µE m^{-2} s^{-1}) in a buffer containing 0.01M 2-(N-morpholine)-ethanesulphonic acid (MES), pH

6.15, 0.05 M KCl, 100 μM $CaCl_2$ to open all stomata. Leaves were homogenized in a blender for 30 seconds and filtered through a 100 μm nylon mesh to collect epidermal fragments. Later on, these fragments were treated with 10 μM of the H_2O_2-sensitive fluorescent dye DCF-DA in the dark for 10 minutes (Zhang et al., 2001). Epidermal fragments were washed and treated twice in fresh phosphate buffer to remove excess of dye for 10 minutes each respectively. For control and ABA treatment, the fragments were treated with appropriate solvents and 100μM ABA respectively for 10 minutes before visualizing by confocal laser scanning microscopy (40x oil immersion lens) using an excitation wavelength of 488 nm and an emission wavelength range of 515–560 nm. For quantification the fluorescence level in the guard cells before and after ABA/PtdIns5P treatment, Adobe Photoshop 5.5 software (Adobe Systems) was used.

2.2.11. HISTOCHEMICAL ß-GLUCORONIDASE (GUS) STAINING

From 5 days to 2 week old seedlings of stably transformed promoter-GUS *A. thaliana* plants were used to examine the expression of ß -Glucoronidase activity as described by Jefferson (1987) with minor modifications. Seedlings were vacuum infiltrated for 10 minutes with substrate solution (100 mM sodium phosphate buffer, pH 7.0, 10 mM EDTA, 0.1% Triton X-100, 0.5 mM potassium ferricyanide, 0.5 mM potassium ferrocyanide and 1 mM 5-bromo-4-chloro-3-indolyl glucuronide) and incubated at 37°C for 8 - 10 hours. The stained seedlings were then washed twice in 70% ethanol for 30 minutes in order to remove chlorophyll from the aerial parts of the seedlings. Photographs were taken by using a Leica MZ FL III binocular equipped with a CCD camera. For image documentation, the Diskus-program (Vers. 4.2, Carl Hilgers, Königswinter, Germany) was used. Stably transformed promoter-GUS plants, challenged with different abiotic stresses and 16 hours after the onset of the stress, were assayed for GUS. For the quantification of GUS staining, images were analysed using ImageJ software (http:/rsb.info.nih.gov/ij/). Pixels were measured in a selected area showing blue color. For background correction, a similar zone without blue color was selected and subtracted to get rid of the background intensity. Mean values for three biological replicates were calculated.

2.2.12. DETERMINATION OF STOMATAL APERTURE AND RELATIVE WATER CONTENT

The abaxial epidermis was peeled from the rosette leaves of 3-week-old plants (wild-type Col-0 and mutants of myotubularins (M1KO, M2KO, DKO and M1OX)) and treated with buffer containing 0.01M 2-(N-morpholine)-ethanesulphonic acid (MES), pH 6.15, 0.05 M KCl, 100μM $CaCl_2$ at 22°C for 2 hours in order to open all stomata (Pei et al., 1997). To

determine the differences in ABA-mediated stomatal closure, previously opened stomata were incubated in 10 µM ABA for 3 h. For control, previously opened stomata were incubated in the above buffer in parallel with no ABA added for 3 h in the light. 40 or more mature stomata of the epidermal strips were investigated in each experiment using a microscope fitted with 40x and 63x objectives.

Relative water content (RWC) was measured as explained by Griffiths and Bray in 1996. Fresh rosette leaves of 6 weeks old, well-watered plants were weighed. For measuring the dry weight, leaves of the plant kept in the same growth room with relative humidity of 30% without water for 7 days were used. Turgid weight was measured by keeping these plants in water, overnight. Water loss was measured by using formula: (RWC = [FW - DW]/[TW - DW], where FW = fresh weight of leaf, DW = dry weight of leaf and TW = rehydrated weight of leaf). For the measurement, 10 separate plants per line were used.

3.   RESULTS

3.1.   EXPRESSION PATTERN OF MYOTUBULARINS

In order to analyze the tissue specific expression pattern of myotubularins in *A. thaliana* in greater detail, wild-type *Arabidopsis* seedlings stably transformed with a AtMTM1prom::GUS and AtMTM2prom::GUS construct (gift from Prof. Zoya Avramova) were examined. Both lines (AtMTM1prom::GUS and AtMTM2prom::GUS) showed GUS activity in numerous plant tissues, like in the vasculature of roots and hypocotyl (Figure 3A and Figure 4A) of 5 days old seedlings under normal condition i.e. 16 hours light and 8 hours dark. There is very little GUS activity observed in the elongation region of the roots. Both AtMTM1prom::GUS and AtMTM2prom::GUS transgenic lines, showed GUS activity in the leaves (clearly netted venation) (Figure 3B and Figure 4B). In 2 weeks old seedlings of AtMTM1prom::GUS and AtMTM2prom::GUS plants, there was an expression observed in trichomes. (Figure 3C and Figure 4D).
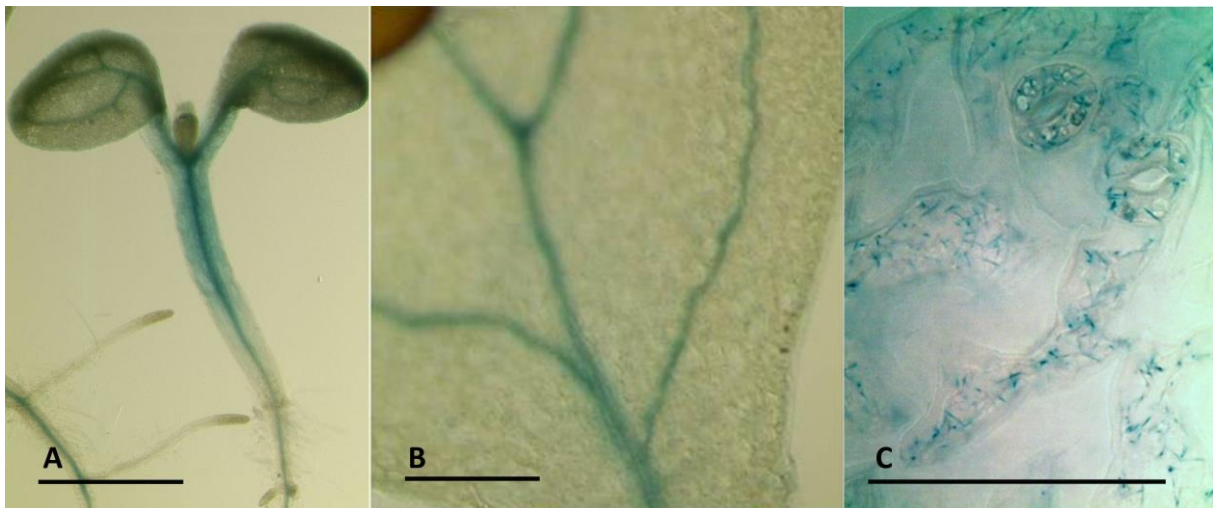
Figure 3: GUS expression pattern of five days old seedlings of AtMTM1 in *Arabidopsis* tissues and organs..

A: AtMTM1 GUS activity in hypocotyl, roots and leaves.

B: Magnified view of leaf showing AtMTM1 GUS expression in veins.

C: AtMTM1 GUS activity in trichomes in a 2 weeks old seedling.

Scale bars: A = 1mm, B = 200 μm, C = 500 μm.
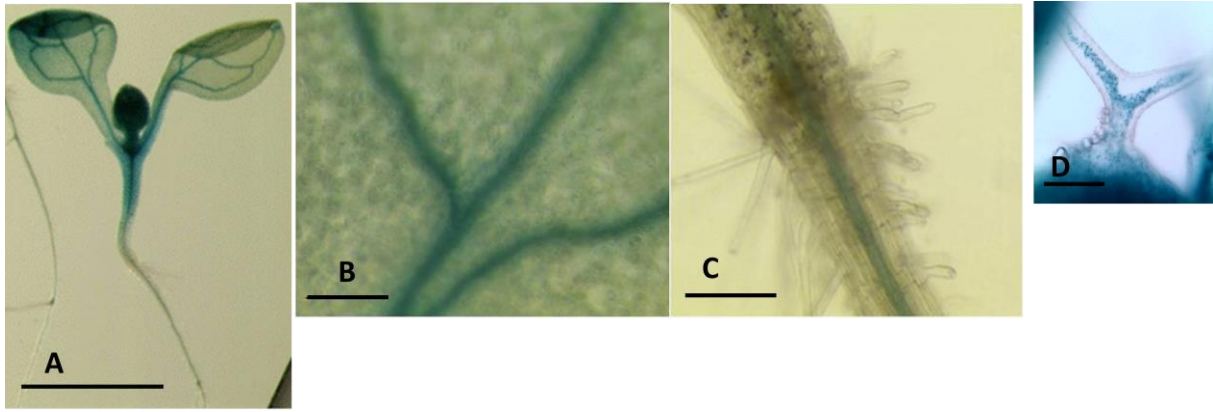
Figure 4: GUS expression of five days old seedlings of AtMTM2 in *Arabidopsis* tissues and organs.

A: AtMTM2 GUS activity in hypocotyl, roots and leaves.

B: Magnified view of leaf showing AtMTM2 GUS expression in veins.

C: Magnified view of root showing AtMTM2 GUS expression in vascular system.

D: GUS activity in trichomes in a 2 weeks old seedling.

Scale bars: A = 1mm, B, C = 200 μm, D = 500 μm.

3.1.1. EXPRESSION ANALYSES UNDER ABIOTIC STRESS CONDITIONS

As plants are sessile organisms, they have to cope with different abiotic stresses which are a part of changing climate. Abiotic stresses mainly include drought (ABA exposure), salinity, extreme temperatures (cold and heat), which adversely affect plant growth and productivity. First, histological expression of AtMTM1prom::GUS and AtMTM2prom::GUS under abiotic stress conditions is analyzed, which will help in determining the physiological functions of these proteins. Therefore, five abiotic stresses were selected to treat 5 days old seedlings.

3.1.1.1. COLD STRESS

When 4 days old seedlings were kept at 4°C for one day, the expression of these proteins diminished in the leaves and was repressed in the root (Figure 5B and Figure 5D). In both AtMTM1prom::GUS and AtMTM2prom::GUS transgenic lines, there was a weak expression in the veins of leaves and hypocotyl (Figure 5A and Figure 5C) with an overall reduction in the level of expression compared to normal condition but no such distinct difference in the level of expression between the two myotubularins was observed.
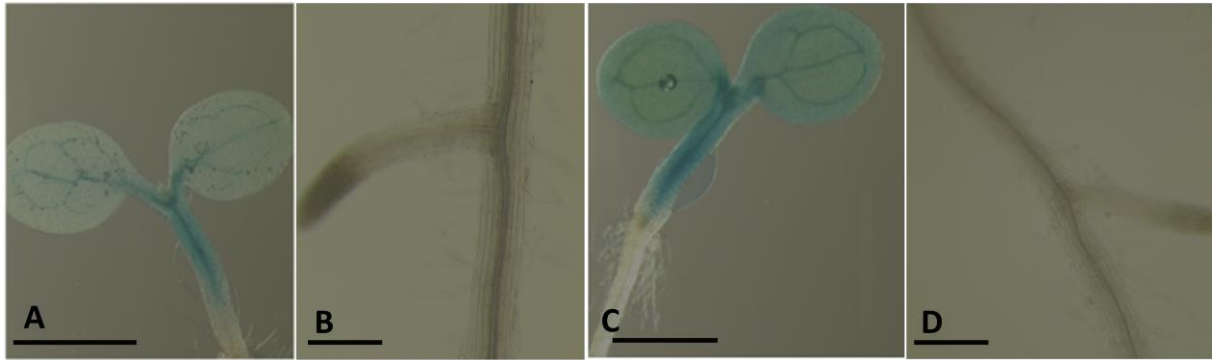
Figure 5: GUS expression of five days old seedlings of AtMTM1 and AtMTM2 in *A. thaliana* during cold stress at 4°C for 24 hours before staining.

A: Weak expression of AtMTM1 GUS activity in leaves and hypocotyl.

B: No expression of AtMTM1 GUS activity in roots.

C: Weak expression of AtMTM2 GUS activity in leaves and hypocotyl.

D: No expression of AtMTM2 GUS activity in roots.

Scale bars: A, C = 1mm, B, D = 500 µm

3.1.1.2.   DARK STRESS

In 5 days old etiolated seedlings, GUS expression was detected only in leaves (Figure 6A and Figure 6C) in both proteins. There was no expression observed in the roots and hypocotyl suggesting promoter activity of both proteins is affected by darkness. But the level of activity of these proteins was at a similar level in the leaves.

Figure 6: GUS expression of five days old seedlings of AtMTM1 and AtMTM2 in *Arabidopsis* during dark stress.

A: Strong AtMTM1 GUS activity in leaves.

B: No expression of AtMTM1 GUS activity in roots.

C: Strong AtMTM2 GUS activity in leaves.

D: No expression of AtMTM2 GUS activity in roots.

Scale bars: A, B, C, D = 200 µm

3.1.1.3.   SALT STRESS

Salt stress also influences the expression of AtMTM1 and AtMTM2. Promoter activity was observed only in leaves and a little in hypocotyl after treatment with 100mM of salt stress to 4 days old seedlings for 1day (Figure 7A and Figure 7C). No expression was observed in the roots for both the myotubularins (Figure 7B and Figure 7D).
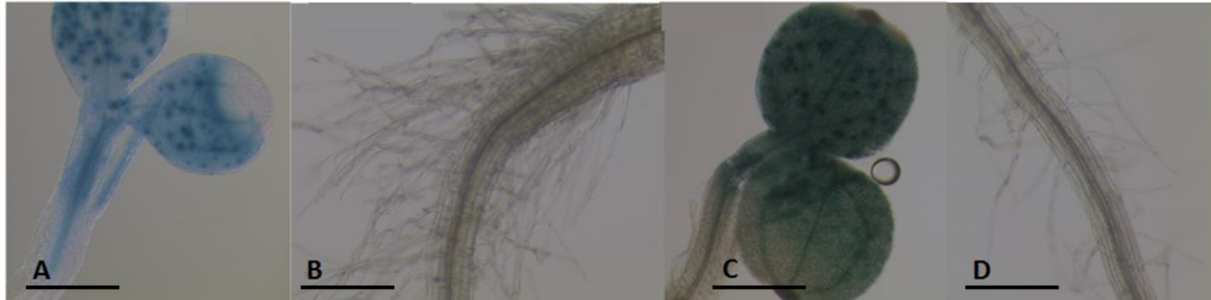
Figure 7: GUS expression of five days old seedlings of AtMTM1 and AtMTM2 in *Arabidopsis* during 100mM salt stress for 24 hours before staining.

A: Strong AtMTM1 GUS activity in leaves and weak AtMTM1 GUS activity in hypocotyl.
B: No expression of AtMTM1 GUS activity in roots.
C: Strong AtMTM2 GUS activity in leaves and weak AtMTM2 GUS activity in hypocotyl.
D: No expression of AtMTM2 GUS activity in roots.
Scale bars: A, B, C, D = 500 μm

3.1.1.4.   ABA EXPOSURE

30μM of ABA exposure for one day increased the promoter activity of AtMTM1 in stable transgenic lines. It showed more expression in roots and leaves of AtMTM1 prom::GUS transgenic lines (Figure 8A and Figure 8B), while no significant elevation was observed in AtMTM2 prom::GUS transgenic lines after 30μM of ABA exposure for one day (Figure 8C and Figure 8D) in comparison to normal condition. Hence ABA exposed seedlings show a difference in the behavior of the two myotubularins. A quantitative comparison in the expression of AtMTM1 and AtMTM2 under different abiotic stresses is shown in Figure 10.
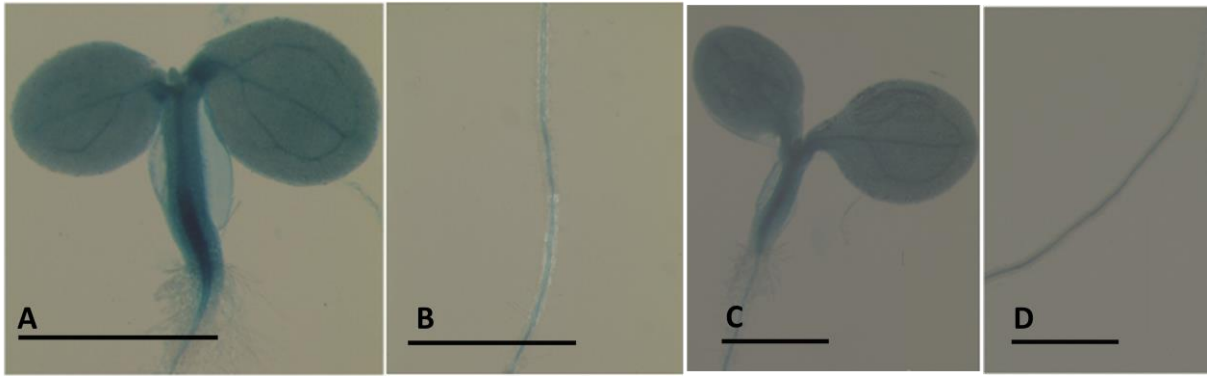
Figure 8: GUS expression of five days old seedlings of AtMTM1 and AtMTM2 in *Arabidopsis* during 30μM ABA exposure for 24 hours prior to staining.

A: Strong expression of AtMTM1 GUS activity in leaves and hypocotyl.

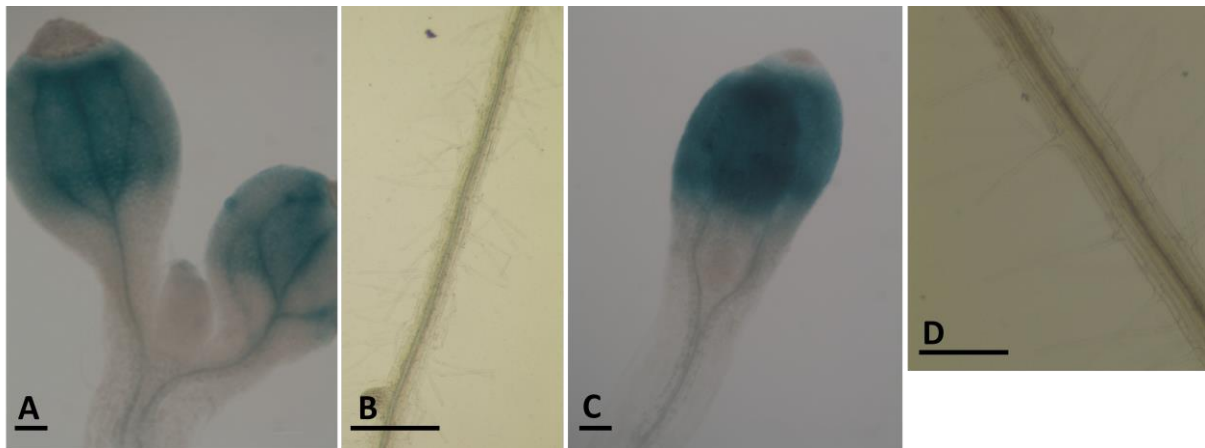B: Strong expression of AtMTM1 GUS activity in vascular system of roots.

C: No significant change observed in the expression of AtMTM2 GUS activity in leaves and hypocotyl.

D: No significant change observed in the expression of AtMTM2 GUS activity in vascular system of roots.

Scale bars: A, B, C, D = 1 mm

3.1.1.5.   HEAT STRESS

High-temperature stress (37°C) was induced in 5 days old seedlings for 2 hours. Heat shock treatment triggered a decrease in AtMTM1 and AtMTM2 gene expression with no expression in roots (Figure 9B and Figure 9D). The expression in the leaves of AtMTM2 was at a slightly higher level compared to AtMTM1 (Figure 9A and Figure 9C). A quantitative comparison in the expression of AtMTM1 and AtMTM2 under different abiotic stresses is shown in Figure 10.

Figure 9: GUS expression of five days old seedlings of AtMTM1 and AtMTM2 in *Arabidopsis* during heat stress at 37°C for 2 hours prior to staining.

A: Weak activity of AtMTM1 GUS activity in leaves and hypocotyl.

B: No expression of AtMTM1 GUS activity in roots.

C: Slightly higher expression of AtMTM2 GUS activity in leaves and hypocotyl in comparison to AtMTM1 GUS activity.

D: No expression of AtMTM2 GUS activity in roots.   Scale bars: A, B, C, D = 500 μm

3.1.1.6.   QUANTIFICATION OF GUS STAINING BY IMAGE ANALYSIS

Quantification of GUS staining revealed that expression of the both genes was affected by abiotic stresses. Under normal conditions, the promoter activity of AtMTM1 and AtMTM2 in stable transgenic lines was almost equivalent, while AtMTM2 showed higher activity in roots as compared to AtMTM1. Decrease in relative intensity of GUS was observed in both AtMTM1 and AtMTM2 promoter activity under dark, cold and heat stress as compared to normal condition. Under dark stress, there was ~40% and ~42% decrease in AtMTM1 and AtMTM2 promoter activity respectively. Similarly, there was ~60% decrease in AtMTM1 promoter activity under both cold and heat stress, while AtMTM2 promoter activity was reduced by ~65% and ~60% under cold and heat stress respectively. Under 100 mM salt stress, there was only ~10% increase in the activities of both genes. Under 30 μM ABA exposure, there was a significant 80% elevation in AtMTM1 promoter activity, while only 10% increment was observed in AtMTM2 promoter activity when compared to control conditions (Figure 10).
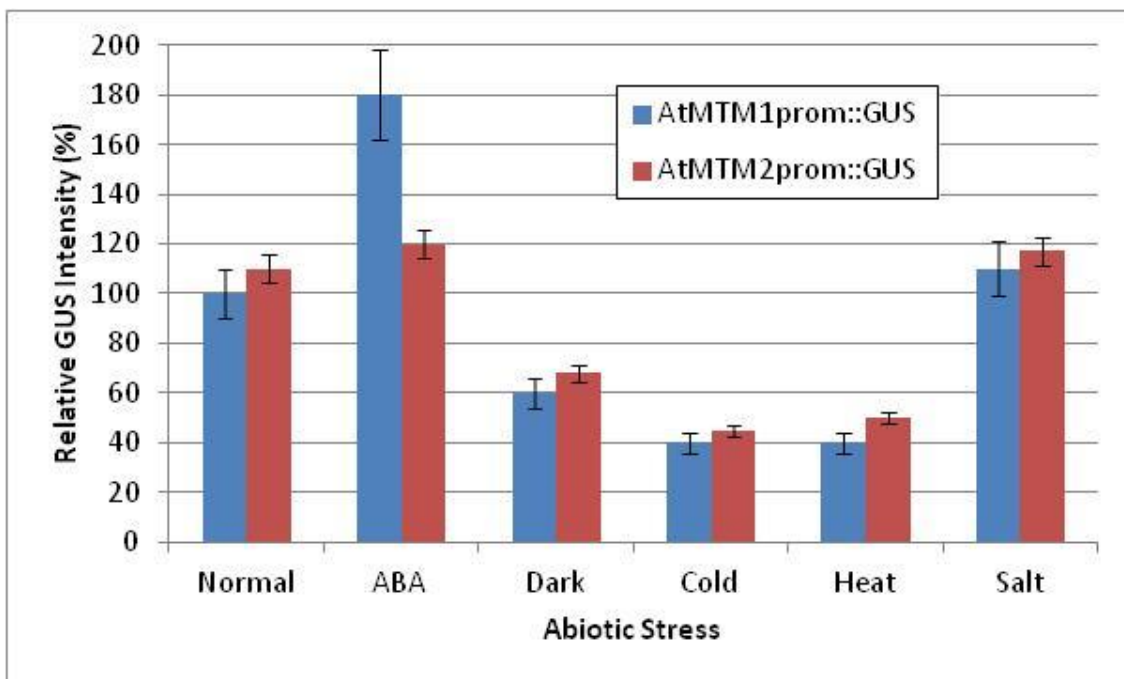
Figure 10: Quantification of GUS expression of AtMTM1 and AtMTM2 under different abiotic stresses like ABA treatment, dark treatment, cold treatment, high temperature and salt treatment.

Blue column (■) represents AtMTM1:GUS activity, while red column (■) represents AtMTM2:GUS activity. The data were measured from 9–12 independent samples. The error bars are the standard deviations.

3.2.   EFFECT OF ABA ON MYOTUBULARIN MUTANTS

3.2.1.   GERMINATION ASSAY

When all the mutants of myotubularins along with wild-type Col-0 were grown under well-watered conditions, they did not show any visible phenotypic alteration. However, AtMTM1 gene affected the sensitivity of seed germination by exogenous application of ABA. As shown in Figure 11, exogenous application of 1μM ABA, Double knock out (DKO) and M1KO plants showed 23% and 26% decrease in the germination rate respectively, while M1OX plants showed 42% decrement and M2KO showed 32% reduction. Col-0 exhibited a diminution of 29% after 1 μM ABA treatment.
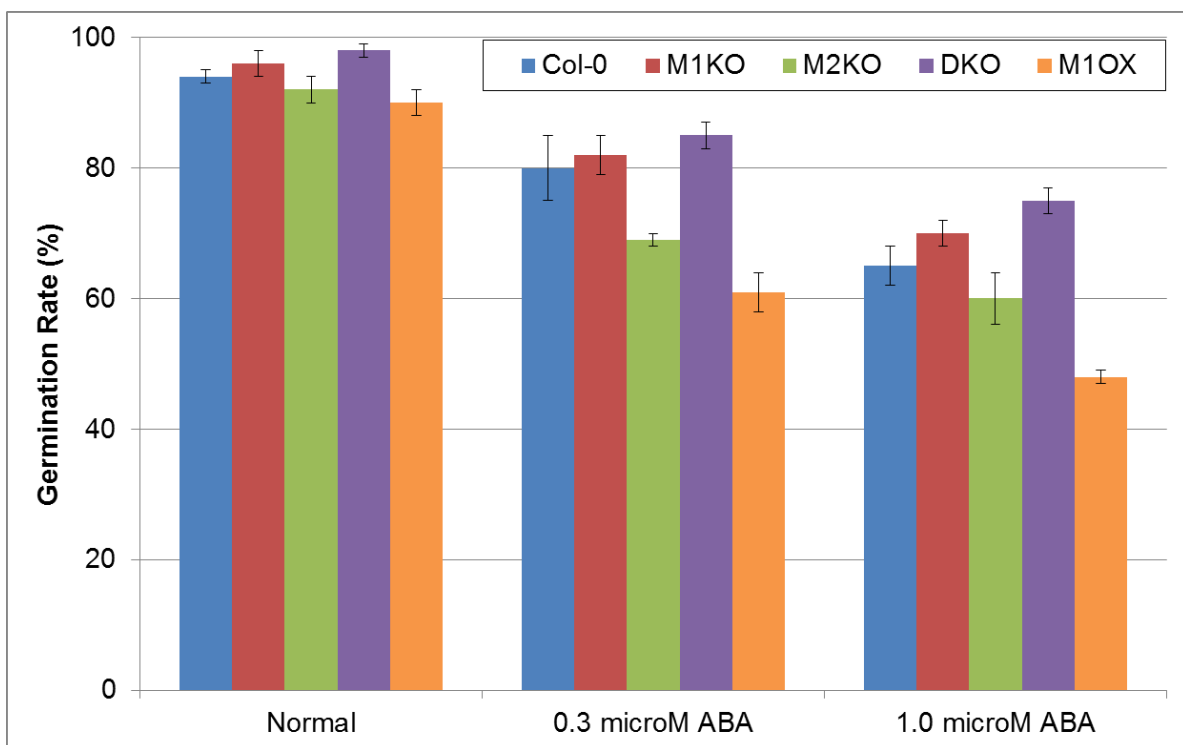
Figure 11: Measurement of germination rate (radicle emergence) for mutants of myotubularins compared to wild-type Col-0 under ABA exposure.

Germination rate scored 5 days after stratification of wild-type Col-0, M1KO, M2KO, DKO and M1OX grown under control conditions or in the presence of 0.3 μM and 1.0 μM ABA. M2KO and M1OX plants showed a decrease in the germination rate under ABA exposure. The data are averages ±SE of three independent experiments, each with a minimum of 60 individual plants.

3.2.2.   RELATIVE WATER CONTENT

Relative water content (RWC) of various mutants along with Col-0 was calculated after 6, 9 and 12 days without water. After 12 days, DKO and M1KO showed significantly higher RWC as compared to M1OX as shown in Figure 12. DKO and M1KO showed respectively

30% and 36% reduction in RWC, while M2KO and M1OX both showed approximately 60% reduction in RWC.
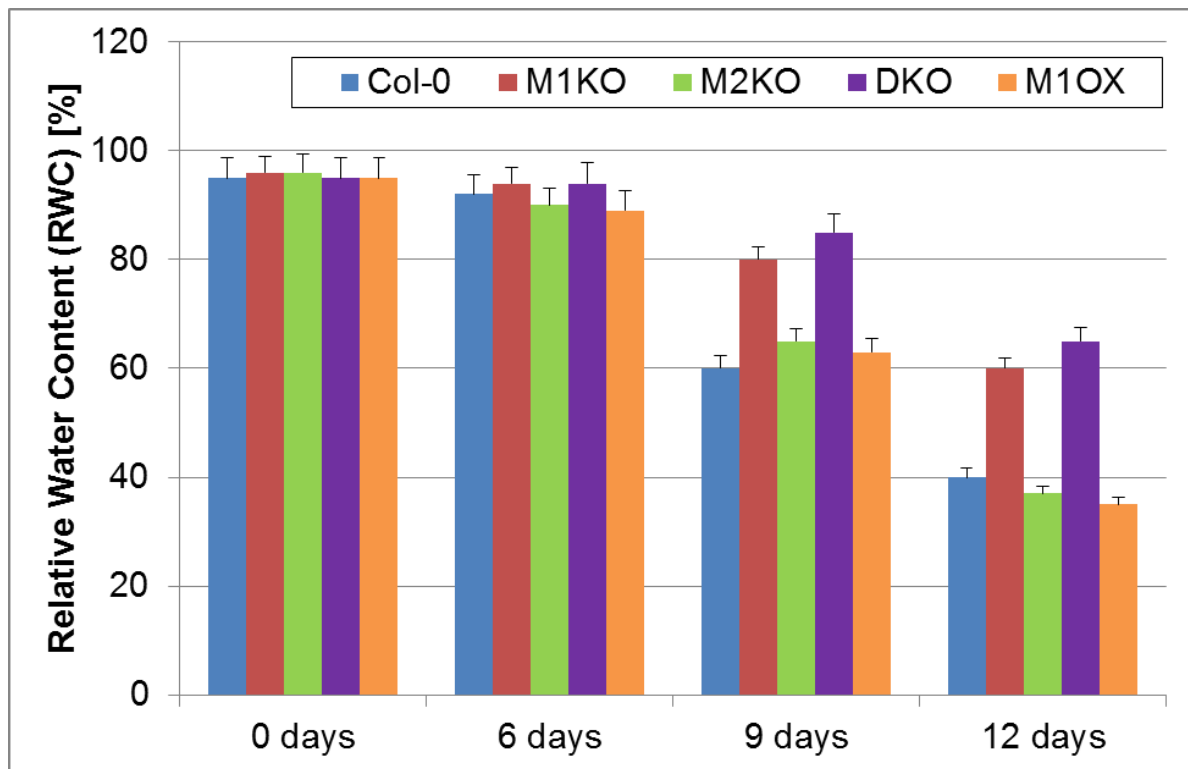
Figure 12: Measurement of relative water content of various mutants of myotubularins along with wild-type Col-0.

Fully expanded leaves of 6 week old plants grown in soil after 6, 9 and 12 days without water were used to determine RWC. M1OX and M2KO plants exhibited less relative water content, while DKO and M1KO plants retained more water as compared to wild-type Col-0. The results are averages ±SE of three independent experiments, each with a minimum of 20 individual plants.

3.2.3. ATMTM1 IMPAIRS THE ABA REGULATION OF STOMATAL APERTURE

The plant hormone abscisic acid (ABA) triggers stomatal closure under drought stress, which helps the plant to survive under stress condition by reducing water loss through transpiration. The responsiveness of stomata of mutants of myotubularins was analyzed in-vitro in response to 10μM ABA using isolated epidermal peels. Pre-opened M1OX stomata failed to close in response to ABA (Figure 13), which is consistent with the inability of M1OX plants to reduce water loss under drought condition. Stomata of M1KO and DKO closed their aperture significantly in response to ABA as shown in Figure 13.
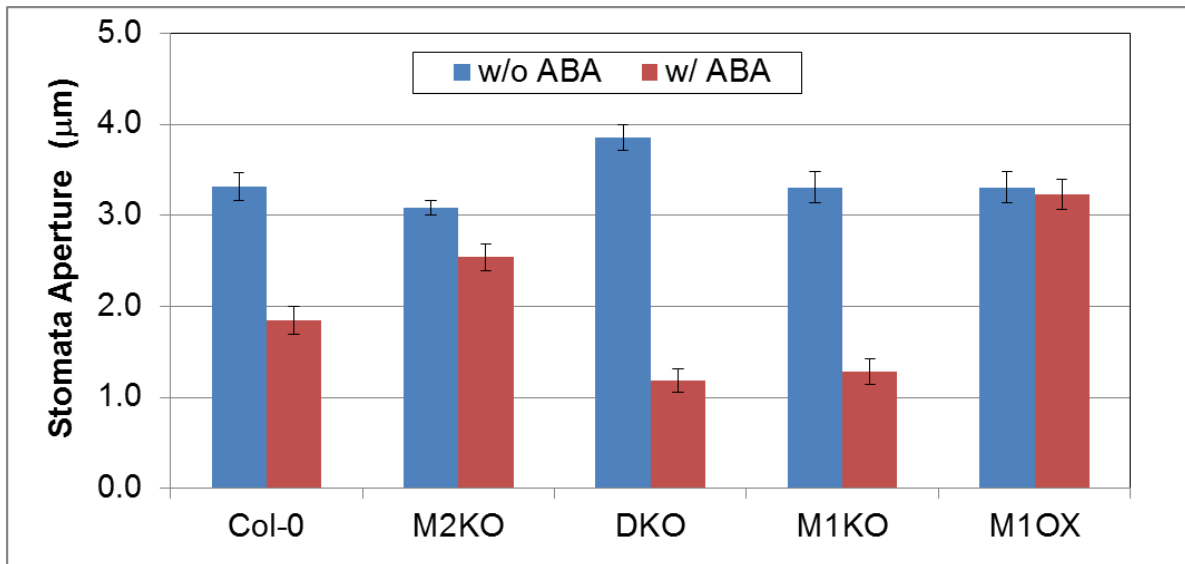
Figure 13: Measurement of stomatal apertures on epidermal peels before and after 10μM ABA treatment.

In each case, blue bars (■) represent stomatal apertures of the guard cells (incubated in the buffer alone) and red bars (■) represent stomatal apertures of the guard cells (incubated in 10 μM ABA). No change in stomatal aperture was observed in M1OX plants, while DKO and M1KO exhibited closing of stomatal aperture after ABA exposure. (The values shown are the mean of two independent experiments, n=40 from 9-12 plants for each experiment)

3.2.4. EXOGENOUS SUPPLY OF ABA AFFECTS ROS LEVELS IN STOMATA

It is well known that ABA increases the cellular level of ROS in Col-0 as it affects the ROS-producing and ROS-scavenging genes which modulate the ROS level. Epidermal peels from the leaves were harvested and kept in the MES buffer for 3 hours under illumination to fully open the stomata. ROS was calculated for control as well as after treatment with 100 μM ABA. Level of ROS in untreated plants was almost equivalent except M1OX, which showed slightly lower level of ROS. In ABA treated plants, M1OX showed ~35% reduction in ROS level, while DKO and M1KO plants showed ~65% and ~40% more increment in ROS level respectively after ABA treatment as Col-0 showed ~ 20% increase in ROS level (Figure 14). This indicates that Myotubularins influence ROS signaling.
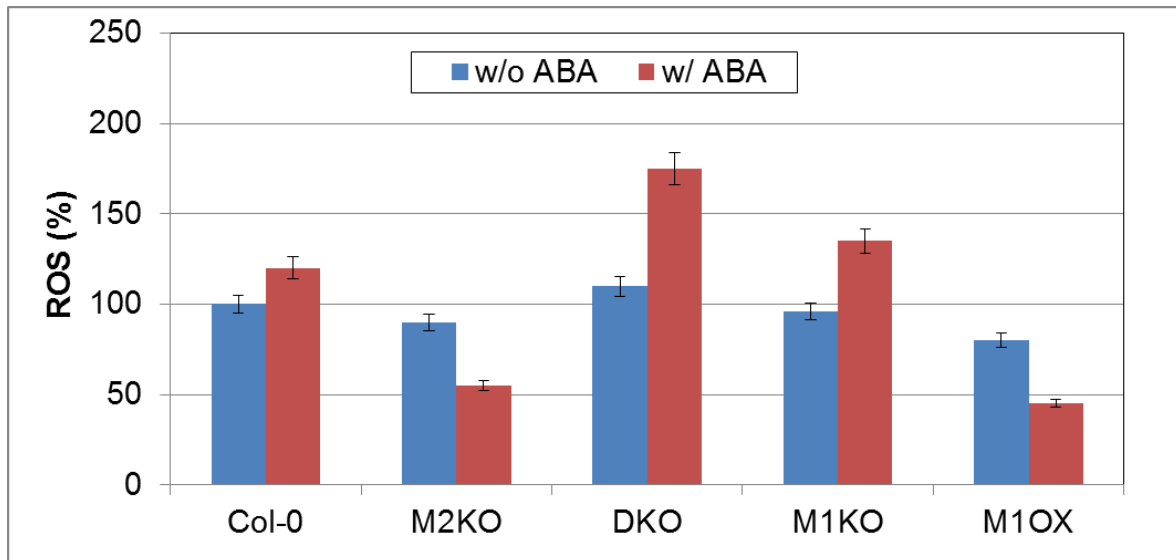
Figure 14: Changes in ROS levels analyzed by measuring 2,7-dichlorofluorescein diacetate fluorescence levels in guard cells with and without ABA (100μM).

In each case, blue bars (■) represent change in ROS level (incubated in the buffer alone) and red bars (■) represent change in ROS level after ABA treatment with wild-type Col-0 as a reference for these measurements. M1KO and DKO showed increment in ROS level after ABA exposure, while M1OX and M2KO exhibited a decreased ROS level as compared to wild-type Col-0 after ABA exposure. The data are averages ±SE of two independent experiments, each with a minimum of 40 individual stomata from 9-12 plants.

3.3. QUANTIFICATION OF ROS AFTER EXOGENOUS SUPPLY OF PTDINS5P

3.3.1. PTDINS5P INHIBITS LIGHT-INDUCED ROS GENERATION IN *ARABIDOPSIS* GUARD CELLS

To check the effect of PtdIns5P on the cellular level of ROS, epidermal peels from the leaves were harvested and kept in MES buffer for 3 hours under illumination in order to fully open the stomata. Under the influence of 1.5μM of PtdIns5P for 1 hour, ROS level was calculated, while for control MES buffer was used for the same duration. Wild-type Col-0 as well as all the mutants of myotubularins showed a decrease in ROS level after treatment of Ptdins5P as compared to Control. Maximum influence of the reduced ROS level was observed in case of M1OX from ~80% to ~30% under the influence of 1.5μM of PtdIns5P, while DKO showed the least effect, changing from 107% to 65% with Col-0 as control at 100% (Figure 15).

Figure 15: Changes in ROS levels were analyzed by measuring 2,7-dichlorofluorescein diacetate fluorescence levels in stomata with and without exogenous supply of 1.5μM PtdIns5P .

In each case, blue bars (█) represent change in ROS level (incubated in the buffer alone) and red bars (█) represent change in ROS level after exogenous PtdIns5P treatment with wild-type Col-0 as a reference for these measurements. ROS level of stomata was reduced in wild-type Col-0 as well as all the mutants of myotubularins after the application of exogenous PtdIns5P but higher reduction has been observed in M1OX plants. The data are averages ±SE of two independent experiments, each with a minimum of 30 individual stomata from 6-8 plants in each experiment.

3.3.2. PTDINS5P TREATMENT DECREASES ROS LEVELS ALSO IN ROOT TISSUES

A quantitative estimate of ROS level was determined by 2′,7′ dichlorodihydrofluorescin-diacetate (DCF-DA). In order to determine the intracellular ROS levels in roots under PtdIns5P conditions, the ROS-sensitive dye was loaded into root cells and after washing with buffer, were investigated using a confocal microscope. ROS accumulation was markedly decreased in PtdIns5P treated roots compared to the control roots. *Arabidopsis* roots of Col-0 and other mutants of myotubularins showed almost similar background intensity under control conditions except M1OX plants. In M1OX, ROS reduced from 68% to 38% after 1.5μM phosphoinositide (PtdIns5P) treatment. Fluorescence was about ~17% lower in M1OX compared with the Col-0 after 1.5μM PtdIns5P treatment. While in M2KO, fluorescence intensity was reduced from 79% to 34%, the intracellular ROS level of root tip treated with 1.5μM PtdIns5P decreased to 47% of the control in wild-type Col-0. ROS level was decreased from 107% to 73% in DKO, while in M1KO, it decreased to 46% from 87% (Figure 16). This

suggests that exogenous supply of PtdIns5P affects ROS level in stomata as well as root tissues.
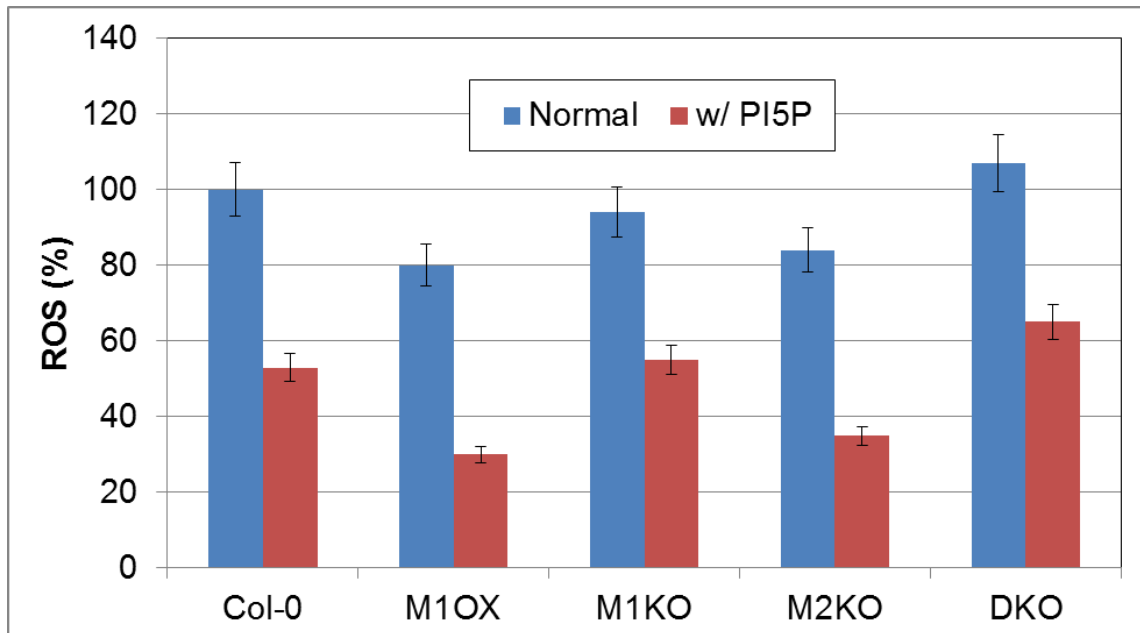

Figure 16: Changes in ROS levels were analyzed by measuring 2,7-dichlorofluorescein diacetate fluorescence levels in root tissues with and without exogenous supply of 1.5μM PtdIns5P.
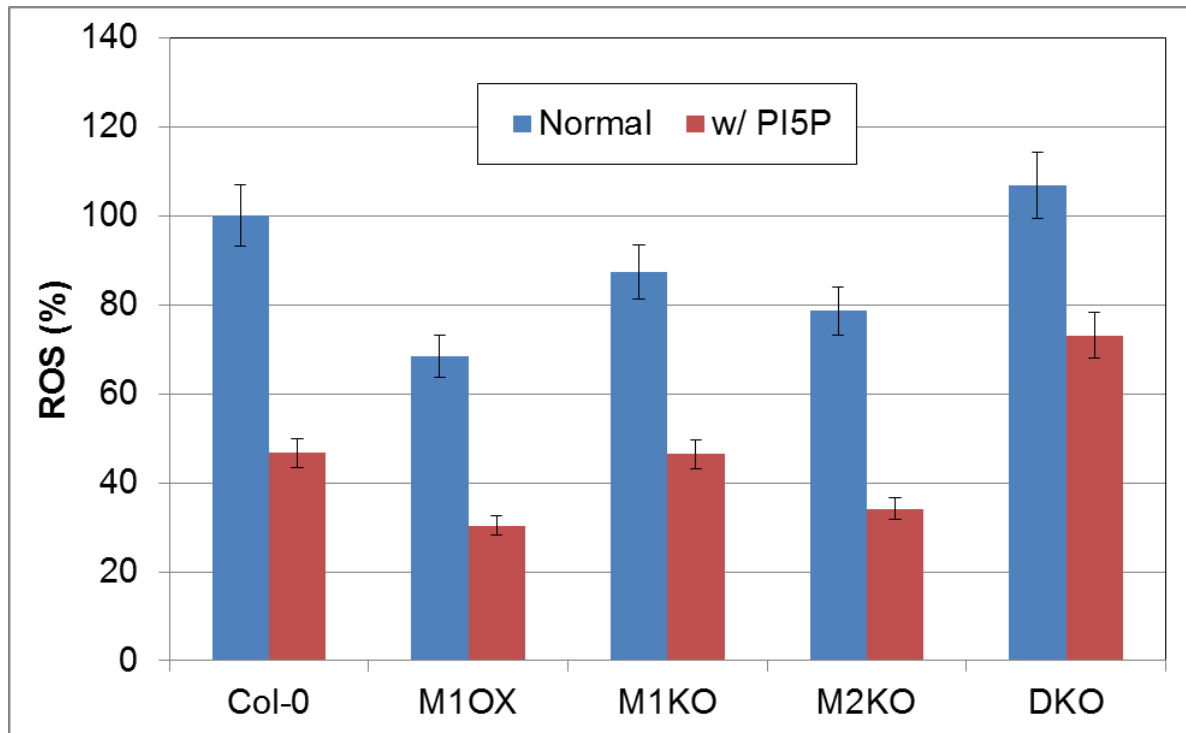
In each case, blue bars (▬) represent change in ROS level (incubated in the buffer alone) and red bars (▬) represent change in ROS level after exogenous PtdIns5P treatment. Wild-type Col-0 is used as a reference for these measurements. Decrease in ROS level has been observed in roots of wild-type Col-0 as well as four mutants of myotubularins after exogenous PtdIns5P treatment. The data are averages ±SE of two independent experiments, each with a minimum of 20 roots.

3.4.   SUBCELLULAR LOCALIZATION OF MYOTUBULAINS

In order to investigate the cellular role and localization of AtMTM1 and AtMTM2 in plant cell, AtMTM1 and AtMTM2 fused to the RFP/GFP under the control of 35S promoter (these constructs are a gift from Prof. Zoya Avramova) were expressed transiently in *N. benthamiana* leaf epidermal cells based on published protocols for DNA integration into the plant genome (Batoko et al., 2000; daSilva et al., 2004) and then observed by Confocal Microscopy. It revealed that both proteins showed different expression. AtMTM1-RFP showed motile punctuate particles of different sizes (or vesciles) near the plasma membrane and throughout the cytoplasm (Figure 17A), while AtMTM2-GFP expressed in a net like structure with some dense patches around the epidermal pavement cells (Figure 17B). One of the aims of this study is to determine the nature of these particulate structures found in

AtMTM1-RFP and to find out the subcellular localization of AtMTM2-GFP. (The term 'vesicles' is used throughout this Thesis for regularly or irregularly shaped punctuate structures of different sizes).
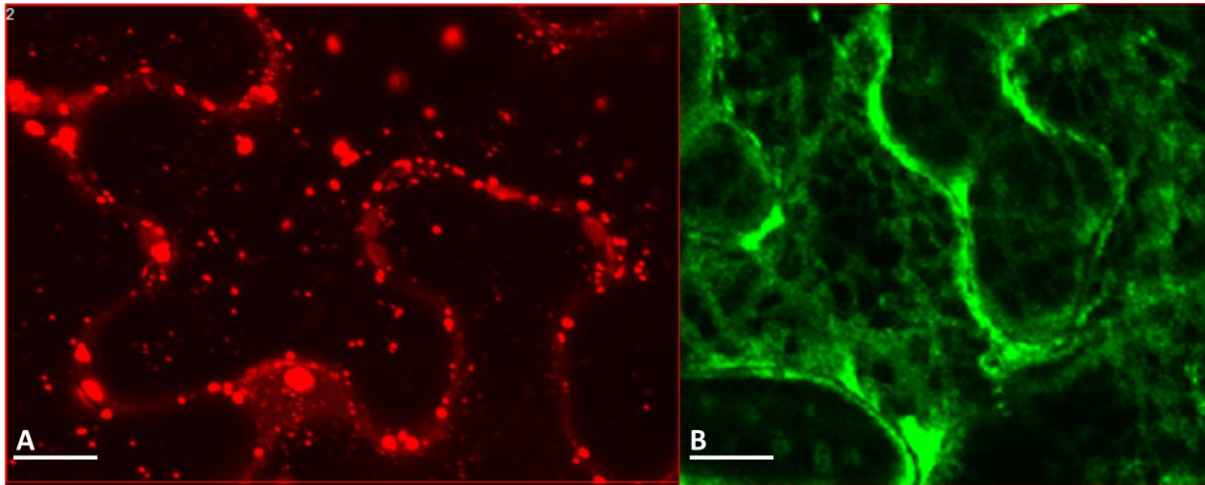
Figure 17: Expression of AtMTM1-RFP and AtMTM2-GFP in transformed epidermal leave cells of tobacco.

A: Z-projection of AtMTM1-RFP showed large number of motile vesicles of different sizes in the cytoplasm and around the plasma membrane.

B: Z-projection of AtMTM2-GFP exhibited net like structure like ER in a projection of the top half of the cell. (Bar: 10 μm)

3.4.1. CO-LOCALIZATION OF ATMTM1-RFP

To find out a possible endosomal identity of the vesicular structures observed in tobacco leaf epidermal cells expressing AtMTM1-RFP, co-expression studies were carried out with plant endosomal markers. Co-expression of AtMTM1-RFP with FVYE-GFP, ARA7-GFP visualizing the late endosomes (Jensen et al., 2001; Heras and Drobak, 2002; Voigt et al., 2005; Golomb et al., 2008) and AtEHD1-GFP (*Arabidopsis* Eps15 homology (EH) domain acts as a endocytic marker) did not co-localize (Figures shown in appendix). AtMTM1-RFP also did not show any co-localization with RabF2b, which label late endosome or pre-vacuolar compartments (Nielsen et al., 2008) (Figure in appendix). Also, AtMTM1-RFP did not localize with RabA1e-YFP which acts as an endosomal recycling marker (Chow et al., 2008) (Figure in appendix). It confirmed that plant myotubularin AtMTM1-RFP does not reside in late endosomes.

In an attempt to ascertain the nature of these punctate motile structures, Golgi markers were co-expressed with AtMTM1-RFP in tobacco leaves. The Golgi apparatus (also called Golgi complex) is divided into distinct cis, medial and trans compartments, each of which consist of one or two adjacent cisternae surrounded by vesicles and distributed throughout the cytoplasm (Staehelin and Moore, 1995; Driouich and Staehelin, 1997; Andreeva et al., 1998; Polishchuk

and Mironov, 2004; Staehelin and Kang, 2008). Various trans-Golgi (TGN) markers were used in co-expression studies e.g. ST-GFP is 58 amino acids of a sialyl transferase fused with GFP (Boevink et al., 1998; Batoko et al., 2000; Brandizzi et al., 2002; Saint-Jore et al., 2002); Venus-SYP61-GFP is a single gene found in syntaxin of plants (SYP), which is mainly localized to TGN (Sanderfoot et al., 2000; Sanderfoot et al., 2001); VTI12-YFP is one of the *Arabidopsis* homologues of the yeast SNARE Vti1p (Zheng et al., 1999); RabA1d-GFP is a member of the RabA subfamily of small Rab GTPases, which is a reliable marker used for studying secretory/recycling vesicles. This and none of three other TGN markers (ST-GFP, Venus-SYP61-GFP and VTI12-YFP) co-localized with AtMTM1-RFP (Figure in appendix). This clearly shows that AtMTM1-RFP does not reside with the early endosome (EE), which by some authors is considered a subset of the TGN (Dettmer et al., 2006).

G-YK (Nelson et al., 2007), a Golgi marker, partially co-localizes with endoplasmic reticulum and highly co-localized with the cis-Golgi. It is derived from Man49-GFP (Saint-Jore-Dupas et al., 2006) replacing GFP with the monomeric yellow fluorescent protein. Co-expression of G-YK with AtMTM1-RFP showed high co-localization. (Figure 18).
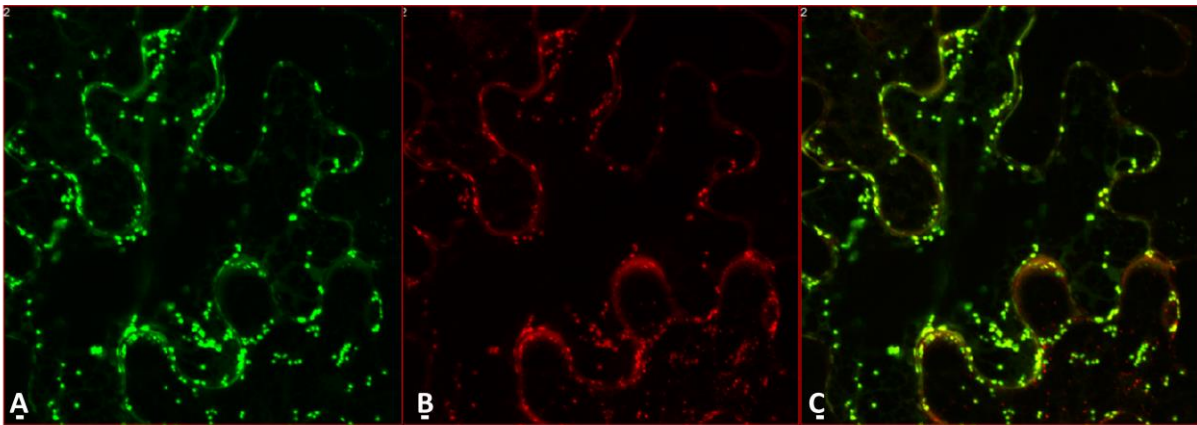
Figure 18: Z-projections of *Nicotiana benthamiana* epidermal leaf cells co-expressing AtMTM1-RFP with G-YK.

A-C: overview of a cell showing G-YK in (A); AtMTM1-RFP in (B) and a merge of the two in (C). Transient co-expression of AtMTM1-RFP with G-YK in transformed tobacco leaves showed a complete co-localization of both constructs (z-stack). (Bar: 10 μm)

3.4.2. CO-LOCALIZATION OF AtMTM2-GFP

Transformed *Agrobacterium tumefaciens* harboring the AtMTM2-GFP construct was infiltrated into the leaf epidermis of *N. benthamiana*. Figure 19B is a single optical section at the middle plane of the cell demonstrating the dense patches around epidermal cells, while Figure 19A is a Z-projection showing network like structure within the whole cell.
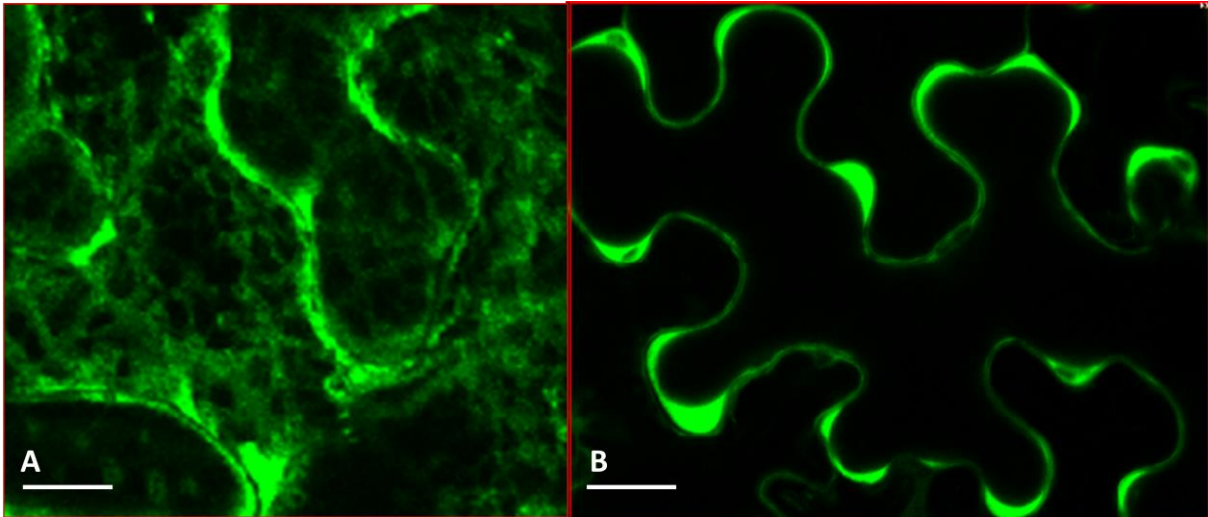
Figure 19: Expression of AtMTM2-GFP in transformed epidermal leaf cells of tobacco**.**

A: Z-projection of AtMTM2-GFP showing network like structure within the whole cell.

B: An overview of an entire cell expressing AtMTM2-GFP showing dense patches around epidermal cells (Single Slice).

(Bar: 10 µm)

The construct AtMTM2-GFP was co-expressed together with HDEL-DsRed, a marker for endoplasmic reticulum (ER). Comparison of expression patterns of the two proteins showed that the network formed by the AtMTM2-GFP completely co-localized with the ER network (Figure 20).
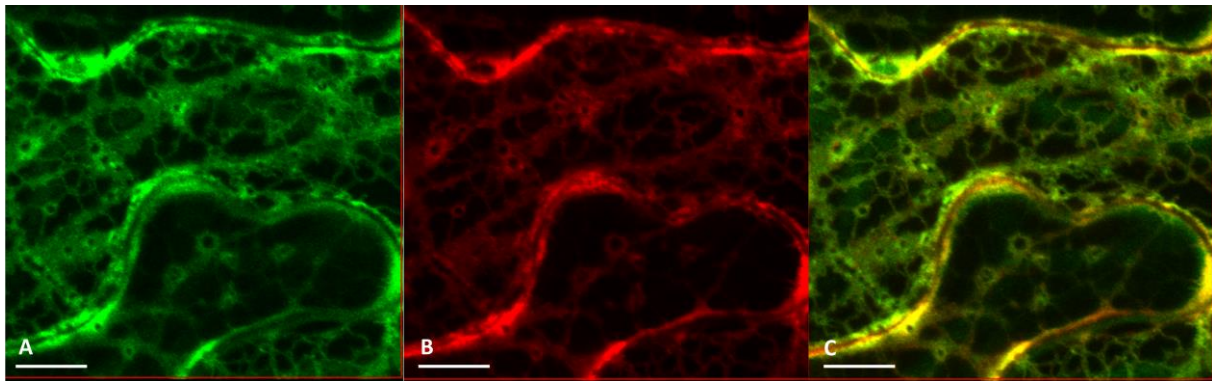
Figure 20: Co-localization of AtMTM2-GFP with ER-RFP (HDEL-DsRed).

A-C: A detailed view of a part of cell showing AtMTM2-GFP in (A); ER-RFP in (B) and a merge of the two in (C). Transient co-expression of AtMTM2-GFP with ER-RFP in transformed tobacco leaves showed a complete co-localization of both constructs (z-stack).

(Bar: 10 µm)

In order to determine, whether expressed AtMTM2-GFP inserts itself in the plasma membrane, tobacco leaves were stained with FM4-64 (an endocytic tracker) which anchors

into the outer lipid leaflet of the plasma membrane and is taken up into the cell by endocytosis via the formation of membrane vesicles (Ribchester et al., 1994; Bolte et al., 2004). CLSM analysis revealed that the bright red fluorescence of FM-4-64 incorporated into the plasma membrane did not co-localize with AtMTM2-GFP in leaf epidermal cells of *N. benthamiana* (Figure 21). It showed that AtMTM2-GFP is not associated with the plasma membrane and is present as dense patches in the concave pockets of cytosol.
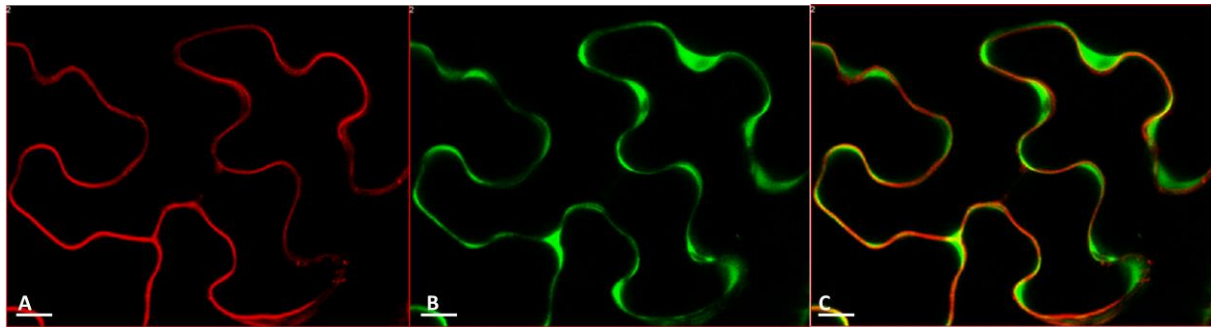
Figure 21: Staining of AtMTM2-GFP with FM4-64.

A-C: Overview of a cell showing FM4-64 infiltrated into tobacco leaf cells containing AtMTM2-GFP; FM4-64 in (A); AtMTM2-GFP in (B) and a merge of the two in (C). No co-localization was observed between FM4-64 and AtMTM2 indicating that AtMTM2 is not associated with the plasma membrane (single slice). (Bar: 10 μm)

3.4.3. ATMTM2-GFP AND ATMTM1-RFP CO-LOCALIZATION

The two plant myotubularins showed a somewhat different localization when co-expressed in tobacco leaves. The question now is whether the co-expression of two active plant MTMs in a transient transformation could change the distribution of one of the two proteins. As in hMTMs, active myotubularins interact with each other and change the subcellular localization e.g. co-expression of active MTMR3 and MTMR4 alters the subcellular localization of each phosphatase (Lorenzo et al., 2006). For this kind of investigation, two AtMTM proteins at a time were co-expressed. The results obtained show a change in AtMTM2-GFP expression, which was earlier showing dense patches around the cell but after its cross co-expression with AtMTM1-RFP, AtMTM2-GFP showed large number of vesicles, which were completely co-localized with vesicles of AtMTM1-RFP (Figure 22). These data lead to the conclusion that the overexpression of one myotubularin protein affects the expression of the other.
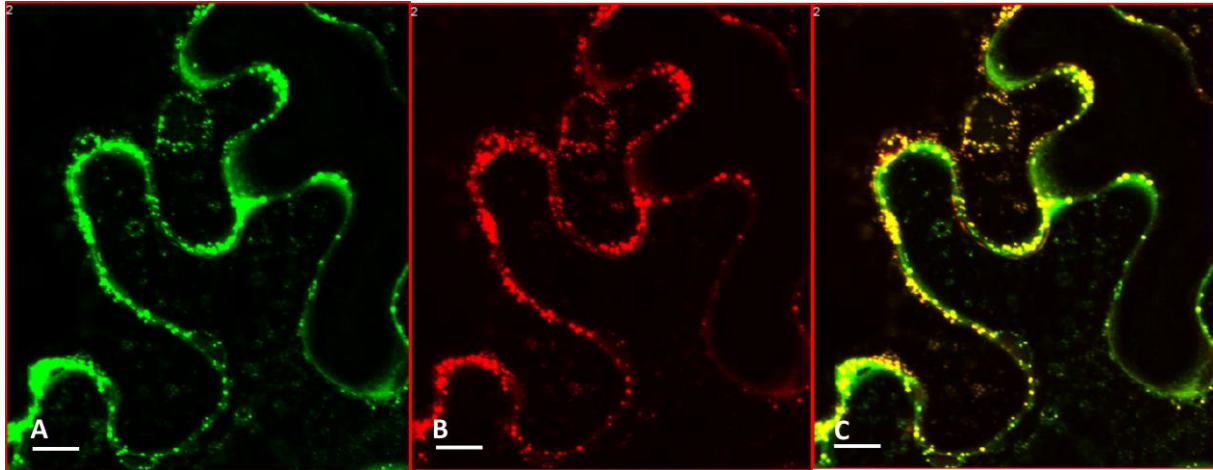
Figure 22: Co-localization of AtMTM1-RFP with AtMTM2-GFP

A-C: A part of cell showing AtMTM2-GFP in (A); AtMTM1-RFP in (B) and a merge of the two in (C). Transient co-expression of in AtMTM1-RFP with AtMTM2-GFP in transformed tobacco leaves showed a complete co-localization of both constructs (z-stack).

(Bar: 10 μm)

3.5. SUBCELLULAR LOCALIZATION OF ISOFORMS OF AtMTM1-RFP

In 2011, Franklin and his colleagues identified a high stoichiometry phosphorylation site on hMTMR2 by mass spectrometry-based methods. Mutation in Serine 58 changed the localization of hMTMR2 to early endocytic structures. They showed that the phosphorylation site, which was 11 amino acids upstream of the PH-GRAM domain of hMTMR2, changed the subcellular localization of hMTMR2 (Franklin et al., 2011). Plant myotubularins contain Serine-rich domain which is found upstream of the SID. As the molecular mechanisms regulating AtMTM1 have been poorly defined, we investigated the role of the Serine-rich and GRAM domains, which might affect AtMTM1 activity.

3.5.1. AtAAF-GFP

One of the isoforms of AtMTM1 is AtAAF, which is AtMTM1 without the Serine-rich domain (amino acids 506-531) located beside the SID but with the intact GRAM domain, as shown in the Figure below.

Figure 23: A schematic depiction of the distribution of protein domains in AtAAF. (For details of domain structure, refer to Section 1.2)

AtAAF-GFP showed a lot of motile vesicles around the plasma membrane and in the cytoplasm as shown in Figure 24A, which gives an overview of a transformed cell after two days of infiltration in tobacco epidermal cells. In a few cells, sometimes AtAAF-GFP showed some signal in the nucleus as well.
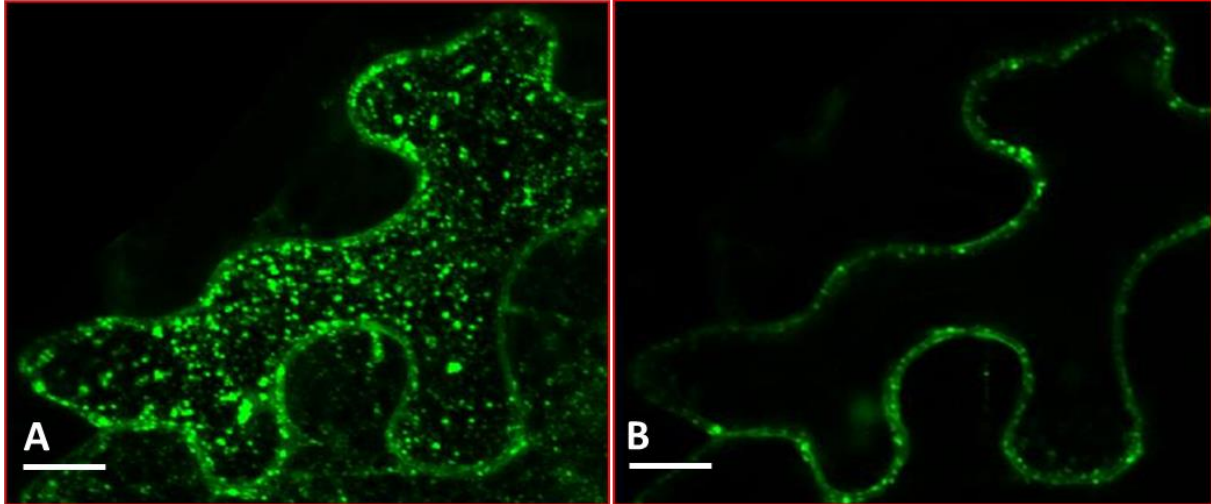
Figure 24: Transient expression of AtAAF-GFP in tobacco leaf after infiltration.

A: Z-projection of AtAAF-GFP showing large number of vesicles throughout the cytoplasm and around the plasma membrane.

B: Single slice showing vesicles around the plasma membrane.

(Bar: 10 μm)

AtAAF-GFP was also co-expressed with a number of markers. It did not show any co-localization with a late endosome maker i.e. FYVE-RFP as well as trans-Golgi marker such as ST-RFP (Figure 25C and Figure 25F).
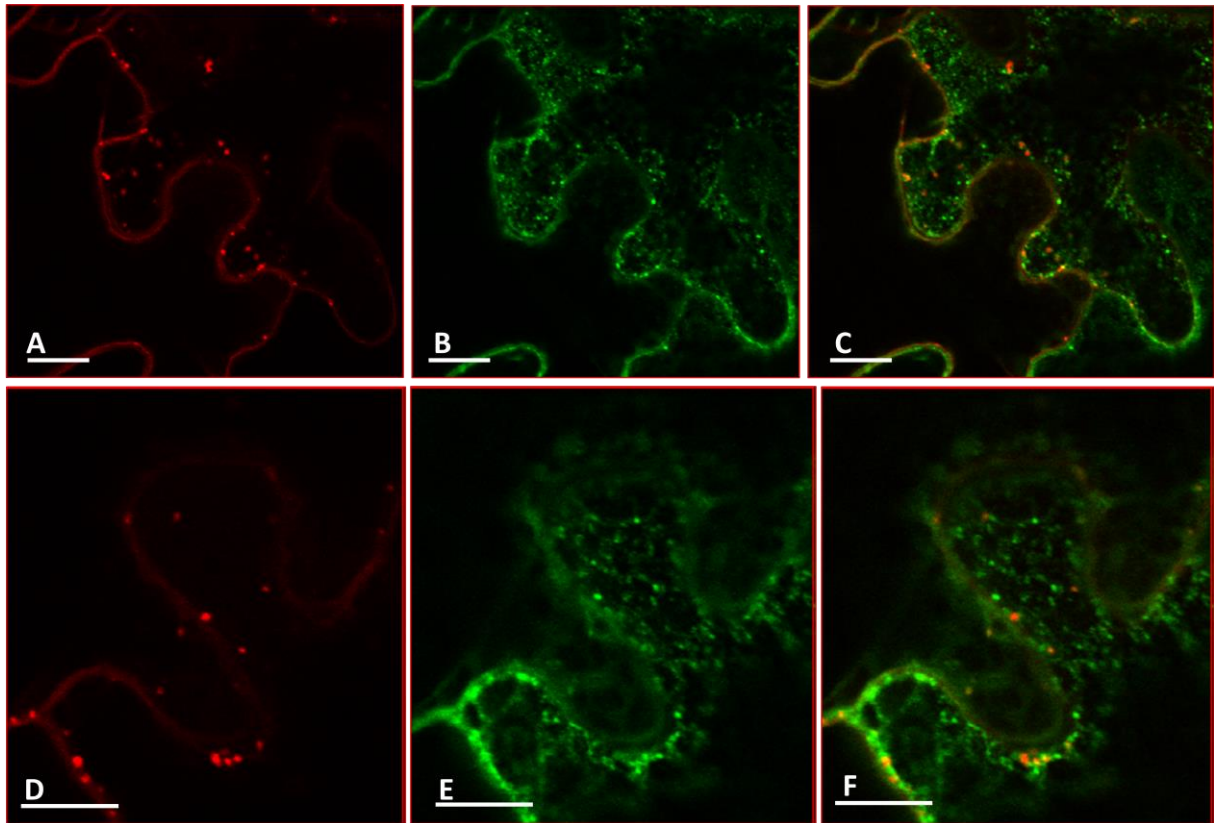
Figure 25: Co-localization of AtAAF-GFP with FYVE-RFP and ST-RFP.

A-F: A detailed view of a part of the cell showing in FYVE-RFP in (A); AtAAF-GFP in (B) and a merge of the two in (C); ST-RFP in (D); AtAAF-GFP in (E) and a merge of the two in (F).Transient co-expression of AtAAF-GFP with FYVE-RFP and ST-RFP in transformed tobacco leaves showed no co-localization with both constructs.

(Bar: 10 μm)

When GFP tagged AtAAF was expressed with HDEL-DsRed, a marker for ER (Haseloff et al., 1997), it exhibited small vesicles of AtAAF-GFP partially co-localized with highly mobile ER tubules (Figure 26C). Partial co-localization of AtAAF-GFP was also seen with G-RK, a marker for the cis-Golgi (Figure 26F).
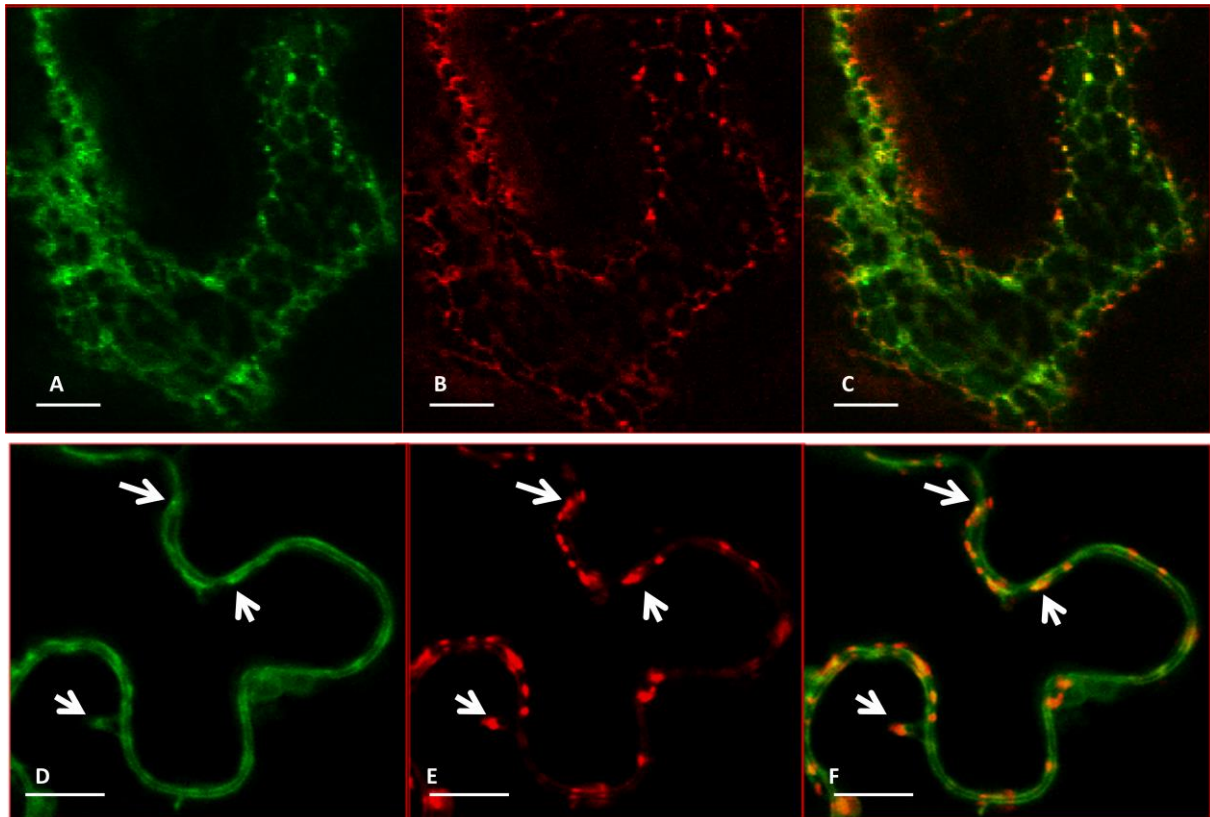
Figure 26: Co-localization of AtAAF-GFP with ER-RFP and G-RK (cis-Golgi marker).

A-F: Part of a cell showing AtAAF-GFP in (A); ER-RFP in (B) and a merge of the two in (C); AtAAF-GFP in (D); G-RK in (E) and a merge of the two in (F). Transient co-expression of in AtAAF-GFP with ER-RFP and G-RK in transformed tobacco leaves showed partial co-localization with both constructs.

(Bar: 10 μm)

3.5.2. ATAAG-GFP

AtAAG is another isoform without the Serine-rich domain (amino acids 506-531) as well as N-terminal sequences including the GRAM domain (amino acids 1-205) as shown in the Figure below.
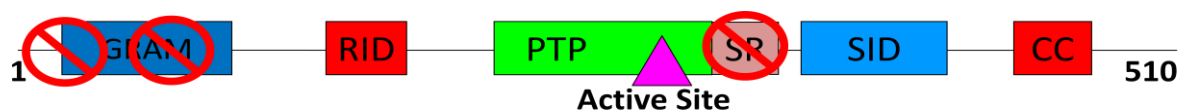
Figure 27: A schematic depiction of the distribution of protein domains in AtAAG. (For details of domain structure, refer to Section 1.2)

AtAAG fusion protein showed highly motile vesicle-like structures of various sizes like AtAAF-GFP after 2 days of infiltration in tobacco epidermal cells (Figure 28A and Figure 28B). In a similar manner like AtAAF-GFP, it also showed nuclear localization in few cells when expressed alone.
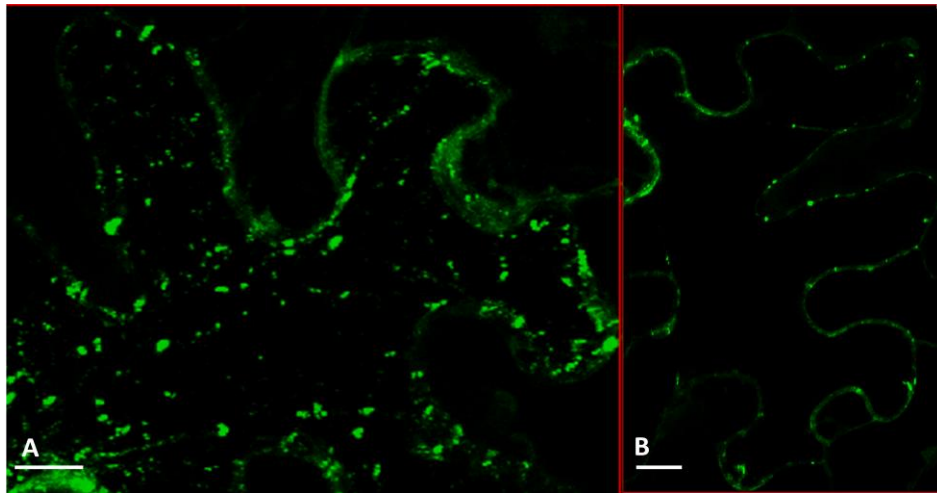
Figure 28: Transient expression of AtAAG-GFP in tobacco leaf cells.

A: Z-projection of AtAAG-GFP showing large number of vesicles of different sizes around the plasma membrane and throughout the cytoplasm.

B: Single optical section of another cell showing vesicles around the plasma membrane.

(Bar: 10 μm)

But it showed a different subcellular localization than AtAAF-GFP. AtAAG-GFP was partially co-localized with FYVE-RFP, a late endosomal marker (Figure 29F) and also with ST-RFP, a trans-Golgi marker (Figure 29C). It did not show any co-localization with HDEL-DsRed, a marker for ER (Figure 29I) as well as with the cis-Golgi marker (G-RK) (Figure 29L).
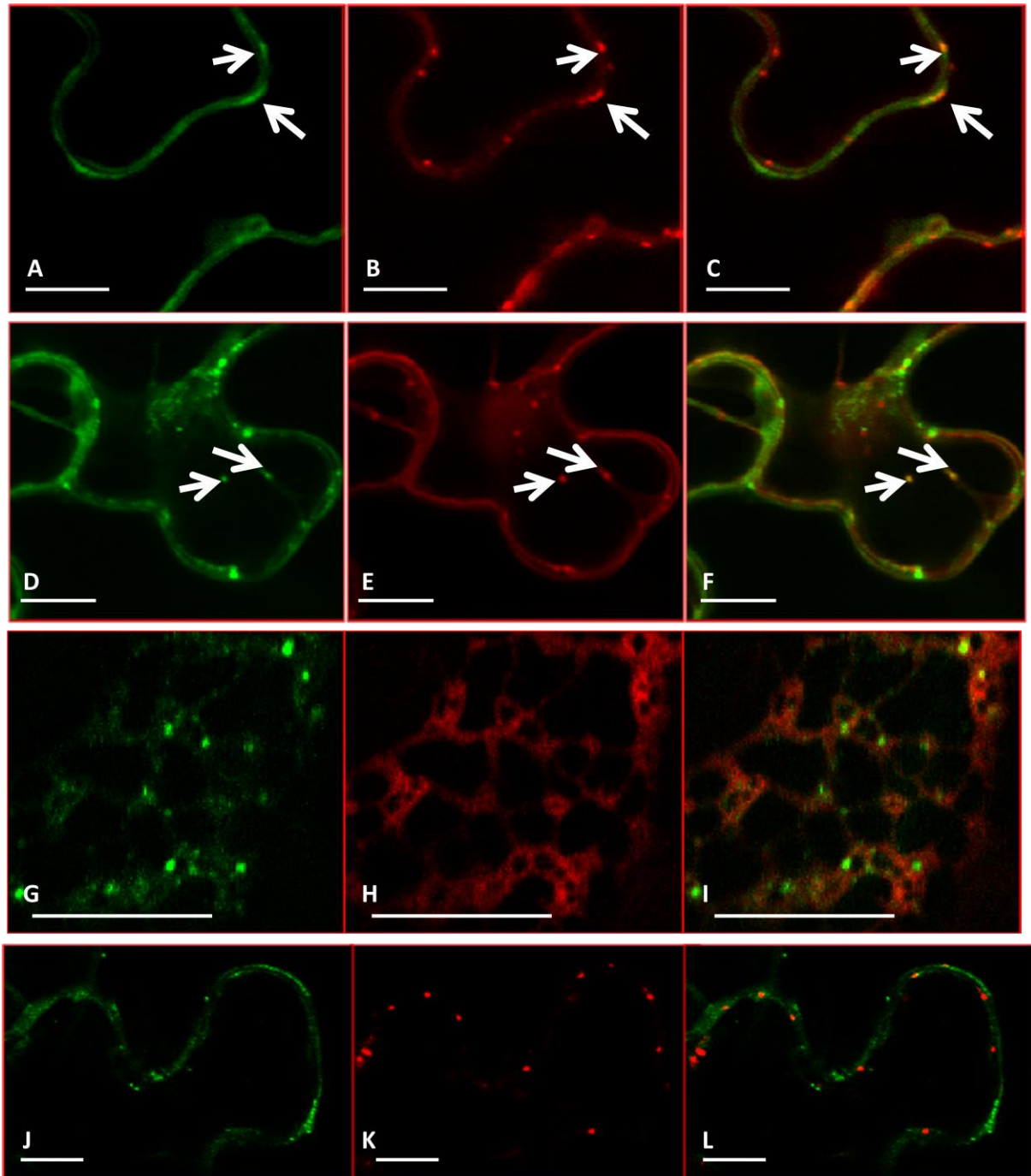
Figure 29: Co-localization of AtAAG-GFP with ST-RFP, FYVE-RFP, ER-RFP and G-RK.

A-F: A part of cell showing AtAAG-GFP in (A); ST-RFP in (B) and a merge of the two in (C); AtAAG-GFP in (D); FYVE-RFP in (E) and a merge of the two in (F). White arrows represent the vesicles which were partially co-localized. Transient co-expression of AtAAG-GFP with ST-RFP and FYVE-RFP in transformed tobacco leaves showed partial co-localization with both constructs.

G-I: A magnified view of a cell showing AtAAG-GFP in (G); ER-RFP in (H) and a merge of the two in (I). No co-localization was observed between AtAAG-GFP and ER-RFP indicating different subcellular localization in comparison to AtAAF-GFP.

J-L: A magnified view of cell showing AtAAG-GFP in (J); G-RK in (K) and a merge of the two in (L). No co-localization was observed between AtAAG-GFP and G-RK indicating different subcellular localization in comparison to AtAAF-GFP.

 (Bar: 10 μm)

3.5.3. ATNP-RFP

To understand the role of the Serine-rich domain, an isoform with intact Serine-rich domain (amino acids 506-539) but without the N-terminal sequence including the GRAM domain (amino acids 1-205), was used i.e. AtNP-RFP as shown in the Figure below.
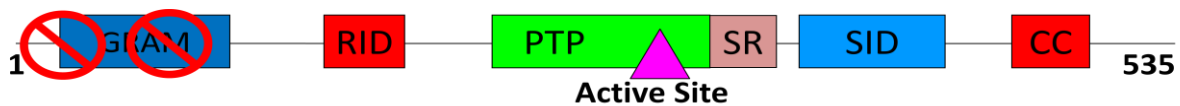
Figure 30: A schematic depiction of the distribution of protein domains in AtNP. (For details of domain structure, refer to Section 1.2)

AtNP-RFP also showed large and small vesicles varying in density around the plasma membrane and throughout the cytoplasm (Figure 31).
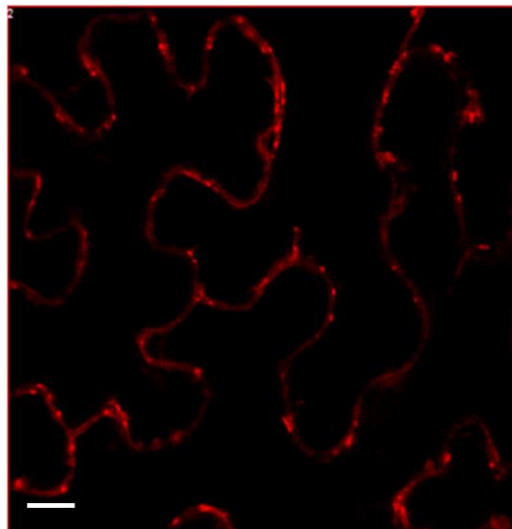
Figure 31: Transient expression of AtNP-RFP in tobacco leaf cells showing vesicles around the plasma membrane similar to AtMTM1.

(Bar: 10 μm)

Unlike AtAAF-GFP and AtAAG-GFP, AtNP-RFP did not show any nuclear localization when expressed alone. It was highly co-localized with G-YK, a cis-Golgi marker like AtMTM1-RFP (Figure 32) indicating that the absence of only GRAM domain with Serine-rich domain still intact, does not affect the subcellular localization of AtNP-RFP.
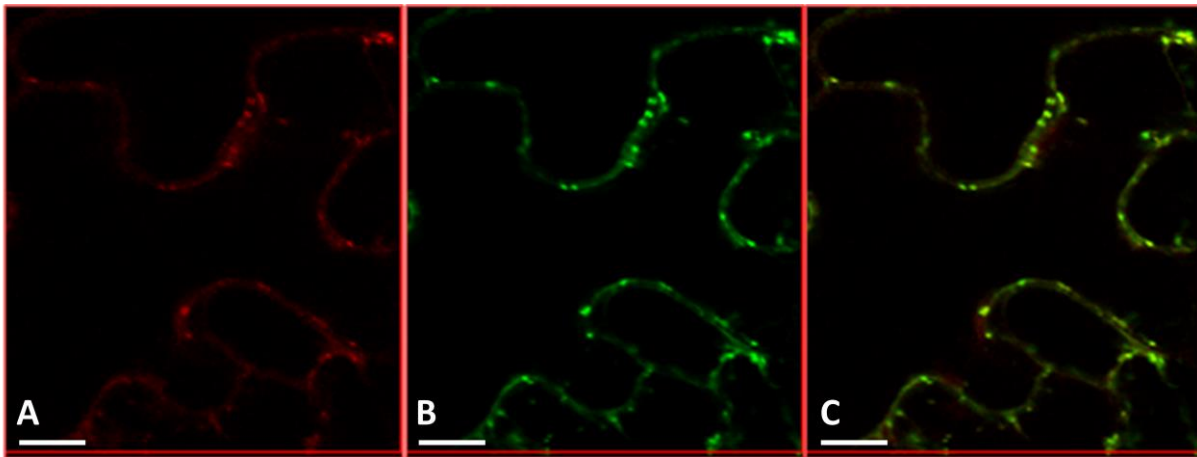
**Figure 32:** Co-localization of AtNP-RFP with G-YK (cis-Golgi marker).

A-C: Part of a cell showing AtNP-RFP in (A); G-YK in (B) and a merge of the two in (C). Transient co-expression of AtNP-RFP with G-YK in transformed tobacco leaf cells showed full co-localization. (Bar: 10 μm)

3.6. CO-LOCALIZATION OF ISOFORMS OF ATMTM1 WITH ATX1 AND THE PHD OF ATX1

It has previously been demonstrated that the effect of elevated level of PtdIns5P, produced by AtMTM1 affects the subcellular localization of ATX1 by infiltrating RFP tagged AtMTM1 in the presence of GFP tagged ATX1 in tobacco leaf cells. Over expression of AtMTM1-RFP in tobacco leaf epithelial cells relocates nuclear ATX1 from the nucleus to the cytoplasm (Ndamukong et al., 2010). Similar result was obtained when AtMTM1-RFP was co-expressed with the PHD-GFP of ATX1. This behavior is consistent with the assumption that the PHD of ATX1 binds with PtdIns5P, which is generated by AtMTM1 and this in turn leads to relocalization of ATX1 from the nucleus to the cytoplasm (Ding et al., 2009). To determine whether the Serine domain regulates AtMTM1 activity towards ATX1, co-expression experiments were conducted.

3.6.1. CO-LOCALIZATION OF ATAAF / ATAAG WITH ATX1-RFP AND PHD-RFP

To examine the functionality of the deletion of the Serine-rich domain, *Nicotiana benthamiana* cells were transformed with AtAAF-GFP and ATX1-GFP. Co-expression of AtAAF-GFP with ATX1-RFP showed AtAAF-GFP signals in the nucleus along with ATX1-RFP (Figure 33F), but AtAAF-GFP was not able to relocate nuclear ATX1 from the nucleus. When PHD-RFP was co-expressed with AtAAF-GFP, AtAAF-GFP expressed itself in the nucleus (Figure 33C) instead of a lot of vesicles in the cytoplasm and around the plasma membrane when AtAAF-GFP was expressed alone.

When AtAAG-GFP (for domain structure, see Figure 27) was co-expressed with ATX1-RFP and PHD-RFP, AtAAG-GFP also appeared in the nucleus along with ATX1 and PHD respectively (Figure 34). Surprisingly, sometimes AtAAF-GFP and AtAAG-GFP were also seen in the nucleus when expressed alone, but quantification showed, that the amount of AtAAF-GFP or AtAAG-GFP when co-expressed with the PHD of ATX1, increased up to approximately 80-90% compared to just 10% without the combination with the PHD of ATX1 (Figure 35).
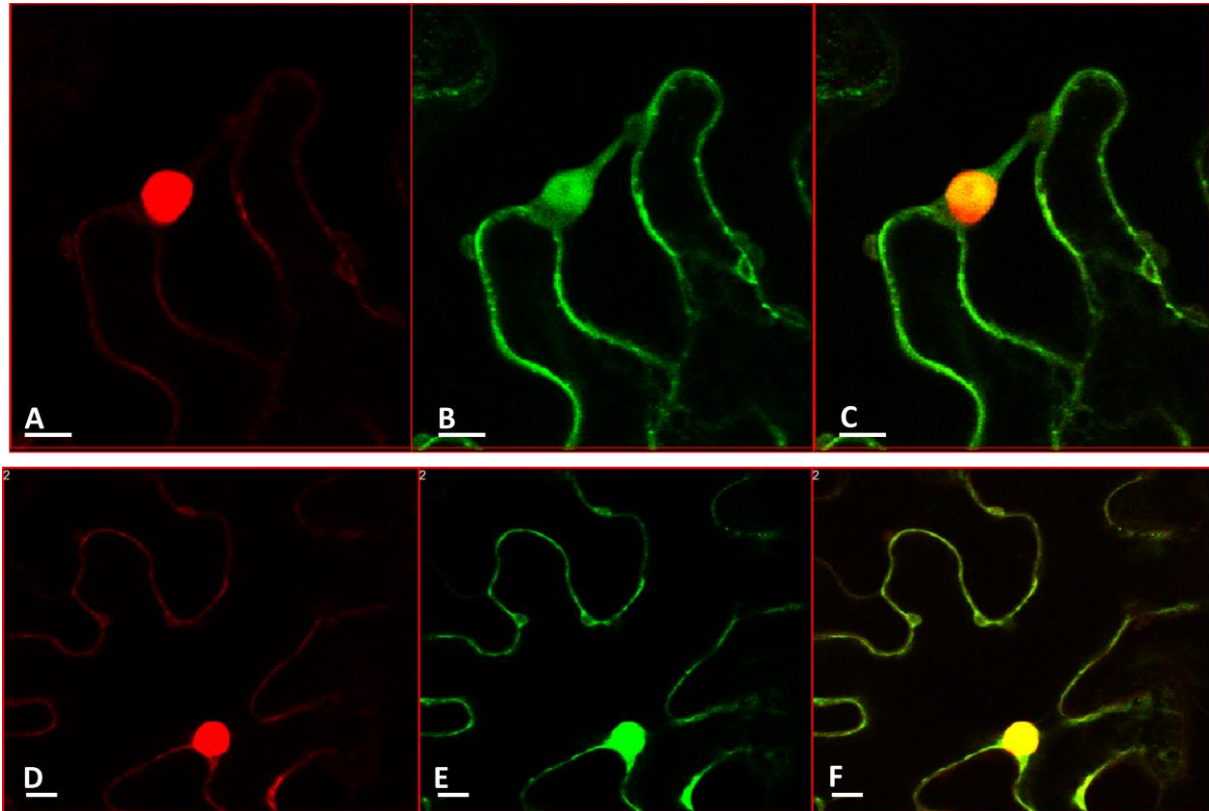
Figure 33: Subcellular distribution of AtAAF co-expressed with PHD and ATX1.

A-C: Part of a cell showing PHD-RFP in (A); AtAAF-GFP in (B) and a merge of the two in (C). Transient co-expression of AtAAF-GFP with PHD-RFP showed GFP signal of AtAAF in the nucleus.

D-F: Part of a cell showing ATX1-RFP in (D); AtAAG-GFP in (E) and a merge of the two in (F). Transient co-expression of AtAAF-GFP with ATX1-RFP showed co-localization in the nucleus.

 (Bar: 10 μm)
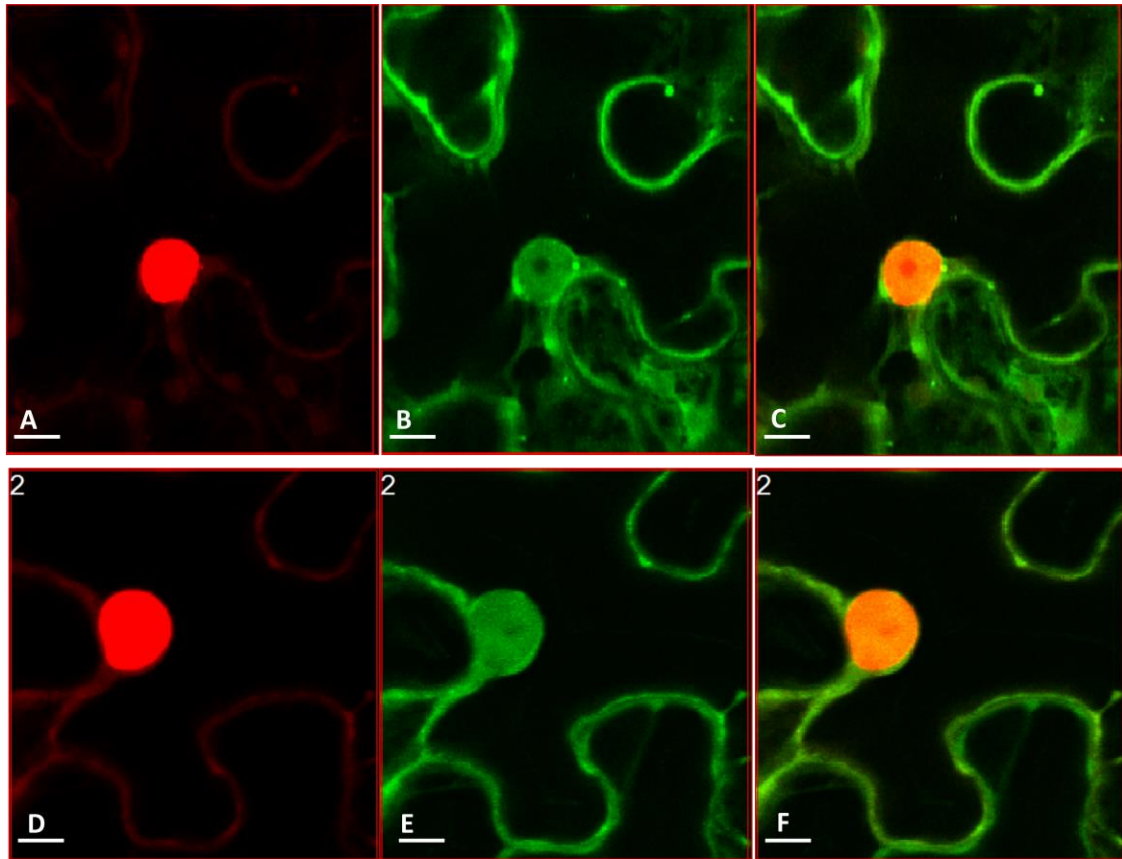
Figure 34: Subcellular distribution of AtAAG-GFP co-expressed with PHD and ATX1.

A-C: Part of a cell showing PHD-RFP in (A); AtAAG-GFP in (B) and a merge of the two in (C). Transient co-expression of AtAAG-GFP with PHD-RFP showed GFP signal of AtAAG in the nucleus.

D-F: Part of a cell showing ATX1-RFP in (D); AtAAG-GFP in (E) and a merge of the two in (F). Transient co-expression of AtAAG-GFP with ATX1-RFP showed co-localization in the nucleus.

(Bar: 10 μm)
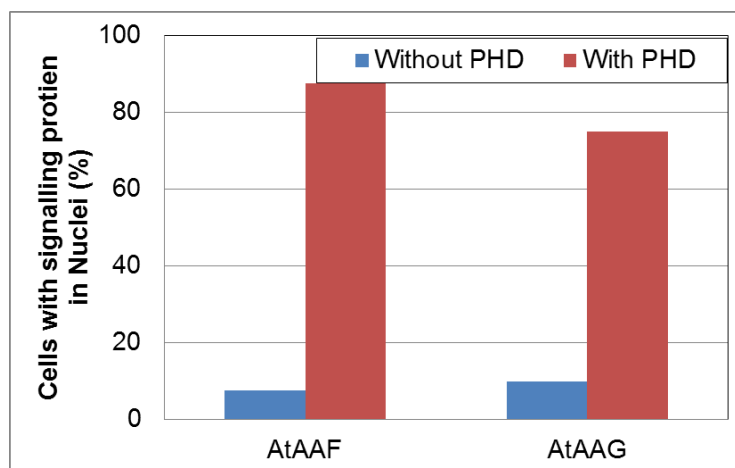
Figure 35: Cells showing nuclear GFP-signal of AtAAF and AtAAG associated with or without the PHD domain of ATX1.

(Number of cells observed, n=40)

3.6.2. Co-localization of AtNP-RFP with ATX1-GFP and PHD-GFP

When another isoform AtNP-RFP, without the GRAM domain but with Serine-rich domain, was co-expressed with ATX1-GFP, no signal of AtNP-RFP was observed in the nucleus. Additionally, it even failed to shift nuclear ATX1 from the nucleus to the cytoplasm (Figure 36F). Similar result was obtained with PHD-GFP after two days of infiltration (Figure 36C). It can be concluded that the interaction of ATX1 or PHD with AtNP-RFP did not affect its subcellular localization.
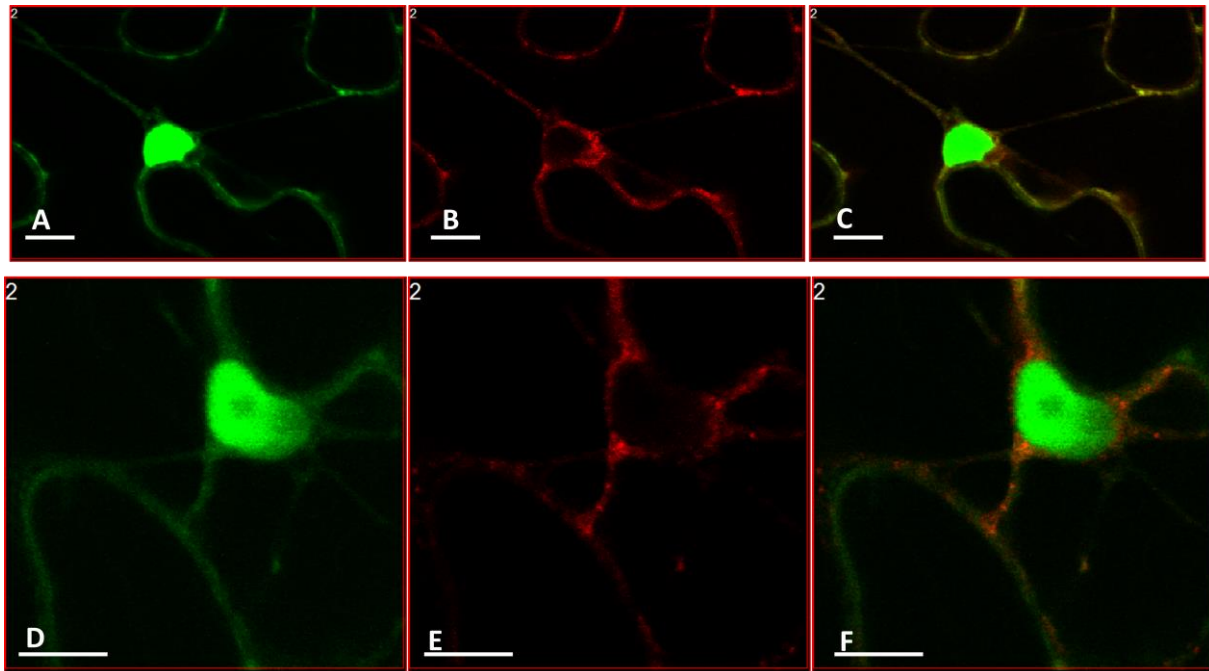
Figure 36: Subcellular distribution of AtNP-RFP co-expressed with PHD and ATX1.

A-C: Part of a cell showing PHD-GFP in (A); AtNP-RFP in (B) and a merge of the two in (C). Transient co-expression of AtNP-RFP with PHD-GFP was not affecting the RFP signal of AtNP.

D-F: Part of a cell showing ATX1-GFP in (D); AtNP-RFP in (E) and a merge of the two in (F). Transient co-expression of AtNP-RFP with ATX1-GFP showed no co-localization in the nucleus.

 (Bar: 10 μm)

3.7. Effect of ABA on the Subcellular Localization of Myotubularins

As discussed in Section 3.2, ABA affects the expression of AtMTM1 as well as mutants of MTMs. In order to find out if ABA has any effect on the subcellular localization of myotubularins, epidermal leaves of tobacco expressing AtMTM1-RFP and AtMTM2-GFP were soaked into 10 μM of ABA solution for 1 hour. An increased number of vesicles of AtMTM1-RFP towards the plasma membrane were observed (Figure 37B). On the other hand,

the localization of AtMTM2-GFP did not show any significant change after exposure of the leaf to 10 µM ABA (Figure 37D).
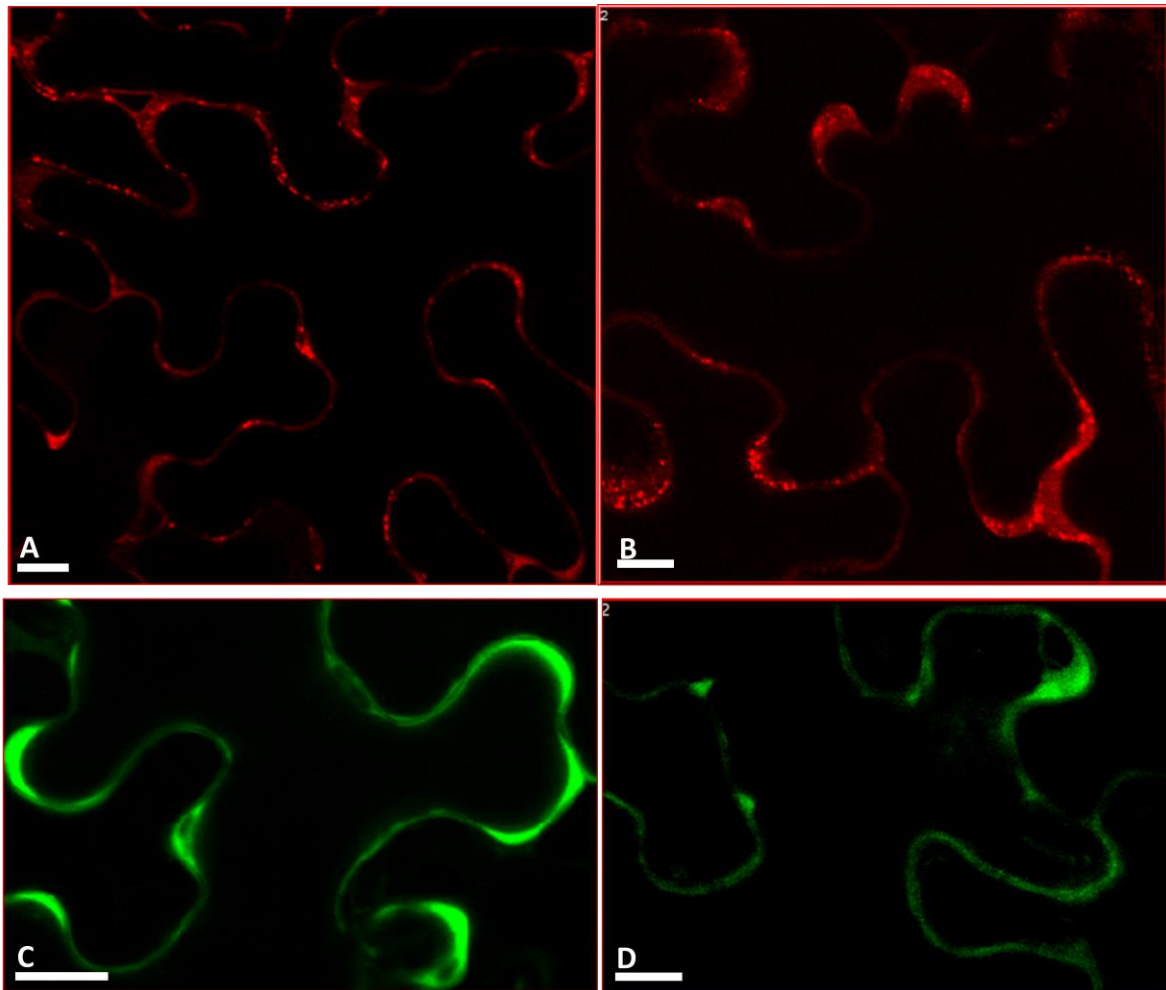
Figure 37: Effect of ABA on subcellular localization of AtMTM1 and AtMTM2.

A-B: Part of a cell showing AtMTM1-RFP signal without ABA in (A); AtMTM1-RFP signal with ABA in (B). Increased number of vesicles of AtMTM1-RFP towards the plasma membrane was observed after 10 µM ABA. C-D: Part of a cell showing AtMTM2-GFP signal without ABA in (C) and AtMTM2-GFP signal under ABA exposure. No significant change observed in the subcellular localization of AtMTM2-GFP after 10 µM ABA. (Bar: 10 µm)

No significant change in subcellular localization was observed when isoforms of AtMTM1-RFP i.e. AtAAF-GFP and AtAAG-GFP were treated with 10 µM of ABA solution (Figure 38).
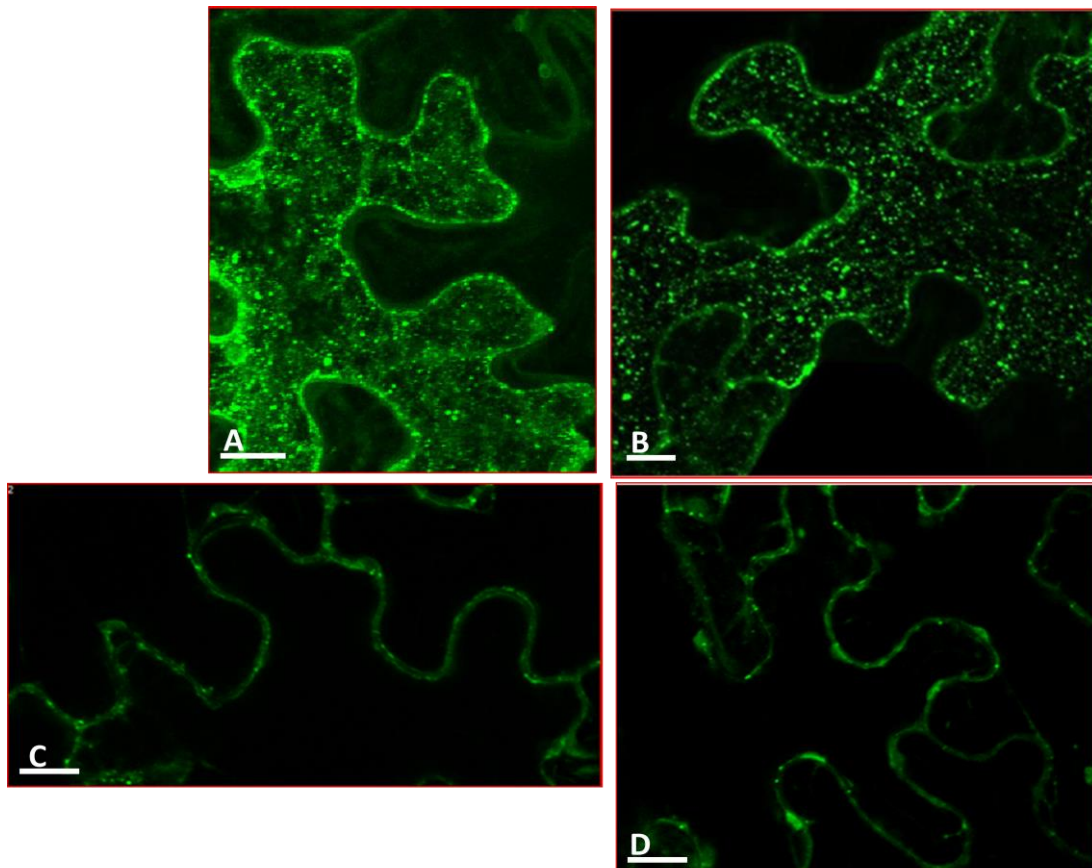
Figure 38: Effect of ABA on subcellular localization of AtAAF and AtAAG.

A-D: Part of a cell showing AtAAF-GFP signal without ABA in (A); AtAAF-GFP signal with ABA in (B); AtAAG-GFP signal without ABA in (C) and AtAAG-GFP signal with ABA in (D). No significant changes were observed in cells expressing either of the two constructs under the influence of 10 μM ABA.
 (Bar: 10 μm)

3.8.   IN-VIVO IMAGING OF PLANT MYOTUBULARINS IN ROOT CELLS

3.8.1.   IN-VIVO IMAGING OF ATAAF-GFP IN ROOT CELLS

Transgenic plants expressing AtAAF-GFP were imaged in-vivo to detect intracellular localization in root cells by CLSM. Due to the ubiquitously expressing 35S promoter, the fluorescence signal and therefore fusion protein expression was seen in all cells of the root cap as well as in the epidermal and cortex cell layers of the root (Figure 39A, F). Stably transformed lines of AtAAF-GFP showed small dot-like structures within the cytoplasm of cells in the elongation zone (Figure 39A) and root hair of these roots (Figure 39C, E). At higher magnification, cortex cells of the transition zone of roots showed green signal in the cytoplasm around the plasma membrane (Figure 39B). In elongating root hair, some vesicles showed green fluorescence (Figure 39D). Out of those vesicles, some were motile and some were stationary.
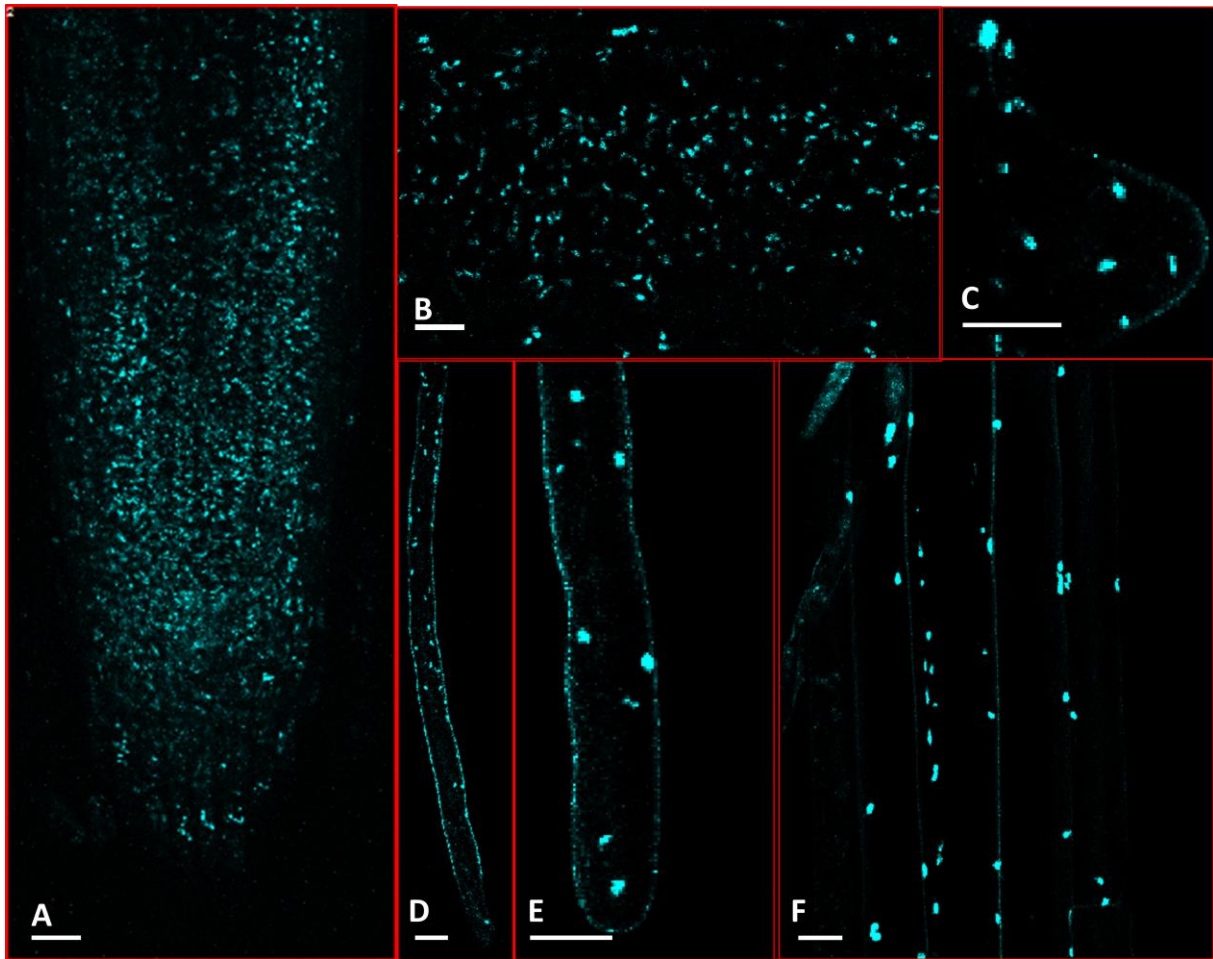
Figure 39: In-vivo visualization of AtAAF-GFP in transgenic *A. thaliana* root cells.

A: Overview of the complete root tip in a median longitudinal optical section, showing large number of vesicles in root cells.

B: Higher magnification of cortex cells of the transition zone revealed vesicles around the vacuole.

C: Projection of a growing root hair of AtAAF -GFP vesicles throughout the cytoplasm.

D-E: Projection of a young, rapidly growing root hair.

F: Epidermis cells of a basal root part.

(Bar: 10μm)

3.8.2. CO-LOCALIZATION OF FM4-64 WITH ATAAF-GFP

In order to examine, whether AtAAF-GFP is of plasma membrane or endosomal origin, five day old seedlings were incubated with FM4-64 for 10 minutes at 4°C and then examined under confocal microscope after washing with 35μM Brefeldin A (BFA) for 60 minutes. The application of BFA along with FM4-64 results in aggregation of endosomal compartments comprising endosomes and elements of the trans-Golgi network, but not the Golgi apparatus and endoplasmic reticulum (Baluska et al., 2002; Samaj et al., 2005). The intracellular pattern of GFP signals in root cells of stable transgenic lines of AtAAF-GFP seedlings did not reveal any co-localization, either with the fluorescent dye or with the BFA compartments, even 60-

90 minutes after application (Figure 40C). These results show that the vesicles of AtAAF-GFP could not be an endosomal organelle.
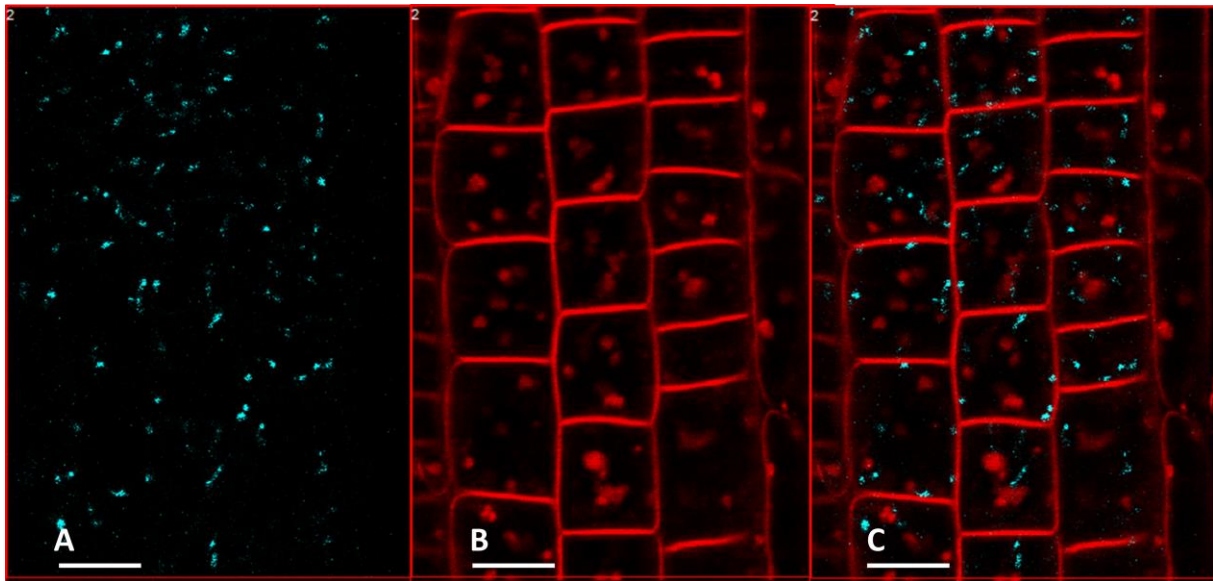
Figure 40: Lack of co-localization of AtAAF-GFP with FM4-64.

A-C: AtAAF-GFP in (A); FM4-64 (B) and merged image of both in (C). FM4-64 pre-incubated cortex cells of the transition zone of AtAAF-GFP treated with BFA for 60 minutes showed no co-localization with BFA induced compartments.

 (Bar: 10μm)

3.8.3. INTRACELLULAR LOCALIZATION OF ATMTM1-RFP IN ROOT CELLS

For the analysis of the intracellular localization of the myotubularin proteins in transgenic *Arabidopsis* lines, AtMTM1-RFP fusion construct was used to transform wild-type Col-0 plants using *Agrobacterium*-mediated gene transfer method (Clough and Bent, 1998). Around 10 transformed lines could be isolated, which were resistant to the selection marker, but all of them showed very low levels of RFP signal. Confocal microscopy of the roots (Figure 41A) revealed that the red fluorescence signal emerged as intracellular punctate pattern around the plasma membrane predominantly abundant within vesicles, which are distributed in the cytoplasm of the cortex cells and excluded from the nuclei (Figure 41C). Some vesicles were motile but some were stationary. The same pattern of organization was seen in the elongating root hair (Figure 41B).
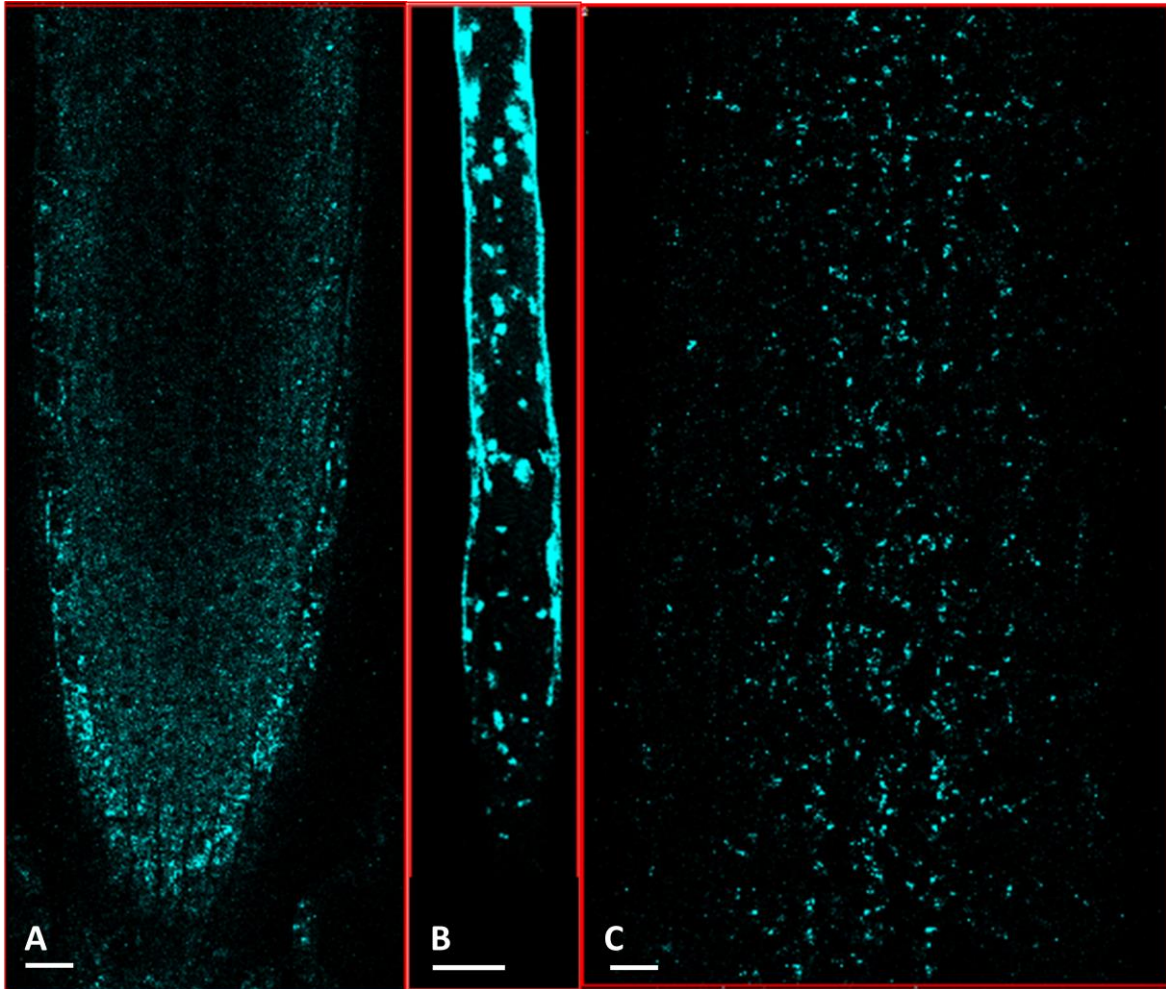
Figure 41: In-vivo visualization of AtMTM1-RFP in transgenic *A. thaliana* root cells.

A: Overview of the complete root tip in a median longitudinal optical section, showing a few vesicles in root cells.

B: Projection of a mature root hair of AtMTM1-RFP vesicles throughout the cytoplasm.

C: Magnified part of transition zone of root.

(Bar: 10 μm)

3.8.4. CO-LOCALIZATION OF FM1-43 WITH ATMTM1-RFP IN STABLE TRANSGENIC LINES

Another lipophilic styryl dye, FM1-43 is used here instead of FM4-64 as an endocytic marker and it has been extensively used in plants in conjuction with BFA-treatment to study endocytotic pathways (Klima and Foissner, 2008; Grebe et al., 2003; Müller et al., 2007).

FM1-43 when applied to the root of transgenic AtMTM1-RFP plants did not reveal any co-localization of the fluorescent dye and the RFP signal after uptake for 10 minutes. The roots of transgenic AtMTM1-RFP were treated with FM-dye and BFA for 60 minutes. Vesicles of AtMTM1-RFP did not accumulate within BFA-induced compartments (Figure 42C). This

indicates that the subcellular localization of AtMTM1-RFP vesicles is the cis-Golgi, as the cis-Golgi Marker does not accumulate within BFA compartments (Baluska et al., 2002).
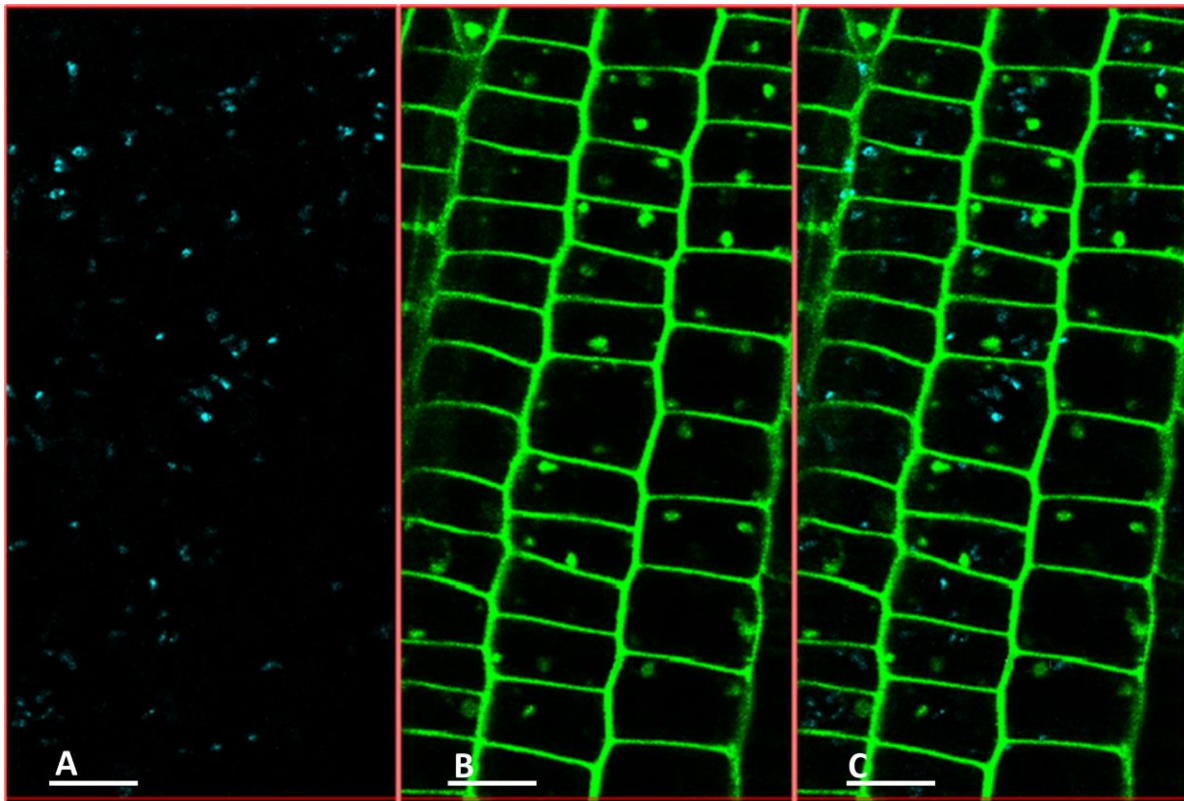
Figure 42: Lack of co-localization of AtMTM1-RFP with FM1-43 treated with BFA.

A-C: Cortex cells of transition zone showing AtMTM1-RFP in (A); FM1-43 in (B) and merged image of both in (C). FM1-43 pre-incubated cortex cells of the transition zone of AtMTM1-RFP treated with BFA for 60 minutes showed no co-localization with BFA induced compartments.

(Bar: 10μm)

3.8.5. IN-VIVO IMAGING OF AtMTM2-GFP IN ROOT CELLS OF TRANSGENIC *ARABIDOSPSIS* LINES

To refine the analysis of intracellular localization of AtMTM2, fusion protein under the control of a 35S promoter was transiently expressed in *Arabidopsis* plants using a floral dipping method (Clough and Bent, 1998) and examined by confocal laser-scanning microscopy. Surprisingly, stable transgenic lines of AtMTM2-GFP showed a somewhat different expression as compared to that shown before in the leaf epidermal cells of tobacco. AtMTM2-GFP stable transformed lines showed intracellular punctate pattern as found before in AtMTM1-RFP expressing plants. AtMTM2 fusion proteins localized to small vesicles with in the cytoplasm in root tip as well as in root hair (Figure 43A, B, C). The transition zone of root tip of stable transgenic lines of AtMTM2 showed vesicles (Figure 43E, F) and at higher

magnification cortex as well as epidermal cells of root showed some vesicles in the cytoplasm in close vicinity to vacuole (Figure 43E).
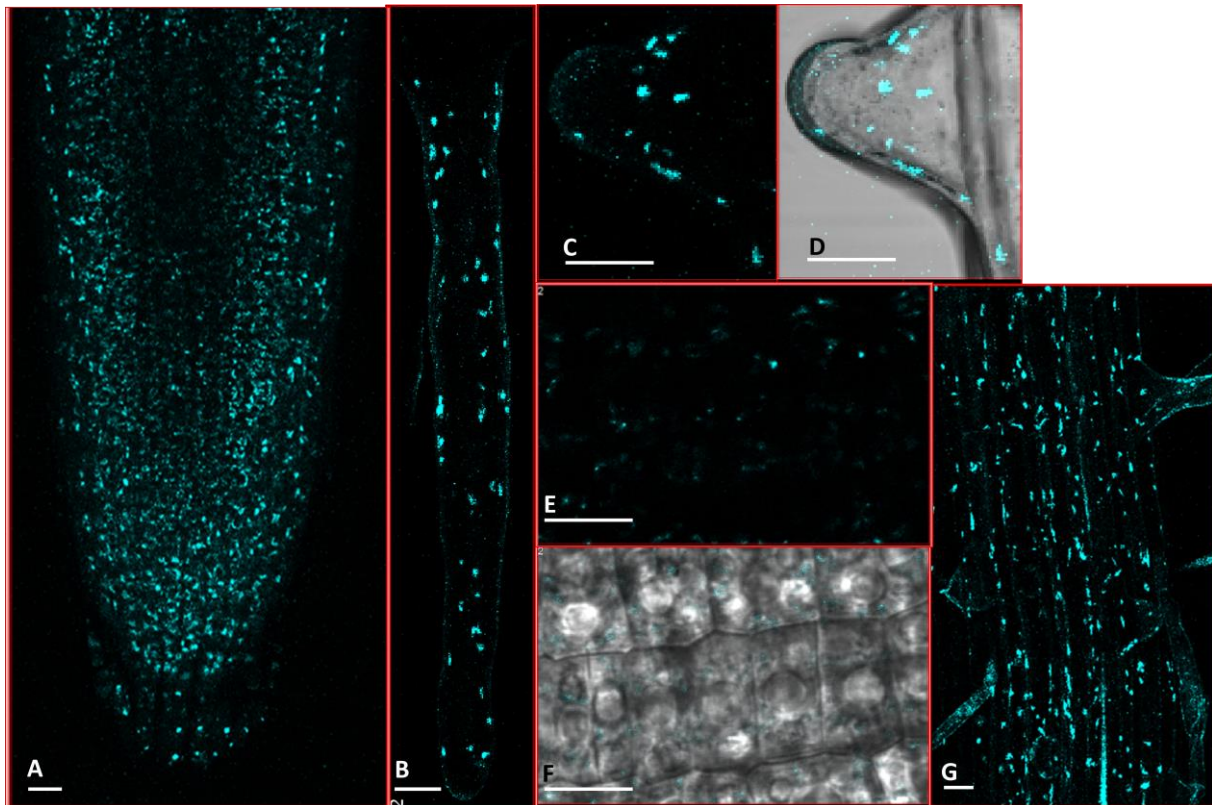
Figure 43: In-vivo visualization of AtMTM2-GFP in transgenic *A. thaliana* root cells.

A: Overview of the complete root tip in a median longitudinal optical section, showing large number of vesicles in root cells.

B: Projection of a growing root hair of AtMTM2-GFP vesicles throughout the cytoplasm.

C-D: Projection of a young, rapidly growing root hair. The corresponding DIC image of growing root hair is shown in D.

E-F: Higher magnification of cortex cells of the transition zone revealed vesicles around the vacuole. The corresponding DIC image is shown in F.

G: Epidermis cells of a basal root.

 (Bar: 10μm)

3.8.6. CO-LOCALIZATION OF FM4-64 WITH AtMTM2-GFP IN TRANSGENIC *ARABIDOPSIS* LINES

FM4-64, when applied for 10 minutes to root hairs of transgenic AtMTM2-GFP plants, did not reveal any co-localization with the GFP signal (Figure 44F). The application of FM4-64 along with BFA (for 60 minutes) resulted in strong FM-dye label in the plasma membrane and BFA-induced compartments (Figure 44B), while the AtMTM2-GFP signal was not affected by BFA and did not co-localize with the BFA induced compartments (Figure 44C). The same kind of result was obtained in cortex cells of the transition zone after incubating roots of

transgenic AtMTM2-GFP in FM4-64 for 10 minutes and kept in BFA for 60 minutes. BFA did not affect the localization of AtMTM2-GFP, i.e., BFA-induced compartments were not labelled. This indicates that the AtMTM2 vesicles are not part of the endocytic network and do not contribute to the formation of BFA-induced compartments. Similar results have been observed when AtMTM2-GFP was infiltrated into *N. benthamiana* co-stained with FM4-64 dye (Figure 21).
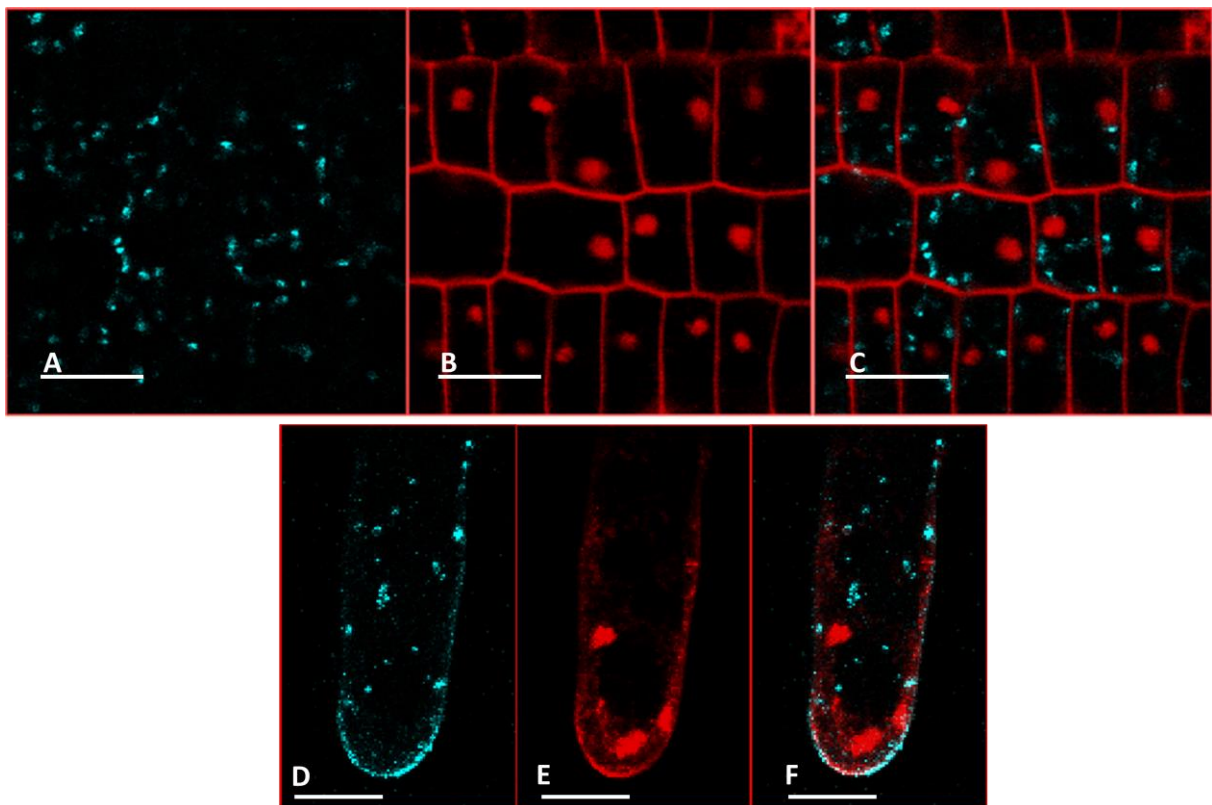
Figure 44: Lack of co-localization of AtMTM2-GFP with FM4-64.

A-C: Cortex cells of transition zone showing AtMTM2-GFP in (A); FM4-64 in (B) and merged image of both in (C). FM4-64 pre-incubated cortex cells of the transition zone of AtMTM2-GFP treated with BFA for 60 minutes showed no co-localization with BFA induced compartments.

D-F: Root hair showing AtMTM2-GFP in (D); FM4-64 in (E) and merged image of both in (F). Root hair from AtMTM2-GFP transgenic seedling incubated for 10 minutes with FM4-64, showed no co-localization.

(Bar: 10μm)

4.   DISCUSSION

4.1.   SUBCELLULAR LOCALIZATION OF PLANT MYOTUBULARINS

Despite sharing a similar structure, the role of plant myotubularins does not appear to be redundant, i.e., they behave in a differentiated manner. Deletion of AtMTM1 elevates the tolerance of plants towards dehydration stress. Also, these proteins show different patterns of intracellular localization in transformed tobacco leaves – AtMTM1-RFP is present in some punctate particles throughout the cytoplasm, while AtMTM2-GFP shows some high, uniform signal at the concave sides of cell wall lobes in epidermal pavement cells (Ding et al., 2012). Since, the subcellular localization of myotubularins was not known in plant so far; one of the aim of this thesis was to clarify this point.

Various markers were used in this study in order to find out the co-localization of AtMTM1-RFP and AtMTM2-GFP. Co-expression experiments of the fluorescently tagged AtMTM1 with the post-Golgi/PVC marker BP-GFP, with the endosomal recycling marker RabA1e-YFP, with the TGN markers RabA1d and SYP61, and with the late endosome markers FYVE-RFP and ARA7-GFP, demonstrated no co-localization with any of the above reporters. These results clearly showed that AtMTM1-RFP containing subcellular structures, possibly vesicles, did not participate in the endosomal recycling process. However, co-expression of AtMTM1-RFP with G-YK, a cis-Golgi marker, showed high co-localization. This shows that AtMTM1 does not co-localize with the trans-Golgi / post-Golgi but does with the cis-Golgi. Stable transgenic plants expressing AtMTM1-RFP fusion construct also showed a lot of vesicles in the root tip as well as inside the root hair, but the expression was too weak. AtMTM1-RFP does not reveal any co-localization with BFA compartments, which also shows that AtMTM1 does not participate in endosomal recycling process.

When tobacco leaf tissue expressing AtMTM2-GFP was stained with FM4-64 dye (an endocytic tracker), confocal imaging revealed that the signal was shown just beneath the plasma membrane but the green fluorescence from AtMTM2 did not show any co-localization with the plasma membrane. Projection of the AtMTM2-GFP image stacks revealed a net like structure which is a peculiar form of the endoplasmic reticulum in tobacco. This is confirmed by the co-expression of AtMTM2 with HDEL-DsRed, a marker for ER, in tobacco. Confocal imaging displayed a complete co-localization with the ER marker. Surprisingly, stable transgenic lines of AtMTM2-GFP showed a somewhat different expression in comparison to the transient expression of AtMTM2-GFP in tobacco. Instead of those dense lobes, AtMTM2 showed lots of vesicles in root tip, root hairs. In tobacco no such granule like structures were

seen. It could be possible that the subcellular localization of AtMTM2 is controlled by some cytosolic factors which are different in *Arabidopsis* and tobacco. To address this question in more detail, further experiments should be conducted by generating stable transgenic lines with AtMTM2-GFP and G-RK (a cis-Golgi marker). On the other hand, it might also be possible that the proper localization of AtMTM2 requires AtMTM1. If the amount of AtMTM2 is exceeding the amount of AtMTM1, then AtMTM2 might mis-localize to other subcellular domains. This scenario is supported by the AtMTM2-AtMTM1 co-expression experiment as well as by the results obtained from stably transformed lines. As obtained by the result of the co-expression study between AtMTM1 and AtMTM2, when expressed together, AtMTM2 highly co-localized with AtMTM1 in tobacco leaf cells. In stable transgenic lines, AtMTM2 shows similar expression as AtMTM1 in *Arabidopsis* root cells, indicating that the two might be interacting.

To investigate the nature of these vesicles in the endocytic recycling process, transformed seedlings expressing AtMTM2-GFP were stained with FM4-64 dye for 10 minutes and then washed with BFA for 60 minutes. Even after 60 minutes, AtMTM2-GFP positive vesicles did not co-localize with the BFA compartments. Similar results have been observed, when AtMTM2 was infiltrated into *N. benthamiana* stained with FM4-64 dye, which did not show any co-localization with each other. These results show that AtMTM2 does not participate in endocytic recycling.

Previous studies on human myotubularins showed that there are active members in the myotubularin family along with inactive ones (Laporte et al., 2003). An interaction was reported between two active myotubularins of human which altered the subcellular localization of each myotubularin (Lorenzo et al., 2006), e.g. when hMTMR4 interacts with hMTMR3, it changes its subcellular localization from endosomes to the Golgi. Since, *A. thaliana* contains two active myotubularins, cross co-transformation of the two plant myotubularins was done in order to reveal any change in their expression after interaction. These experiments showed that there was a high co-localization between these two active myotubularins: AtMTM2-GFP, when expressed alone, was not showing any vesicle-localization but it did when co-expressed with AtMTM1-RFP, which by itself also labels a large number of vesicles around the plasma membrane and throughout the cytoplasm, when expressed alone, demonstrating an analogy to active human myotubularins. These results support the hypothesis that myotubularins play an important role in trafficking between the ER and the cis-Golgi. Further studies should address their potential functions in the

trafficking and verify this hypothesis by generating transgenic lines expressing different ER exit sites (ERES) markers and AtMTMs together.

4.2.   EFFECTS OF ABA ON *ARABIDOPSIS* MYOTUBULARINS

One of the aims of this thesis was to analyze the expression of myotubularins under different abiotic stresses. To this end, stable transgenic GUS lines under the control of the native AtMTM1 and AtMTM2 promoters, respectively, were submitted to different abiotic stresses. Under normal condition, AtMTM2 showed higher expression in roots in comparison to leaves, while AtMTM1 showed higher expression in leaves in comparison to roots. These results are consistent with the previously reported RT-PCR analysis data (Ding et al., 2012). While both myotubularins lost their expression in roots and showed dominant expression only in leaves in response to environmental stresses like cold stress, dark stress, salt stress and heat stress, but under 30 μM ABA exposure, AtMTM1 showed higher expression in roots. At the same time negligible change in the expression of AtMTM2 was observed under 30 μM ABA exposure. Quantification of the GUS staining intensity showed 60% elevation in AtMTM1 promoter activity in comparison to AtMTM2 under ABA exposure.

It was previously reported that deletion of AtMTM1 increased the plant's tolerance towards drought stress. M1OX plants were more sensitive towards water stress as compared to M1KO and DKO mutants. M1KO and DKO mutants showed a higher relative water content (RWC) after 9 and 12 days without water indicating that these mutants are enduring drought stress better in comparison to M1OX, M2KO and wild-type Col-0 plant.

ABA ($C_{15} H_{20} O_4$) is a plant hormone formed from terpenoids which are synthesized from 2C-methyl-D-erythritol-4-phosphate (MEP) pathway (Nambara and Marion-Poll, 2005). Under different environmental stresses, particularly drought (Zhu, 2002), the level of ABA increased in order to provide tolerance to the plant for its survival (Giraudat et al., 1994; Lee et al., 2006). Subcellular localization of AtMTM1-RFP changed in response to ABA treatment, while there was no significant effect observed on the subcellular localization of AtMTM2-GFP after ABA treatment. These results show that ABA mainly affects the activity of AtMTM1.

During drought stress, ABA is produced in response to soil water deficit which brings a variety of physiological effects in plants to acclimatize under stress conditions. One of the major hurdles is to decrease water loss from transpiration by regulating stomatal closure of plant leaves during drought stress. ABA induces stomatal closure by altering osmotic potential of guard cells in times of deficient water. Measurement of stomatal aperture in the

absence or presence of exogenously applied ABA revealed that M1KO and DKO mutants confer enhanced sensitivity towards ABA-induced stomatal closure. Consistent with this, M1KO and DKO mutants also exhibited an enhanced capacity to conserve water, as revealed by RWC measured in detached leaves under dehydration conditions. M1OX and M2KO were more sensitive to exogenously applied ABA in comparison to M1KO and DKO mutants which was revealed here by the germination assay (Section 3.2.1). All together, these results indicate that absence of AtMTM1 elevated the plant's resistance towards ABA exposure as DKO also showed resistance under ABA exposure. Next step was to check the ROS activity, as ABA affects ROS production as well.

4.3. MYOTUBULARINS RELATIONSHIP WITH ROS SIGNALING

As discussed above, ABA affects the expression of AtMTM1 and leads to many physiological changes like reducing the germination rate, inhibition of stomatal closure and inability to conserve water. One of the major ABA mediated responses is production of ROS. In response to a variety of environmental changes, plants control the regulation of ROS level. ABA activates calcium-permeable channels, which leads to loss of guard cell turgor by outflow of ions from the cell and this in turn results in stomatal closing (Schroeder and Hagiwara, 1989; Kim et al., 2010). ROS levels are controlled during this complex regulatory network by regulating various ROS-scavenging and ROS-producing genes (Fryer et al., 2003; Kwak et al., 2003; Zhu and Scandalios 1994).

Myotubularins are the enzymes which use two substrates PtdIns3P and PtdIns(3,5)P$_2$ in order to produce two products PtdIns and PtdIns5P respectively. Previous studies show that PtdIns3P plays an important role in the generation of ROS in response to ABA in guard cells (Park et al., 2003). ROS was measured in response to applied ABA in various mutants of myotubularins along with wild-type Col-0 for control. An abrupt increase in ROS level was reported in M1KO and DKO mutants after application of ABA to the guard cells and these mutants survived under dehydration stress. It might be because of the positive effect of ROS production on these mutants which is well in agreement with the suggested positive signaling role of ROS (Foyer and Noctor, 2005). On the other hand, a decrease in ROS level was observed in M1OX and M2KO after ABA exposure. During dehydration stress, ABA plays a pivotal role which increases ROS production. These results show that AtMTM1 affects ROS signaling process under ABA exposure.

Another major product of myotubularins is PtdIns5P. From previous studies it was reported that during dehydration stress, the cellular level of PtdIns5P was increased by 70% in M1OX in comparison to M1OX in non-stressed condition. On the other hand, in M1KO, there was a

negligible increase in PtdIns5P level after dehydration stress (Ndamukong et al., 2010). To test the hypothesis further, that PtdIns5P plays a role in ROS generation, guard cells of various myotubularin mutants along with Col-0 were treated with 1.5μM PtdIns5P in order to see its effect on ROS production. The ROS level was significantly reduced in M1OX after PtdIns5P treatment in guard cells as M1OX produces more PtdIns5P in comparison to others. A similar result was obtained when the roots of myotubularin mutants were treated with an appropriate concentration of PtdIns5P. These results show that the ROS level was reduced after treatment with PtdIns5P. This is an important result indicating that PtdIns5P emerges as a second messenger in the ROS homeostasis for plant cells analogous to animal cells. In animal cells, PI5P emerges as a second messenger in ROS homeostasis (Keune et al., 2013). The proposed model for the hypothetical pathway is summarized in the Figure 45.
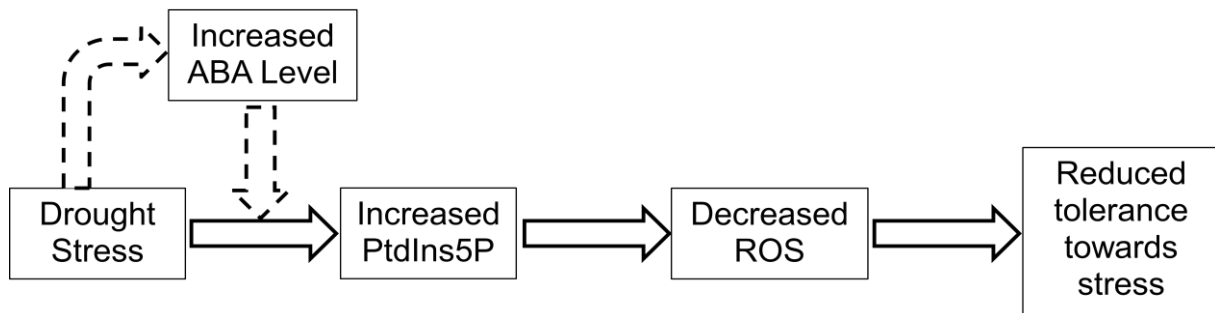
Figure 45: Hypothetical signalling pathway: Increased ABA level during drought stress leading to a reduced tolerance in myotubularin mutants towards stress due to the reduced ROS level.

4.4. IMPORTANCE OF THE SERINE-RICH DOMAIN AND GRAM DOMAIN

In 2009, two plant myotubularins (AtMTM1 and AtMTM2) were characterized which were encoded by the At3g10550 and At5g04540 genes showing 77% identity and 85% similarity to each other (Ding et al., 2009). They were 38% identical to human MTMR2 while showing 59% similarity (Ding et al., 2009). Both proteins contain a conserved PH-GRAM domain, a RID, a CC domain as well as a catalytic domain along with SID, which is a similar domain structure as in hMTMR2 (Laporte et al., 2002a; Begley et al., 2003). Despite of these similarities, these proteins behave in different manners. For instance, they show different affinity towards substrates like PtdIns3P and PtdIns(3,5)P$_2$. AtMTM1 exhibited higher phosphatase activity in comparison to AtMTM2. Dehydration tolerance in *Arabidopsis thaliana* increased in response to dehydration stress by the deletion of AtMTM1 (Ding et al., 2012). During drought stress, AtMTM1 increased the cellular level of PtdIns5P which in turn decreased the activity of ATX1 as well as WRKY70 transcripts. AtMTM1 changed the subcellular localization of ATX1 by shifting it from the nucleus to the cytoplasm by interacting with the PHD of ATX1 (Ndamukong et al., 2010). To summarize, an increased level of PtdIns5P due to an increased
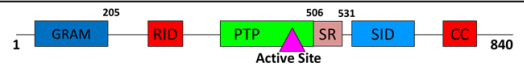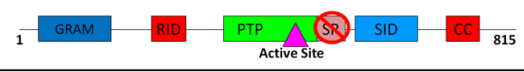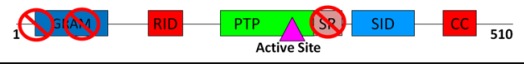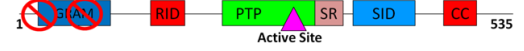
lipid 3'-phosphatase activity of AtMTM1 during drought stress kept ATX1 in the cytoplasm only.

Previous studies showed that subcellular localization of hMTMR2 does not reside in suborganellar structures (Laporte et al., 2002a; Berger et al., 2003; Kim et al., 2003). In 2011, Franklin and his collaborators found a phosphorylation site on Serine 58 (Ser[58]), which is approximately 11 amino acids upstream of the PH-GRAM domain of hMTMR2, by mass spectrometry-based methods. This phosphorylation site was found to be responsible for restricting its localization to endocytic membranes. The phosphomimetic S58A mutant, which is devoid of this phosphorylation site, displayed localization to early endocytic structures.

In order to understand the importance of the Serine-rich domain, which is present upstream of the SID and GRAM domain in AtMTM1, three constructs i.e. AtAAF-GFP (without the Serine-rich domain present near SID), AtAAG-GFP (without the Serine-rich domain as well as N-terminal sequences including the GRAM domain) and AtNP-RFP (without the GRAM domain including the N-terminal sequences but with the Serine-rich domain intact) were constructed (a generous gift of Prof. Zoya Avramova, University of Nebraska School of Biological Sciences, Nebraska, USA). Subcellular localization of AtAAF-GFP showed that this protein partially co-localizes with an ER marker (HDEL) and a cis-Golgi marker (G-YK), while AtAAG-GFP partially co-localizes with FYVE (late endosome marker) and ST-RFP (TGN marker). AtAAG-GFP did neither co-localize with the ER marker nor with the cis-Golgi marker. These results would mean that deletion of this Serine-rich domain affects the localization of AtMTM1. Deletion of both the Serine-rich domain as well as the GRAM domain changes AtMTM1 localization to endocytic structures. AtNP-RFP did not show any change in localization in comparison to AtMTM1, which would mean that despite the deletion of the GRAM domain, the subcellular localization does not change due to the presence of Serine-rich domain.

Previous results showed that there is a relationship between AtMTM1 and ATX1 (Ndamukong et al., 2010). To see whether this Serine-rich domain or GRAM domain would affect the activity of AtMTM1 towards ATX1, co-transformation of these constructs was done with ATX1 or PHD. Co-expression of AtAAF-GFP or AtAAG-GFP with either ATX1 or with just the PHD of ATX1 showed nuclear localization of both partners in the co-expressed pairs. While co-expression of AtNP-RFP with ATX1-GFP or PHD-GFP did not affect the cytoplasmic localization of AtNP-RFP, AtNP lost its ability to change the subcellular localization of ATX1 or the PHD of ATX1 i.e. from the nucleus to the cytoplasm. Deletion of the Serine-rich domain causes relocalization of AtMTM1 from the cytoplasm to the nucleus

with or without the presence of the GRAM domain and also inhibits the capability of AtMTM1 to relocate nuclear ATX1 from the nucleus to the cytoplasm. Deletion of only the GRAM domain does not affect the localization of either AtMTM1 or ATX1 and also inhibits the capability of AtMTM1 to relocate nuclear ATX1 from the nucleus to the cytoplasm. It showed that presence of these two domains i.e. the GRAM and Serine-rich domains together in AtMTM1 cause relocation of nuclear ATX1 from the nucleus to the cytoplasm (Table 1). Further studies should address a possible regulatory role of Serine phosphorylation or dephosphorylation in the interaction between AtMTM1 and ATX1.

Construct	Representation of the structure of the construct	Expression of respective constructs alone	Expression of nuclear ATX1 with respective constructs	Expression of respective constructs with ATX1
AtMTM1	1 — GRAM (205) — RID — PTP — Active Site — SR (506 531) — SID — CC — 840	Cytoplasm	Cytoplasm	Cytoplasm
AtAAF	1 — GRAM — RID — PTP — Active Site — (SR) — SID — CC — 815	Cytoplasm	Nucleus	Nucleus
AtAAG	1 — (GRAM) — RID — PTP — Active Site — (SR) — SID — CC — 510	Cytoplasm	Nucleus	Nucleus
AtNP	1 — (GRAM) — RID — PTP — Active Site — SR — SID — CC — 535	Cytoplasm	Nucleus	Cytoplasm

Table 1: Co-localization of ATX1 with different isoforms of AtMTM1.

Deletion of SR domain causes relocalization of AtMTM1 from the cytoplasm to the nucleus with or without the presence of the GRAM domain and also inhibits the capability of AtMTM1 to relocate nuclear ATX1 from the nucleus to the cytoplasm.

Presence of both the GRAM and SR domains causes relocation of nuclear ATX1 from the nucleus to the cytoplasm.

Deletion of only the GRAM domain does not affect the localization of either AtMTM1 or ATX1 and also inhibits the capability of AtMTM1 to relocate nuclear ATX1 from the nucleus to the cytoplasm.

As shown in Section 3.7, ABA affects the subcellular localization of AtMTM1. In order to check the effect of ABA on subcellular localization of AtAAF-GFP and AtAAG-GFP, transformed pieces of tobacco leaves containing these constructs treated with 10 μM ABA solution for 1 hour did not show any significant effect on the localization pattern of AtAAF-GFP and AtAAG-GFP. It could be due to the inability of these constructs to relocate nuclear ATX1 from the nucleus to the cytoplasm. Diminution of ATX1 activity affects a variety of cellular signals which in turn affects plant growth.

5.   SUMMARY

In 2009, plant myotubularins were discovered (Ding et al., 2009). Since then, although plant myotubularins represent a very new and important topic of research, very little is known about their function, localization and behavior. Hence the aim of this thesis was to enhance the understanding about the functioning of myotubularins in *A. thaliana*.

Despite being 77% identical, each of these proteins has their own functionality which was shown by different localization pattern and different behavior under stress. As a part of this work, the expression pattern of myotubularins was studied under normal condition as well as under different abiotic stresses like dark, cold, heat, salt and ABA using AtMTM1prom::GUS and AtMTM2prom::GUS transgenic lines. Both genes are present in vascular tissue of root, leaves, hypocotyl and trichomes under normal condition. Under dark, cold, salt and heat stress, the expression was mainly in leaves and hypocotyl, while no expression in root was observed. On the other hand, under ABA exposure, the promoter activity of AtMTM1 was enhanced in the vascular tissue of root and hypocotyl, while slight increase was observed in leaves. At the same time, AtMTM2 showed no significant change in its expression under ABA exposure. Quantification of GUS intensity revealed that promoter activity of both the genes AtMTM1 and AtMTM2 decreased after dark (-40% and -42% respectively), cold (-60% and -65% respectively) and heat stress (-60% for both). Slight increment was observed under salt stress (+10% for both), but after 30μM ABA treatment, there was a significant increment in promoter activity of AtMTM1 (+80%) as compared to AtMTM2 (+10%).

Over-expression of AtMTM1 led to the failure of stomatal closure in response to ABA exposure. Also, AtMTM2 as well as double knock out showed a significant closure in their stomatal aperture under ABA effect indicating that only AtMTM1 hinders stomatal closure during ABA exposure. In addition, ABA exposure also aids the ROS production in plants, which help the plant to survive under stress condition. While over-expression of AtMTM1 led to a reduction in ROS level (-35%), AtMTM2 and double knockout showed a significant increase in ROS level under ABA exposure (+40% and +65% respectively).

As myotubularins use PtdIns3P, PtdIns(3,5)P$_2$ phosphoinositides as a substrate and form PtdIns and PtdIns5P respectively, it was deemed important for this research to check the effect of exogenous supply of PtdIns5P on the ROS level. It was found that PtdIns5P, when supplied externally, inhibits ROS generation in guard cells of wild-type Col-0 and all mutants of myotubularins. Maximum influence of the reduced ROS level was observed in the M1OX mutant plants from ~80% down to ~30% under the influence of 1.5μM of PtdIns5P, while the

DKO mutant showed the least effect, changing from 107% to 65% with wild-type Col-0 as control at 100%. This indicates that the myotubularins affect ROS signaling significantly via PtdIns5P.

Co-localization of RFP tagged AtMTM1 and GFP tagged AtMTM2 with various markers showed that AtMTM1 is present in the cis-Golgi and AtMTM2 is present in endoplasmic reticulum. Co-localization showed that the interaction between active myotubularins of plant might play an important role in the trafficking between the ER and the cis-Golgi. Cross co-localization of AtMTM2 with AtMTM1 changed the subcellular localization of AtMTM2, from a net like structure to large number of vesicles like in AtMTM1, which were highly co-localizing with each other.

Three isoforms of AtMTM1 i.e. AtAAF-GFP (without the Serine-rich domain present near SID), AtAAG-GFP (without the Serine-rich domain as well as N-terminal sequences including the GRAM domain) and AtNP-RFP (without the GRAM domain including N-terminal sequences but with Serine-rich domain intact) were studied in order to understand the role of different domains of AtMTM1. It was found that the deletion of the Serine-rich domain, with or without the GRAM domain, affected the localization pattern which is confirmed by different localization of AtAAF and AtAAG. AtAAF showed partial co-localization with the ER and the cis-Golgi marker, while AtAAG showed partial co-localization with the FYVE and the trans-Golgi markers. However, the deletion of only the GRAM domain did not change the localization of AtMTM1. In addition to this, it was found that the Serine-rich domain was involved in re-location of AtMTM1 from the cytoplasm to the nucleus as co-expression studies of AtAAF and AtAAG with ATX1 and the PHD of ATX1 showed nuclear instead of cytoplasmic localization. On the other hand, the deletion of only the GRAM domain affects the ability of AtMTM1 to relocate nuclear ATX1 from the nucleus to the cytoplasm. These data suggest that these two domains together affect activity of AtMTM1 which in turn affects the activity of ATX1.

6. REFERENCES

Aggarwal, C., Łabuz, J. and Gabrys, H. (2013) Phosphoinositides play differential roles in regulating Phototropin1- and Phototropin2- mediated chloroplast movements in *Arabidopsis*. PLoS One 8, e55393.

Alvarez-Venegas, R., Abdallat, A.A., Guo, M., Alfano, J.R. and Avramova, Z. (2007) Epigenetic control of a transcription factor at the cross section of two antagonistic pathways. Epigenetics 2, 106–113.

Alvarez-Venegas, R., Pien, S., Sadder, M., Witmer, X., Grossniklaus, U. and Avramova, Z. (2003) ATX-1, An *Arabidopsis* homolog of Trithorax has histone methylase activity and activates flower homeotic genes. Curr. Biol. 13:627-37.

Alvarez-Venegas, R., Sadder, M., Hlavacka, A., Baluska, F., Xia, Y., Lu, G., Firsov, A., Sarath, G., Moriyama, H., Dubrovsky, J.G. and Avramova, Z. (2006) The *Arabidopsis* homolog of trithorax, ATX1, binds phosphatidylinositol 5-phosphate, and the two regulate a common set of target genes. Proc. Natl. Acad. Sci. USA, 103, 6049–6054.

Andreeva, A.V., Kutuzov, M.A., Evans, D.E. and Hawes, C. (1998) The structure of the Golgi apparatus: A hundred year of questions. J. Exp. Bot. 49, 1281–1291.

Aparicio-Fabre, R., Guill´en, G., Estrada, G., Olivares-Grajales, J., Gurrola, G. and S´anchez, F. (2006) Profilin tyrosine phosphorylation in poly-l-proline-binding regions inhibits binding to phosphoinositide 3-kinase in *Phaseolus vulgaris*. Plant J. 47:491–500.

Arcaro, A. and Wymann, M.P. (1993) Wortmannin is a potent phosphatidylinositol 3-kinase inhibitor: the role of phosphatidylinositol 3,4,5-trisphosphate in neutrophil responses. Biochem. J. 296, 297–301.

Auger, K.R., Serunian, L.A., Soltoff, S.P., Libby, P. and Cantley, L.C. (1989) PDGF-dependent tyrosine phosphorylation stimulates production of novel polyphosphoinositides in intact cells. Cell 57, 167–175.

Azzedine, H., Bolino, A., Taieb, T., Birouk, N., Di, D.M., Bouhouche, A., Benamou, S., Mrabet, A., Hammadouche, T., Chkili, T., Gouider, R., Ravazzolo, R., Brice, A., Laporte, J. and LeGuern, E. (2003) Mutations in MTMR13, a new pseudophosphatase homologue of MTMR2 and Sbf1, in two families with an autosomal recessive demyelinating form of Charcot-Marie-Tooth disease associated with early-onset glaucoma. Am. J. Hum. Genet. 72, 1141-1153.

Backer, J.M. (2008) The regulation and function of Class III PI3Ks: novel roles for Vps34. Biochem. J. 410, 1–17.

Baluska, F., Hlavacka, A., Samaj, J., Palme, K., Robinson, D.G., Matoh, T., McCurdy, D.W., Menzel, D. and Volkmann, D. (2002) F-Actin dependent endocytosis of cell wall pectins in Meristematic root cells. Insights from Brefeldin A-induced compartments. Plant Physiol. 130, 422-431.

Batoko, H., Zheng, H.Q., Hawes, C. and Moore, I. (2000) A Rab1 GTPase is required for transport between the endoplasmic reticulum and Golgi apparatus and for normal Golgi movement in plants. Plant Cell 12, 2201–2218.

Begley, M.J. and Dixon, J.E. (2005) The Structure and regulation of myotubularin phosphatases. Curr. Opin. Struct. Biol. 15, 614-620.

Begley, M.J., Taylor, G.S., Brock, M.A., Ghosh, P., Woods, V.L. and Dixon, J.E. (2006) Molecular basis for substrate recognition by MTMR2, a myotubularin family phosphoinositide phosphatase. Proc. Natl. Acad. Sci. USA 103, 927-932.

Begley, M.J., Taylor, G.S., Kim, S.A., Veine, D.M., Dixon, J.E. and Stuckey, J.A. (2003) Crystal structure of a phosphoinositide phosphatase, MTMR2: insights into myotubular myopathy and Charcot-Marie-Tooth syndrome. Mol. Cell. 12, 1391-1402.

Berger, P., Berger, I., Schaffitzel, C., Tersar, K., Volkmer, B. and Suter, U. (2006) Multi-level regulation of myotubularin-related protein-2 phosphatase activity by myotubularin-related protein-13/set-binding factor-2. Hum. Mol. Genet. 15, 569-579.

Berger, P., Bonneick, S., Willi, S., Wymann, M. and Suter, U. (2002) Loss of phosphatase activity in myotubularin-related protein 2 is associated with Charcot-Marie-Tooth disease type 4B1. Hum. Mol. Genet. 11, 1569-1579.

Berger, P., Schaffitzel, C., Berger, I., Ban, N. and Suter, U. (2003) Membrane association of myotubularin-related protein 2 is mediated by a pleckstrin homology-GRAM domain and a coiled-coil dimerization module. Proc. Natl. Acad. Sci. USA 100, 12177-12182.

Bloch, D., Lavy, M., Efrat, Y., Efroni, I., Bracha-Drori, K., Abu-Abied, M., Sadot, E. and Yalovsky, S. (2005) Ectopic expression of an activated RAC in *Arabidopsis* disrupts membrane cycling. Mol. Biol. Cell 16, 1913–1927.

Blondeau, F., Laporte, J., Bodin, S., Superti-Furga, G., Payrastre, B. and Mandel, J.L. (2000) Myotubularin, a phosphatase deficient in myotubular myopathy, acts on phosphatidylinositol 3-kinase and phosphatidylinositol 3-phosphatase pathway. Hum. Mol. Genet. 9, 2223-2229.

Boevink, P., Oparka, K., Santa Cruz, S., Martin, B., Betteridge, A. and Hawes, C. (1998) Stacks on tracks: The plant Golgi apparatus traffics on an actin / ER network. Plant J. 15, 441–447.

Bolino, A. (2000) Charcot-Marie-Tooth type 4B is caused by mutations in the gene encoding myotubularin-related protein-2. Nature Genet. 25, 17-19.

Bolte, S., Talbot, C., Boutte, Y., Catrice, O., Read, N.D. and Satiat-Jeunemaitre, B. (2004) FM-dyes as experimental probes for dissecting vesicle trafficking in living plant cells. J. Microsc. 214, 159-173.

Boronenkov, I.V. and Anderson, R.A. (1995) The sequence of phosphatidylinositol- 4-phosphate 5-kinase defines a novel family of lipid kinases. J. Biol. Chem. 270, 2881–2884.

Bosgraaf, L. and Van Haastert, P.J. (2003) Roc, a Ras/GTPase domain in complex proteins. Biochim. Biophys. Acta 1643, 5–10.

Boss, W.F. and Im, Y.J. (2012) Phosphoinositide signaling. Annu. Rev. Plant Biol. 63, 409–429.

Brandizzi, F., Snapp, E.L., Roberts, A.G., Lippincott-Schwartz, J. and Hawes, C. (2002) Membrane protein transport between the endoplasmic reticulum and the Golgi in tobacco leaves is energy dependent but cytoskeleton independent: Evidence from selective photobleaching. Plant Cell 14, 1293–1309.

Brearley, C.A. and Hanke, D.E. (1992) 3- and 4-phosphorylated phosphatidylinositols in the aquatic plant *Spirodela polyrhiza L.* Biochem. J. 283, 255–260.

Bright, J., Desikan, R., Hancock, J.T., Weir, I.S. and Neill, S.J. (2006) ABA-induced NO generation and stomatal closure in *Arabidopsis* are dependent on H_2O_2 synthesis. Plant J. 45,113-122.

Chow, C.M., Neto, H., Foucart, C. and Moore, I. (2008) Rab-A2 and Rab-A3 GTPases define a trans-Golgi endosomal membrane domain in *Arabidopsis* that contributes substantially to the cell plate. Plant Cell 20, 101–123.

Clarke, J., Letcher, A.J., D'Santos, C.S., Halstead, J.R., Irvine, R.F. and Divecha, N. (2001) Inositol lipids are regulated during cell cycle progression in the nuclei of murine erythroleukaemia cells. Biochem. J. 357, 905–910.

Clough, S.J. and Bent, A.F. (1998) Floral dip: a simplified method for *Agrobacterium-*mediated transformation of *Arabidopsis thaliana*. Plant J. 16, 735–743.

Cooke, F.T., Dove, S.K., McEwen, R.K., Painter, G., Holmes, A.B., Hall, M.N., Michell, R.H. and Parker, P.J. (1998) The stress-activated phosphatidylinositol 3-phosphate 5-kinase Fab1p is essential for vacuole function in *S. cerevisiae*. Curr. Biol. 8, 1219–1222.

Corvera, S., D'Arrigo, A. and Stenmark, H. (1999) Phosphoinositides in membrane traffic. Curr. Opin. Cell Biol. 11, 460-465.

Cui, X., Vivo, I., Slany, R., Miyamoto, A., Firestein, R. and Cleary, M.L. (1998) Association of SET domain and myotubularin-related proteins modulates growth control. Nat. Genet. 18, 331-337.

daSilva, L.L., Snap, E.L., Deneck, J., Lippincott-Schwartz, J., Hawes, C. and Brandizzi, F. (2004) Endoplasmic reticulum export sites and Golgi bodies behave as single mobile secretory units in plant cells. Plant Cell 16, 1753-1771.

de Gouyon, B.M., Zhao, W., Laporte, J., Mandel, J.L., Metzenberg, A. and Herman, G.E. (1997) Characterization of mutations in the myotubularin gene in twenty six patients with X-linked myotubular myopathy. Hum. Mol. Genet. 6, 1499-1504.

Denu, J.M. and Dixon, J.E. (1998) Protein tyrosine phosphatases: mechanisms of catalysis. Curr. Opin. Chem. Biol. 2, 633–641.

Dettmer, J., Hong-Hermesdorf, A., Stierhof, Y.D. and Schumacher, K. (2006) Vacuolar H+-ATPase activity is required for endocytic and secretory trafficking in *Arabidopsis*. Plant Cell 18, 715–730.

Dharmasiri, S., Swarup, R., Mockaitis, K., Dharmasiri, N., Singh, S.K., Kowalchyk, M., Marchant, A., Mills, S., Sandberg, G., Bennett, M.J. and Estelle, M. (2006) AXR4 is required for localization of the auxin influx facilitator AUX1. Science 312, 1218–1220.

Di Paolo, G. and De Camilli, P. (2006) Phosphoinositides in cell regulation and membrane dynamics. Nature 443, 651–657.

Ding, Y., Lapko, H., Ndamukong, I., Xia, Y., Al-Abdallat, A., Lalithambika, S., Sadder, M., Saleh, A., Fromm, M., Riethoven, J.J., Lu, G. and Avramova, Z. (2009) The *Arabidopsis* chromatin modifier ATX1, the myotubularin-like AtMTM and the response to drought. Plant Signal. Behav. 4, 1049–1058.

Ding, Y., Ndamukong, I., Zhao, Y., Xia, Y., Riethoven, J., Jones, D.R., Divecha, N. and Avramova, Z. (2012) Divergent functions of the myotubularin (MTM) homologs AtMTM1 and AtMTM2 in *Arabidopsis thaliana*: evolution of the plant MTM family. Plant J. 70, 866–878.

Dodd, I.C. (2003) Hormonal interactions and stomatal responses. J. Plant Growth Regul. 22, 32–46.

Doerks, T., Strauss, M., Brendel, M. and Bork, P. (2000) GRAM, a novel domain in glucosyltransferases, myotubularins and other putative membrane-associated proteins. Trends Biochem. Sci. 25, 483–485.

Dong, X.P., Shen, D., Wang, X., Dawson, T., Li, X., Zhang, Q., Cheng, X., Zhang, Y., Weisman, L.S., Delling, M. and Xu, H. (2010) PI(3,5)P(2) controls membrane

trafficking by direct activation of mucolipin Ca^{2+} release channels in the endolysosome. Nat. Commun. 1, 38.

Dove, S.K., Cooke, F.T., Douglas, M.R., Sayers, L.G., Parker, P.J. and Michell, R.H. (1997) Osmotic stress activates phosphatidyl-D-inositol 3,5-bisphosphate synthesis in yeast. Nature 390, 187-192.

Dove, S.K., Dong, K., Kobayashi, T., Williams, F.K. and Michell, R.H. (2009) Phosphatidylinositol 3,5-bisphosphate and Fab1p/PIKfyve underPPIn endo-lysosome function. Biochem J. 419, 1-13.

Driouich, A. and Staehelin, L.A. (1997) The plant Golgi apparatus: Structural organization and functional properties. The Golgi Apparatus, Berger, E.G. and Roth, J., eds. (Basel: Birkhauser Verlag), 275–301.

Du, G., Altshuller, Y.M., Vitale, N., Huang, P., Chasserot-Golaz, S., Morris, A.J., Bader, M.F. and Frohman, M.A. (2003) Regulation of phospholipase D1 subcellular cycling through coordination of multiple membrane association motifs. J. Cell Biol. 162, 305-315.

Emans, N., Zimmermann, S. and Fischer, R. (2002) Uptake of a fluorescent marker in plant cells is sensitive to brefeldin A and wortmannin. Plant Cell 14, 71–86.

Fabre, S., Reynaud, C. and Jalinot, P. (2000) Identification of functional PDZ domain binding sites in several human proteins. Mol. Biol. Rep. 27, 217–224.

Fardeau, M. (1992) Congenital myopathies. Skeletal muscle pathology, Mastaglia, F.L. and Lord Walton of Detchant, eds. (Edinburgh: Churchill Livingstone), 237-281.

Feng, X., Hara, Y. and Riabowol, K. (2002) Different HATS of the ING1 gene family. Trends Cell Biol. 12, 532–538.

Firestein, R. and Cleary, M.L. (2001) Pseudo-phosphatase Sbf1 contains an N-terminal GEF homology domain that modulates its growth regulatory properties. J. Cell Sci. 114, 2921-2927.

Firestein, R., Cui, X., Huie, P. and Claery, M.L. (2000) Set domain dependent regulation of transcriptional silencing and growth control by SUV39H1, a mammalian ortholog of *Drosophila* Su(var)3–9. Mol. Cell Biol. 20, 4900–4909.

Foyer, C.H. and Noctor, G. (2005) Oxidant and antioxidant signalling in plants: a re-evaluation of the concept of oxidative stress in a physiological context. Plant Cell Environ. 28, 1056–1071.

Franklin, N.E., Taylor, G.S. and Vacratsis, P.O. (2011) Endosomal targeting of the Phosphoinositide 3-Phosphatase MTMR2 is regulated by an N-terminal phosphorylation site. J. Biol. Chem. 286, 15841–15853.

Fryer, M.J., Ball, L., Oxborough, K., Karpinski, S., Mullineaux, P.M. and Baker, N.R. (2003) Control of ascorbate peroxidase 2 expression by hydrogen peroxide and leaf water status during excess light stress reveals a functional organisation of *Arabidopsis* leaves. Plant J. 33, 691–705.

Fyodorov, D.V. and Kadonaga, J.T. (2002) Binding of Acf1 to DNA involves a WAC motif and is important for ACF-mediated chromatin assembly. Mol. Cell. Biol. 22, 6344–6353.

Gaullier, J.M., Simonsen, A., D'Arrigo, A., Bremnes, B., Stenmark, H. and Aasland, R. (1998) FYVE fingers bind PtdIns(3)P. Nature 394, 432-433.

Gillooly, D.J., Morrow, I.C., Lindsay, M., Gould, R., Bryant, N.J., Gaullier, J.M., Parton, R.G. and Stenmark, H. (2000) Localization of phosphatidylinositol 3 phosphate in yeast and mammalian cells. EMBO J. 19, 4577-4588.

Gillooly, D.J., Simonsen, A. and Stenmark, H. (2001) Cellular functions of phosphatidylinositol 3-phosphate and FYVE domain proteins. Biochem. J. 355, 249–58.

Giraudat, J., Parcy, F., Bertauche, N., Gosti, F. and Leung, J. (1994) Current advances in abscisic acid action and signaling. Plant Mol. Biol. 26, 1557–1577.

Golomb, L., Abu-Abied, M., Belausov, E. and Sadot, E. (2008) Different subcellular localizations and functions of *Arabidopsis* myosin VIII. BMC Plant Biol. 8, 3.

Gozani, O., Karuman, P., Jones, D.R., Ivanov, D., Cha, J., Lugovskoy, A.A., Baird, C.L., Zhu, H., Field, S.J., Lessnick, S.L., Villasenor, J., Mehrotra, B., Chen, J., Rao, V.R., Brugge, J.S., Ferguson, C.G., Payrastre, B., Myszka, D.G., Cantley, L.C., Wagner, G., Divecha, N., Prestwich, G.D. and Yuan, J. (2003) The PHD finger of the chromatin-associated protein ING2 functions as a nuclear phosphoinositide receptor. Cell 114, 99–111.

Grebe, M., Xu, J., Möbius, W., Ueda, T., Nakano, A., Geuze, H.J., Rook, M.B. and Scheres, B. (2003) *Arabidopsis* sterol endocytosis involves actin-mediated trafficking via ARA6-positive early endosomes. Curr. Biol. 13, 1378-1387.

Griffiths, A. and Bray, E.A. (1996) Shoot induction of ABA-requiring genes in response to soil drying. J. Exp. Bot. 47, 1525–1531.

Guittard, G., Gerard, A., Dupuis-Coronas, S., Tronchere, H., Mortier, E., Favre, C., Olive, D., Zimmermann, P., Payrastre, B. and Nunés, J.A. (2009) Cutting edge: Dok-1 and Dok-

2 adaptor molecules are regulated by phosphatidylinositol 5-phosphate production in T cells. J. Immunol. 182, 3974–3978.

Guittard, G., Mortier, E., Tronchere, H., Firaguay, G., Gerard, A., Zimmermann, P., Payrastre, B. and Nunés, J.A. (2010) Evidence for a positive role of PtdIns5P in T-cell signal transduction pathways. FEBS Lett. 584, 2455–2460.

Haseloff, J., Siemering, K.R., Prasher, D.C. and Hodge, S. (1997) Removal of a cryptic intron and subcellular localization of green fluorescent protein are required to mark transgenic *Arabidopsis* plants brightly. Proc. Natl. Acad. Sci. USA 94, 2122-2127.

Heckmatt, J.Z., Sewry, C.A., Hodes, D. and Dubowitz, V. (1985) Congential Centronuclear (myotubular) myopathy: a clinical pathological and genetic study in eight children. Brain. 108, 941-964.

Heras, B. and Drobak, B.K. (2002) PARF-1: an *Arabidopsis thaliana* FYVE-domain protein displaying a novel eukaryotic domain structure and phosphoinositide affinity. J. Exp. Bot. 53, 565–567.

Herron, M.D., Hackett, J.D., Aylward, F.O. and Michod, R.E. (2009) Triassic origin and early radiation of multicellular volvocine algae. Proc. Natl. Acad. Sci. USA 106, 3254–3258.

Hirano, T. and Sato, M.H. (2011b) *Arabidopsis* FAB1A/B is possibly involved in the recycling of auxin transporters. Plant Signal. Behav. 6, 583-585.

Hirano, T., Matsuzawa, T., Takegawa, K. and Sato, M.H. (2011a) Loss-of-function and gain-of-function mutations in FAB1A/B impair endomembrane homeostasis, conferring pleiotropic developmental abnormalities in *Arabidopsis*. Plant Physiol. 155, 797-807.

Hobbie, L. and Estelle, M. (1995) The axr4 auxin-resistant mutants of *Arabidopsis thaliana* define a gene important for root gravitropism and lateral root initiation. Plant J. 7, 211–220.

Hutter, H. (2004) Five-colour in-vivo imaging of neurons in *Caenorhabditis elegans*. J. Microsc. 215, 213-218.

Jensen, R.B., La Cour, T., Albrethsen, J., Nielsen, M. and Skriver, K. (2001) FYVE zinc-finger proteins in the plant model *Arabidopsis thaliana*: identification of PtdIns3P-binding residues by comparison of classic and variant FYVE domains. Biochem. J. 359, 165– 173.

Jones, D.R., Bultsma, Y., Keune, W.J., Halstead, J.R., Elouarrat, D., Mohammed, S., Heck, A.J., D'Santos, C.S. and Divecha, N. (2006) Nuclear PtdIns5P as a transducer of stress signaling: an in-vivo role for PIP4Kβ. Mol. Cell 23, 685–695.

Jung, J.Y., Kim, Y.W., Kwak, J.M., Hwang, J.U., Young, J., Schroeder, J.I., Hwang, I. and Lee, Y. (2002) Phosphatidylinositol 3- and 4-phosphate are required for normal stomatal movements. Plant Cell 14, 2399–2412.

Katso, R., Okkenhaug, K., Ahmadi, K., White, S., Timms, J. and Waterfield, M.D. (2001) Cellular function of phosphoinositide 3-kinases: implications for development, homeostasis, and cancer. Annu. Rev. Cell Dev. Biol. 17, 615–675.

Kerk, D. and Moorhead, G.B. (2010) A phylogenetic survey of myotubularin genes of eukaryotes: distribution, protein structure, evolution, and gene expression. BMC Evol. Biol. 10, 196.

Keune, W.J., Jones, D.R. and Divecha, N. (2013) PtdIns5P and Pin1 in oxidative stress signaling. Adv. Biol. Regul. 53, 179-89.

Kihara, A., Noda, T., Ishihara, N. and Ohsumi, Y. (2001) Two distinct Vps34 phosphatidylinositol 3-kinase complexes function in autophagy and carboxypeptidase Y sorting in *Saccharomyces cerevisiae*. J. Cell Biol. 152, 519–530.

Kim, D.H., Eu, Y.J., Yoo, C.M., Kim, Y.W., Pih, K.T., Jin, J.B., Kim, S.J., Stenmark, H. and Hwang, I. (2001) Trafficking of phos- phatidylinositol 3-phosphate from the trans-Golgi network to the lumen of the central vacuole in plant cells. Plant Cell 13, 287–301.

Kim, S.A., Taylor, G.S., Torgersen, K.M. and Dixon, J.E. (2002) Myotubularin and MTMR2, phosphatidylinositol 3-phosphatases mutated in myotubular myopathy and type 4B Charcot–Marie–Tooth disease. J. Biol. Chem. 277, 4526–4531.

Kim, S.A., Vacratsis, P.O., Firestein, R., Cleary, M.L. and Dixon, J.E. (2003) Regulation of myotubularin-related (MTMR)2 phosphatidylinositol phosphatase by MTMR5, a catalytically inactive phosphatase. Proc. Natl. Acad. Sci. USA 100, 4492-4497.

Kim, T.H., Bohmer, M., Hu, H., Nishimura, N. and Schroeder, J.I. (2010) Guard cell signal transduction network: advances in understanding abscisic acid, CO_2, and Ca^{2+} signaling. Annu. Rev. Plant Biol. 61, 561-591.

Klima, A. and Foissner, I. (2008) FM dyes label sterol-rich plasma membrane domains and are internalized independently of the cytoskeleton in characean intermodal cells. Plant Cell Physiol. 49, 1508–1521.

Kwak, J.M., Mori, I.C., Pei, Z.M., Leonhardt, N., Torres, M.A., Dangl, J.L., Bloom, R.E., Bodde, S., Jones, J.D.G. and Schroeder, J.I. (2003) NADPH oxidase AtrbohD and AtrbohF genes function in ROS-dependent ABA signaling in *Arabidopsis*. EMBO J. 22, 2623–2633.

Laporte, J., Bedez, F., Bolino, A. and Mandel, J.L. (2003) Myotubularins, a large disease-associated family of cooperating catalytically active and inactive phosphoinositide phosphatases. Hum. Mol. Genet. 12, 285-292.

Laporte, J., Blondeau, F., Buj-Bello, A. and Mandel, J.L. (2001) The myotubularin family: from genetic diseases to phosphoinositide metabolism. Trends Genet. 17, 221-228.

Laporte, J., Blondeau, F., Buj-Bello, A., Tentler, D., Kretz, C., Dahl, N. and Mandel, J.L. (1998) Characterization of the myotubularin dual specificity phosphatase gene family from yeast to human. Hum. Mol. Genet. 7, 1703-1712.

Laporte, J., Blondeau, F., Gansmuller, A., Lutz, Y., Vonesch, J.L. and Mandel, J.L. (2002a) The PtdIns3P phosphatase myotubularin is a cytoplasmic protein that also localizes to Rac1-inducible plasma membrane ruffles. J. Cell Sci. 115, 3105–3117.

Laporte, J., Hu, L.J., Kretz, C., Mandel, J.L., Kioschis, P., Coy, J.F., Klauck, S.M., Poustka, A. and Dahl, N. (1996) A gene mutated in X-linked myotubular myopathy defines a new putative tyrosine phosphatase family conserved in yeast. Nat. Genet. 13, 175-82.

Laporte, J., Liaubet, L., Blondeau, F., Tronchere, H., Mandel, J.L. and Payrastre, B. (2002b) Functional redundancy in the myotubularin family. Biochem. Biophys. Res. Commun. 291, 305–312.

Lecompte, O., Poch, O. and Laporte, J. (2008) PtdIns5P regulation through evolution: roles in membrane trafficking? Trends Biochem. Sci. 33, 453–460.

Lee, C.B., Kim, S. and McClure, B. (2009) A pollen protein, NaPCCP, that binds Pistil Arabinogalactan proteins also binds Phosphatidylinositol 3-Phosphate and associates with the pollen tube endomembrane system. Plant Physiol. 149, 791–802.

Lee, G.J., Kim, H., Kang, H., Jang, M., Lee, D.W., Lee, S. and Hwang, I. (2007) EpsinR2 interacts with Clathrin adaptor protein-3, AtVTI12, and Phosphatidylinositol-3-Phosphate. Implications for EpsinR2 function in protein trafficking in plant cells. Plant Physiol. 143, 1561–1575.

Lee, K.H., Piao, H.L., Kim, H.Y., Choi, S.M., Jiang, F., Hartung, W., Hwang, I., Kwak, J.M. and Lee, I.J. (2006) Activation of glucosidase via stress-induced polymerization rapidly increases active pools of abscisic acid. Cell 126, 1109-1120.

Lee, S.H., Jin, J.B., Song, J., Min, M.K., Park, D.S., Kim, Y.W. and Hwang, I. (2002) The intermolecular interaction between the PH domain and the C-terminal domain of *Arabidopsis* dynamin-like 6 determines lipid binding specificity. J. Biol. Chem. 277, 31842–31849.

Lee, Y., Bak. G., Choi, Y., Chuang, W., Cho, H. and Lee, Y. (2008) Roles of Phosphatidylinositol 3-Kinase in root hair growth. Plant Physiol. 147, 624–635.

Leshem, Y., Seri, L. and Levine, A. (2007) Induction of phosphatidylinositol 3-kinase-mediated endocytosis by salt stress leads to intracellular production of reactive oxygen species and salt tolerance. Plant J. 51, 185–197.

Levchenko, V., Konrad, K.R., Dietrich, P., Roelfsema, M.R. and Hedrich, R. (2005) Cytosolic abscisic acid activates guard cell anion channels without preceding Ca^{2+} signals. Proc. Natl. Acad. Sci. USA 102, 4203–4208.

Levivier, E., Goud, B., Souchet, M., Calmels, T.P., Mornon, J.P. and Callebaut, I. (2001) uDENN, DENN, and dDENN: indissociable domains in Rab and MAP kinases signaling pathways. Biochem. Biophys. Res. Commun. 287, 688-695.

Li, S., Tiab, L., Jiao, X., Munier, F.L., Zografos, L., Frueh, B.E., Sergeev, Y., Smith, J., Rubin, B., Meallet, M.A., Forster, R.K., Hejtmancik, J.F. and Schorderet, D.F. (2005) Mutations in PIP5K3 are associated with Francois–Neetens mouchetee fleck corneal dystrophy. Am. J. Hum. Genet. 77, 54–63.

Lorenzo, O., Urbe, S. and Clague, M.J. (2005) Analysis of phosphoinositide binding domain properties within the myotubularin-related protein MTMR3. J. Cell Sci. 118, 2005-2012.

Lorenzo, O., Urbe, S. and Clague, M.J. (2006) Systematic analysis of myotubularins: heteromeric interactions, subcellular localisation and endosome related functions. J. Cell Sci. 119, 2953-2959.

Maniatis, T., Fritsch, E. F. and Sambrook, J. (1982) Molecular cloning, a laboratory manual. Cold Spring Harbor Laboratory, Cold Spring, NY, 545.

Manta, P., Mamali, I., Zambelis, T., Aquaviva, T., Kararizou, E. and Kalfakis, N. (2006) Immunocytochemical study of cytoskeletal proteins in centronuclear myopathies. Acta Histochem. 108, 271–6.

Marchant, A., Kargul, J., May, S.T., Muller, P., Delbarre, A., Perrot-Rechenmann, C. and Bennett, M.J. (1999) AUX1 regulates root gravitropism in *Arabidopsis* by facilitating auxin uptake within root apical tissues. EMBO J. 18, 2066–2073.

Mason, D., Mallo, G.V., Terebiznik, M.R., Payrastre, B., Finlay, B.B., Brumell, J.H., Rameh, L. and Grinstein, S. (2007) Alteration of epithelial structure and function associated with $PtdIns(4,5)P_2$ degradation by a bacterial phosphatase. J. Gen. Physiol.129, 267–83.

Meijer, H. J. and Munnik, T. (2003) Phospholipid-based signaling in plants. Annu. Rev. Plant Biol. 54, 265–306.

Meijer, H.J.G., Berrie, C.P., Lurisci, C., Divecha, N., Musgrave, A. and Munnik, T. (2001) Identification of a new polyphosphoinositide in plants, phosphatidylinositol 5-phosphate and its accumulation upon osmotic stress. Biochem. J. 360, 491-498.

Meijer, H.J.G., Divecha, N., van den Ende, H., Musgrave, A. and Munnik, T. (1999) Hyperosmotic stress induces rapid synthesis of phosphatidyl-D-inositol 3,5-bisphosphate in plant cells. Planta 208, 294–298.

Merchant, S.S., Prochnik, S.E., Vallon, O., Harris, E.H., Karpowicz, S.J., Witman, G.B., Terry. A., Salamov, A., Fritz-Laylin, L.K., Maréchal-Drouard, L., Marshall, W.F., Qu, L.H., Nelson, D.R., Sanderfoot, A.A., Spalding, M.H., Kapitonov, V.V., Ren, Q., Ferris, P., Lindquist, E., Shapiro, H., Lucas, S.M., Grimwood, J., Schmutz, J., Cardol, P., Cerutti, H., Chanfreau, G., Chen, C.L., Cognat, V., Croft, M.T., Dent, R., Dutcher, S., Fernández, E., Fukuzawa, H., González-Ballester, D., González-Halphen, D., Hallmann, A., Hanikenne, M., Hippler, M., Inwood, W., Jabbari, K., Kalanon, M., Kuras, R., Lefebvre, P.A., Lemaire, S.D., Lobanov, A.V., Lohr, M., Manuell, A., Meier, I., Mets, L., Mittag, M., Mittelmeier, T., Moroney, J.V., Moseley, J., Napoli, C., Nedelcu, A.M., Niyogi, K., Novoselov, S.V., Paulsen, I.T., Pazour, G., Purton, S., Ral, J.P., Riaño-Pachón, D.M., Riekhof, W., Rymarquis, L., Schroda, M., Stern, D., Umen, J., Willows, R., Wilson, N., Zimmer, S.L., Allmer, J., Balk, J., Bisova, K., Chen, C.J., Elias, M., Gendler, K., Hauser, C., Lamb, M.R., Ledford, H., Long, J.C., Minagawa, J., Page, M.D., Pan, J., Pootakham, W., Roje, S., Rose, A., Stahlberg, E., Terauchi, A.M., Yang, P., Ball, S., Bowler, C., Dieckmann, C.L., Gladyshev, V.N., Green, P., Jorgensen, R., Mayfield, S., Mueller-Roeber, B., Rajamani, S., Sayre, R.T., Brokstein, P., Dubchak, I., Goodstein, D., Hornick, L., Huang, Y.W., Jhaveri, J., Luo, Y., Martínez, D., Ngau, W.C., Otillar, B., Poliakov, A., Porter, A., Szajkowski, L., Werner, G., Zhou, K., Grigoriev, I.V., Rokhsar, D.S. and Grossman, A.R. (2007) The *Chlamydomonas* genome reveals the evolution of key animal and plant functions. Science 318, 245–250.

Michell, R.H., Heath, V.L., Lemmon, M.A. and Dove, S.K. (2006) Phosphatidylinositol 3,5-bisphosphate: metabolism and cellular functions. Trends Biochem. Sci. 31, 52–63.

Mikami, K., Katagiri, T., Iuchi, S., Yamaguchi-Shinozaki, K. and Shinozaki, K. (1998) A gene encoding phosphatidylinositol-4- phosphate 5-kinase is induced by water stress and abscisic acid in *Arabidopsis thaliana*. Plant J. 15, 563–568.

Mochizuki, Y. and Majerus, P.W. (2003) Characterization of myotubularin-related protein 7 and its binding partner, myotubularin-related protein 9. Proc. Natl. Acad. Sci. USA 100, 9768-9773.

Mori, I.C., Pinontoan, R., Kawano, T. and Muto, S. (2001) Involvement of superoxide generation in salicylic acid-induced stomatal closure in *Vicia faba*. Plant Cell Physiol. 42, 1383-1388.

Morishita, M., Morimoto, F., Kitamura, K., Koga, T., Fukui, Y., Maekawa, H., Yamashita, I. and Shimoda, C. (2002) Phosphatidylinositol 3-phosphate 5-kinase is required for the cellular response to nutritional starvation and mating pheromone signals in *Schizosaccharomyces pombe*. Genes Cells. 7, 199–215.

Mueller-Roeber, B. and Pical, C. (2002) Inositol phospholipid metabolism in *Arabidopsis*: characterized and putative isoforms of inositol phospholipid kinase and phosphoinositide-specific phospholipase C. Plant Physiol. 130, 22–46.

Müller, J., Mettbach, U., Menzel, D. and Samaj, J. (2007) Molecular dissection of endosomal compartments in plants. Plant Physiol. 145, 293-304.

Murashige, T. and Skoog, F. (1962) A revised medium for rapid growth and bio-assay with tobacco tissue cultures. Plant Physiol. 15, 473-497.

Nambara, E. and Marion-Poll, A. (2005) Abscisic acid biosynthesis and catabolism. Annu. Rev. Plant Biol. 56, 165-185.

Nandurkar, H.H., Caldwell, K.K., Whisstock, J.C., Layton, M.J., Gaudet, E.A., Norris, F.A., Marjerus, P.W. and Mitchell, C.A. (2001) Characterization of an adapter subunit to a phosphatidylinositol (3)P 3-phosphatase: Identification of a myotubularin-related protein lacking catalytic activity. Proc. Natl. Acad. Sci. USA 98, 9499–9504.

Nandurkar, H.H., Layton, M., Laporte, J., Selan, C., Corcoran, L., Caldwell, K.K., Mochizuki, Y., Majerus, P.W. and Mitchell, C.A. (2003) Identification of myotubularin as the lipid phosphatase catalytic subunit associated with the 3-phosphatase adapter protein, 3-PAP. Proc. Natl. Acad. Sci. USA 100, 8660-8665.

Ndamukong, I., Jones, D., Lapko, H., Divecha, N. and Avramova, Z. (2010) Phosphatidylinositol 5-phosphate links dehydration stress to the activity of A*rabidopsis* trithorax-like factor ATX1. PLoS One 5, e13396.

Nelson, B.K., Cai, X. and Nebenführ, A. (2007) A multicolored set of in-vivo organelle markers for co-localization studies in *Arabidopsis* and other plants. Plant J. 51, 1126–1136.

Niebuhr, K., Giuriato, S., Pedron, T., Philpott, D.J., Gaits, F., Sable, J., Sheetz, M.P., Parsot, C., Sansonetti, P.J. and Payrastre, B. (2002) Conversion of PtdIns(4,5)P$_2$ into PtdIns(5)P by the *S. flexneri* effector IpgD reorganizes host cell morphology. Embo J. 21, 5069–5078.

Nielsen, E., Cheung, A.Y. and Ueda, T. (2008) The regulatory RAB and ARF GTPases for vesicular trafficking. Plant Physiol. 147, 1516–1526.

Obara, K., Sekito, T., Niimi, K. and Ohsumi, Y. (2008) The Atg18-Atg2 complex is recruited to autophagic membranes via phosphatidylinositol 3-phosphate and exerts an essential function. J. Biol. Chem. 283, 23972–80.

Odorizzi, G., Babst, M. and Emr, S.D. (2000) Phosphoinositide signaling and the regulation of membrane trafficking in yeast. Trends Biochem. Sci. 25, 229-235.

Park, K.Y., Jung, J.Y., Park, J., Hwang, J.U., Kim, Y.W., Hwang, I. and Lee, Y. (2003) A role for phosphatidylinositol 3-phosphate in abscisic acid-induced reactive oxygen species generation in guard cells. Plant Physiol. 132, 92–98.

Pei, Z.M., Kuchitsu, K., Ward, J.M., Schwarz, M. and Schroeder, J.I. (1997) Differential abscisic acid regulation of guard cell slow anion channels in *Arabidopsis* wild-type and abi1 and abi2 mutants. Plant Cell 9, 409–423.

Pendaries, C., Tronchere, H., Racaud-Sultan, C., Gaits-Iacovoni, F., Coronas, S., Manenti, S., Gratacap, M.P., Plantavid, M. and Payrastre B. (2005) Emerging roles of phosphatidylinositol monophosphates in cellular signaling and trafficking. Adv. Enzyme Regul. 45, 201–214.

Polishchuk, R.S. and Mironov, A.A. (2004) Structural aspects of Golgi function. Cell Mol. Life Sci. 61, 146–158.

Previtali, S.C., Zerega, B., Sherman, D.L., Brophy, P.J., Dina, G., King, R.H., Salih, M.M., Feltri, L., Quattrini, A., Ravazzolo, R., Wrabetz, L., Monaco, A.P. and Bolino, A. (2003) Myotubularin-related 2 protein phosphatase and neurofilament light chain protein, both mutated in CMT neuropathies, interact in peripheral nerve. Hum. Mol. Genet. 12, 1713-1723.

Rameh, L.E., Tolias, K.F., Duckworth, B.C. and Cantley, L.C. (1997) A new pathway for synthesis of phosphatidylinositol-4,5-bisphosphate. Nature 390, 192-196.

Rea, S., Eisenhaber, F., O'Carroll, D., Strahl, B., Sun, Z.W., Schmidt, M., Opravil, S., Mechtler, K., Pontig, C., Allis, D.C. and Jenuwein, T. (2000) Regulation of chromatin structure by site-specific histone H3 methyltransferases. Nature 406, 593-599.

Ribchester, R., Mao, F. and Betz, W. (1994) Optical measurements of activity-dependent membrane recycling in motor nerve terminals of mammalian skeletal muscle. Proc. Biol. Sci. 255, 61-66.

Roberts, H.F., Clarke, J.H., Letcher, A.J., Irvine, R.F. and Hinchliffe, K.A. (2005) Effects of lipid kinase expression and cellular stimuli on phosphatidylinositol 5-phosphate levels in mammalian cell lines. FEBS Lett. 579, 2868–2872.

Robinson, F.L. and Dixon, J.E. (2005) The phosphoinositide-3-phosphatase MTMR2 associates with MTMR13, a membrane-associated pseudophosphatase also mutated in type 4B Charcot-Marie-Tooth disease. J. Biol. Chem. 280, 31699-31707.

Robinson, F.L. and Dixon, J.E. (2006) Myotubularin phosphatases: policing 3-phosphoinositides. Trends Cell Biol. 16, 403-412.

Ron, M. and Avni, A. (2004) The receptor for the fungal Elicitorethylene-inducing Xylanase is a member of a resistance-like gene family in tomato. Plant Cell 16, 1604–1615.

Saint-Jore, C.M., Evins, J., Batoko, H., Brandizzi, F., Moore, I. and Hawes, C. (2002) Redistribution of membrane proteins between the Golgi apparatus and endoplasmic reticulum in plants is reversible and not dependent on cytoskeletal networks. Plant J. 29, 661–678.

Saint-Jore-Dupas, C., Nebenführ, A., Boulaflous, A., Follet-Gueye, M.L., Plasson, C., Hawes, C., Driouich, A., Faye, L. and Gomord, V. (2006) Plant N-glycan processing enzymes employ different targeting mechanisms for their spatial arrangement along the secretory pathway. Plant Cell 18, 3182–3200.

Samaj, J., Baluska, F., Voigt, B., Schlicht, M., Volkmann, D. and Menzel, D. (2004) Endocytosis, actin cytoskeleton, and signaling. Plant Physiol. 135, 1150–1161.

Samaj, J., Read, N.D., Volkmann, D., Menzel, D. and Baluska, F. (2005) The endocytic network in plants. Trends Cell Biol. 15, 425-433.

Sanderfoot, A.A., Assaad, F.F. and Raikhel, N.V. (2000) The *Arabidopsis* Genome: an abundance of soluble N-ethylmaleimide sensitive factor receptors. Plant Physiol. 124, 1558–1569.

Sanderfoot, A.A., Kovaleva, V., Bassham, D.C. and Raikhel, N.V. (2001) Interactions between syntaxins identify at least five SNARE complexes within the Golgi/prevacuolar system of the *Arabidopsis* cell. Mol. Biol. Cell 12, 3733–3743.

Sarkes, D. and Rameh, L.E. (2010) A novel HPLC-based approach makes possible the spatial characterization of cellular PtdIns5P and other phosphoinositides. Biochem. J. 428, 375–384.

Sbrissa, D. and Shisheva, A. (2005) Acquisition of unprecedented phosphatidylinositol 3,5-bisphosphate rise in hyperosmotically stressed 3T3-L1 adipocytes, mediated by ArPIKfyve–PIKfyve pathway. J. Biol. Chem. 280, 7883–7889

Sbrissa, D., Ikonomov, O., Deeb, R. and Shisheva, A. (2002) Phosphatidylinositol 5-phosphate biosynthesis is linked to PIKfyve and is involved in osmotic response pathway in mammalian cells. J. Biol. Chem. 277, 47276-84.

Schaletzky, J., Dove, S.K., Short, B., Lorenzo, O., Clague, M.J. and Barr, F.A. (2003) Phosphatidylinositol-5-phosphate activation and conserved substrate specificity of the myotubularin phosphatidylinositol 3-phosphatases. Curr. Biol. 13, 504-509.

Schroeder, J.I., Allen, G.J., Hugouvieux, V., Kwak, J.M. and Waner, D. (2001) Guard cell signal transduction. Annu. Rev. Plant Physiol. Plant Mol. Biol. 52, 627–658.

Schroeder, J.I. and Hagiwara, S. (1989) Cytosolic calcium regulates ion channels in the plasma membrane of *Vicia faba* guard cells. Nature 338, 427–30.

Senderek, J., Bergmann, C., Weber, S., Ketelsen, U.P., Schorle, H., Rudnik-Schoneborn, S., Buttner, R., Buchheim, E. and Zerres, K. (2003) Mutation of the SBF2 gene, encoding a novel member of the myotubularin family, in Charcot-Marie-Tooth neuropathy type 4B2/11p15. Hum. Mol. Genet. 12, 349-356.

Sewry, C.A. (1998) The role of immunohistochemistry in congenital myopathies. Neuromuscul. Disord. 8, 394-400.

Shen, W. and Forde, B.J. (1989) Efficient transformation of *Agrobacterium* spp. by high voltage electroporation. Nucl. Acids Res. 17, 8385.

Siegel, R.S., Xue, S., Murata, Y., Yang, Y., Nishimura, N., Wang, A. and Schroeder, J.I. (2009) Calcium elevation-dependent and attenuated resting calcium-dependent abscisic acid induction of stomatal closure and abscisic acid-induced enhancement of calcium sensitivities of S-type anion and inward-rectifying channels in *Arabidopsis* guard cells. Plant J. 59, 207–220.

Spiro, A., Shy, G. and Gonatas, N. (1966) Myotubular myopathy. Persistence of fetal muscle in an adolescent boy. Arch. Neurol. 14, 1–14.

Staehelin, L.A. and Kang, B.H. (2008) Nanoscale architecture of endoplasmic reticulum export sites and of Golgi membranes as determined by electron tomography. Plant Physiol. 147, 1454–1468.

Staehelin, L.A. and Moore, I. (1995) The plant Golgi apparatus: structure, functional organization and trafficking mechanisms. Ann. Rev. Plant Physiol. Plant Mol. Biol. 46, 261–288.

Stassen, M.J., Bailey, D., Nelson, S., Chinwalla, V. and Harte, P.J. (1995) The *Drosophila* trithorax proteins contain a novel variant of the nuclear receptor type DNA binding domain and an ancient conserved motif found in other chromosomal proteins. Mech. Dev. 52, 209-223.

Stephens, L., Cooke, F.T., Walters, R., Jackson, T., Volinia, S., Gout, I., Waterfield, M.D. and Hawkins, P.T. (1994) Characterization of a phosphatidylinositol-specific phosphoinositide 3-kinase from mammalian cells. Curr. Biol. 4, 203–214.

Stevenson, J.M., Perera, I.Y., Heilmann, I., Persson, S. and Boss, W.F. (2000) Inositol signaling and plant growth. Trends Plant Sci. 5, 252-258.

Swarbreck, D., Wilks, C., Lamesch, P., Berardini, T.Z., Garcia-Hernandez, M., Foerster, H., Li, D., Meyer, T., Muller, R., Ploetz, L., Radenbaugh, A., Singh, S., Swing, V., Tissier, C., Zhang, P. and Huala, E. (2007) The *Arabidopsis* information resource (TAIR): gene structure and function annotation. Nucleic Acids Res. 36, D1009-14.

Swarup, R., Kargul, J., Marchant, A., Zadik, D., Rahman, A., Mills, R., Yemm, A., May, S., Williams, L., Millner, P., Tsurumib, S., Mooref, I., Napierd, R., Kerrg, I.D. and Bennetta, M.J. (2004) Structure-function analysis of the presumptive *Arabidopsis* auxin permease AUX1. Plant Cell 16, 3069–3083.

Taylor, G.S., Maehama, T. and Dixon, J.E. (2000) Myotubularin, a protein tyrosine phosphatase mutated in myotubular myopathy, dephosphorylates the lipid second messenger, phosphatidylinositol 3-phosphate. Proc. Natl. Acad. Sci. USA 97, 8910-8915.

Tosch, V., Rohde, H.M., Tronchère, H., Zanoteli, E., Monroy, N., Kretz, C., Dondaine, N., Payrastre, B., Mandel, J.L. and Laporte, J. (2006) A novel PtdIns3P and PtdIns(3,5)P_2 phosphatase with an inactivating variant in centronuclear myopathy. Hum. Mol. Genet. 15, 3098–3106.

Tsujita, K., Itoh, T., Ijuin, T., Yamamoto, A., Shisheva, A., Laporte, J. and Takenawa, T. (2004) Myotubularin regulates the function of the late endosome through the GRAM domain-phosphatidylinositol 3,5-bisphosphate interaction. J. Biol. Chem. 279, 13817-13824.

Ungewickell, A., Hugge, C., Kisseleva, M., Chang, S.C., Zou, J., Feng, Y., Galyov, E.E., Wilson, M. and Majerus, P.W. (2005) The identification and characterization of two phosphatidylinositol-4,5-bisphosphate 4-phosphatases. Proc. Natl. Acad. Sci. USA 102, 18854–18859.

Vahisalu, T., Kollist, H., Wang, Y.F., Nishimura, N., Chan, W.Y., Valerio, G., Lamminmäki, A., Brosché, M., Moldau, H., Desikan, R., Schroeder, J.I. and Kangasjärvi, J. (2008) SLAC1 is required for plant guard cell S-type anion channel function in stomatal signalling. Nature 452, 487–491.

Van Gijsegem, F., Genin, S. and Boucher, C. (1993) Conservation of secretion pathways for pathogenicity determinants of plant and animal bacteria. Trends Microbiol. 1, 175-180.

Vanhaesebroeck, B., Leevers, S.J., Ahmadi, K., Timms, J., Katso, R., Driscoll, P.C., Woscholski, R., Parker, P.J. and Waterfield, M.D. (2001) Synthesis and function of 3-phosphorylated inositol lipids. Annu. Rev. Biochem. 70, 535-602.

Vermeer, J.E.M. and Munnik, T. (2010) Imaging lipids in living plants. Lipid Signaling in Plants, Plant Cell Monogr. 16, Munnik, T. ed., (Berlin: Springer Verlag), 185-199.

Voigt, B., Timmers, A.C.J., Samaj, J., Müller, J., Baluska, F. and Menzel, D. (2005) GFP-FABD2 fusion construct allows in-vivo visualization of the dynamic actin cytoskeleton in all cells of A*rabidopsis* seedlings. Eur. J. Cell Biol. 84, 595-608.

Walker, D.M., Urbe, S., Dove, S.K., Tenza, D., Raposo, G. and Clague, M.J. (2001) Characterization of MTMR3, an inositol lipid 3-phosphatase with novel substrate specificity. Curr. Biol. 11, 1600-1605.

Wallgren-Pettersson, C., Clarke, A., Samson, F., Fardeau, M., Dubowitz, V., Moser, H., Grimm, T., Barohn, R.J. and Barth, P.G. (1996) The myotubular myopathies: differential diagnosis of the X- linked recessive autosomal dominant, and autosomal recessive forms and present state of DNA studies. J. Med. Genet. 32, 673-679.

Wang, X. (2004) Lipid signaling. Curr. Opin. Plant Biol. 7, 329–336.

Welters, P., Takegawa, K., Emr, S.D. and Chrispeels, M.J. (1994) ATVPS34, a PtdIns 3-kinase of *Arabidopsis thaliana* is an essential protein with homology to a calcium-dependent lipid-binding domain. Proc. Natl. Acad. Sci. USA 91, 11398–11402.

Wendy, F.B. and Yang, J.I. (2012) Phosphoinositide signaling. Annu. Rev. Plant Biol. 63, 409–29.

Whiteford, C.C., Brearley, C.A. and Ulug, E.T. (1997) Phosphatidylinositol 3,5-bisphosphate defines a novel PI 3-kinase pathway in resting mouse fibroblasts. Biochem. J. 323, 597–601.

Whitley, P., Hinz, S. and Doughty, J. (2009) *Arabidopsis* FAB1/PIKfyve proteins are essential for development of viable pollen. Plant Physiol. 151, 1812-1822.

Wishart, M.J. and Dixon, J.E. (2002) PTEN and myotubularins phosphatases: from 3-phosphoinositide dephosphorylation to disease. Phosphatase and tensin homolog deleted on chromosome ten. Trends Cell Biol. 12, 579–585.

Wishart, M.J., Taylor, G.S., Slama, J.T. and Dixon, J.E. (2001) PTEN and myotubularin phosphoinositide phosphatases: Bringing bioinformatics to the lab bench. Curr. Opin. Cell Biol. 13, 172–181.

Yamamoto, A., DeWald, D.B., Boronenkov, I.V., Anderson, R.A., Emr, S.D. and Koshland, D. (1995) Novel PI(4)P 5-kinase homologue, Fab1p, essential for normal vacuole function and morphology in yeast. Mol. Biol. Cell 6, 525–539.

Yamashiro, C.T., Kane, P.M., Wolczyk, D.F., Preston, R.A. and Stevens, T.H. (1990) Role of vacuolar acidification in protein sorting and zymogen activation: a genetic analysis of the yeast vacuolar proton-translocating ATPase. Mol. Cell Biol. 10, 3737-3749.

Yoon, M.S., Du, G., Backer, J.M., Frohman, M.A. and Chen, J. (2011) Class III PI-3 kinase activates phospholipase D in an amino acid-sensing mTORC1 pathway. J. Cell Biol. 195, 435-447.

Yoshimura, S., Gerondopoulos, A., Linford, A., Rigden, D.J. and Barr, F.A. (2010) Family wide characterization of the DENN domain Rab GDP-GTP exchange factors. J. Cell Biol. 191, 367-381.

Zhang, X., Zhang, L., Dong, F., Gao, J., Galbraith, D.W. and Song, C.P. (2001) Hydrogen peroxide is involved in abscisic acid-induced stomatal closure in *Vicia faba*. Plant Physiol. 126, 1438–1448.

Zhao, R., Qi, Y., Chen, J. and Zhao, Z.J. (2001) FYVE-DSP2, a FYVE domain containing dual specificity protein phosphatase that dephosphorylates phosphatidylinositol 3-phosphate. Exp. Cell Res. 265, 329-338.

Zheng, H., Fischer-von-Mollard, G., Kovaleva, V., Stevens, T.H. and Raikhel, N.V. (1999) The plant vesicle-associated SNARE AtVTI1a likely mediates vesicle transport from the trans-Golgi network to the prevacuolar compartment. Mol. Biol. Cell 10, 2251–2264.

Zhu, D. and Scandalios, J.G. (1994) Differential accumulation of manganese-superoxide dismutase transcripts in maize in response to abscisic acid and high osmoticum. Plant Physiol. 106, 173–178.

Zhu, J.K. (2002) Salt and drought stress signal transduction in plants. Annu. Rev. Plant Biol. 53, 247–273.

Zonia, L. and Munnik, T. (2004) Osmotically induced cell swelling versus cell shrinking elicits specific changes in phospholipid signals in tobacco pollen tubes. Plant Physiol. 134, 813–823.

Zou, J., Chang, S.C., Marjanovic, J. and Majerus, P.W. (2009) MTMR9 increases MTMR6 enzyme activity, stability, and role in apoptosis. J. Biol. Chem. 284, 2064-2071.
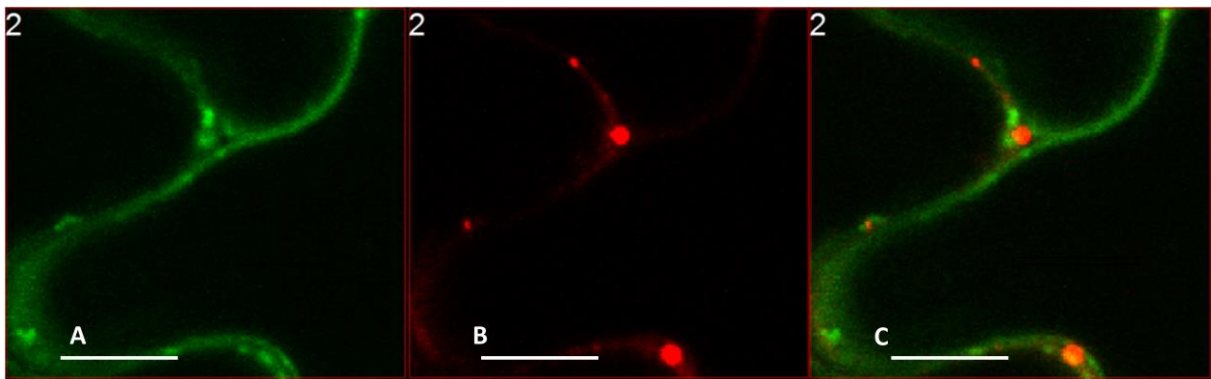
7.   APPENDIX

## 7.1.   CO-EXPRESSION OF DIFFERENT FLUORESCENT MARKERS WITH AtMTM1
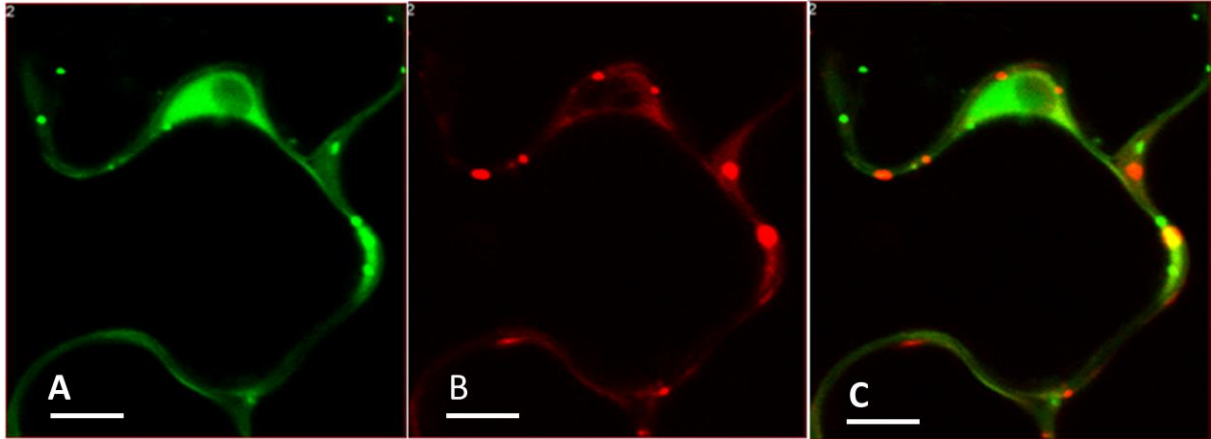
Figure 46: Subcellular distribution of AtMTM1-RFP co-expressed with FYVE-GFP.

A-C: A part of cell showing FYVE-GFP in (A); AtMTM1-RFP in (B) and a merge of the two in (C). Transient co-expression shows no co-localization.
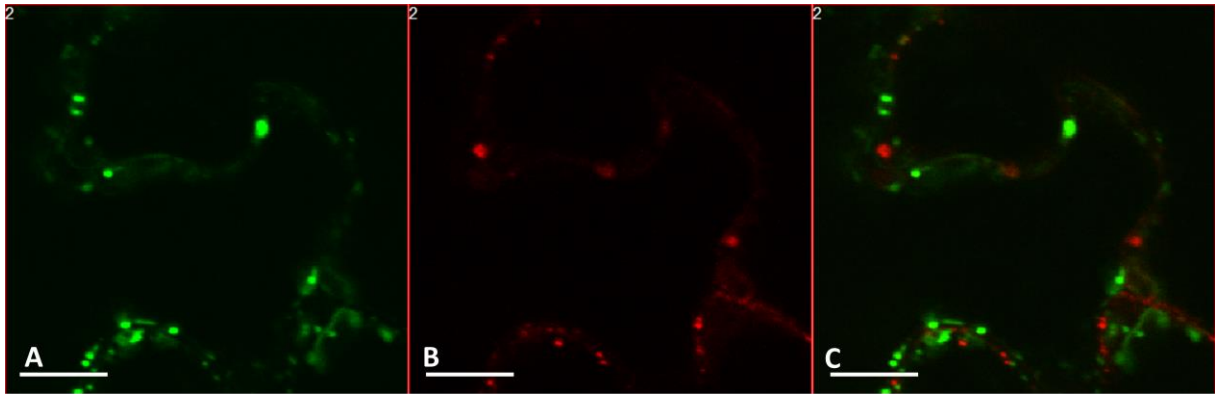

Figure 47: Subcellular distribution of AtMTM1-RFP co-expressed with ARA7-GFP.

A-C: A part of cell showing ARA7-GFP in (A); AtMTM1-RFP in (B) and a merge of the two in (C). Transient co-expression shows no co-localization.
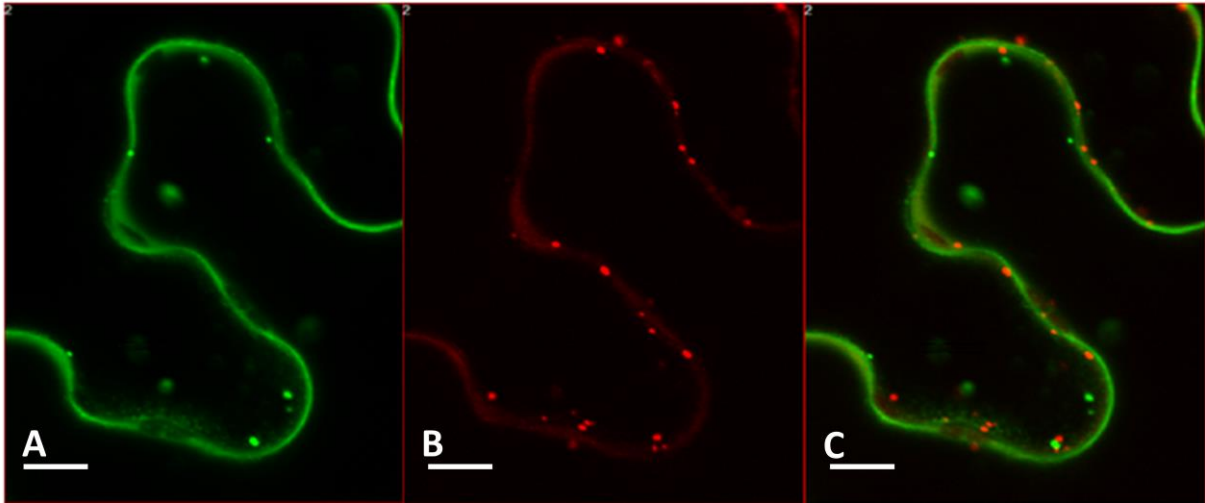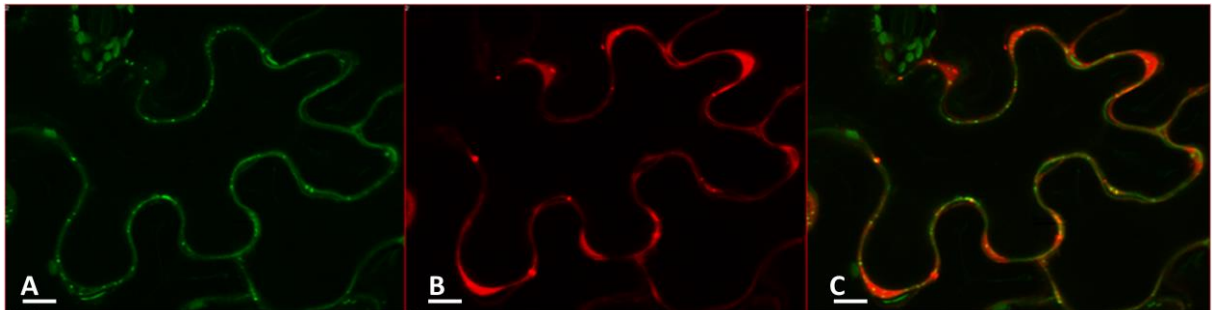
Figure 48: Subcellular distribution of AtMTM1-RFP co-expressed with EHD1-GFP.

A-C: A part of cell showing EHD1-GFP in (A); AtMTM1-RFP in (B) and a merge of the two in (C). Transient co-expression shows no co-localization.
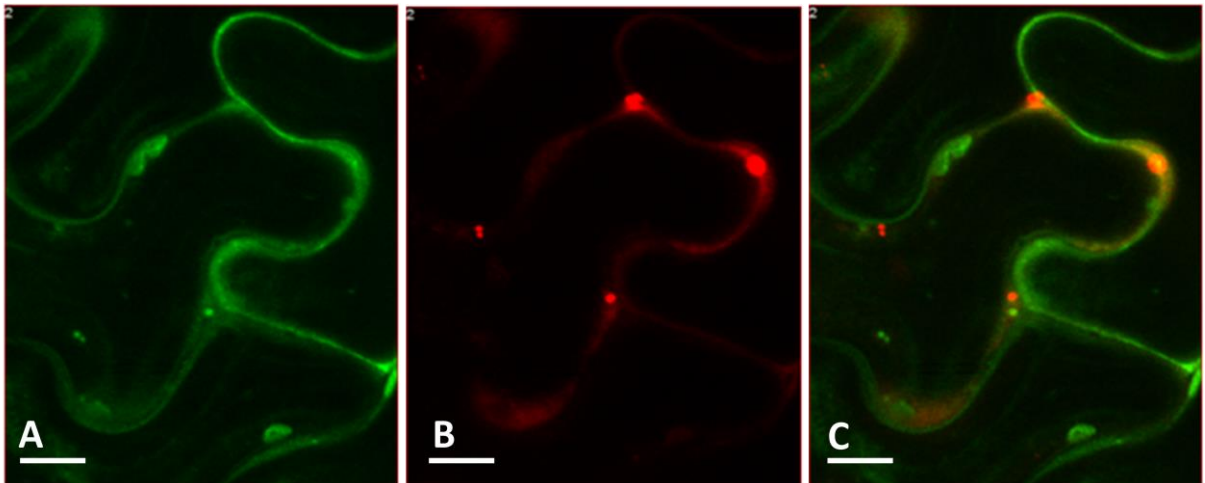
Figure 49: Subcellular distribution of AtMTM1-RFP co-expressed with RabF2b-GFP.

A-C: A part of cell showing RabF2b-GFP in (A); AtMTM1-RFP in (B) and a merge of the two in (C). Transient co-expression shows no co-localization.
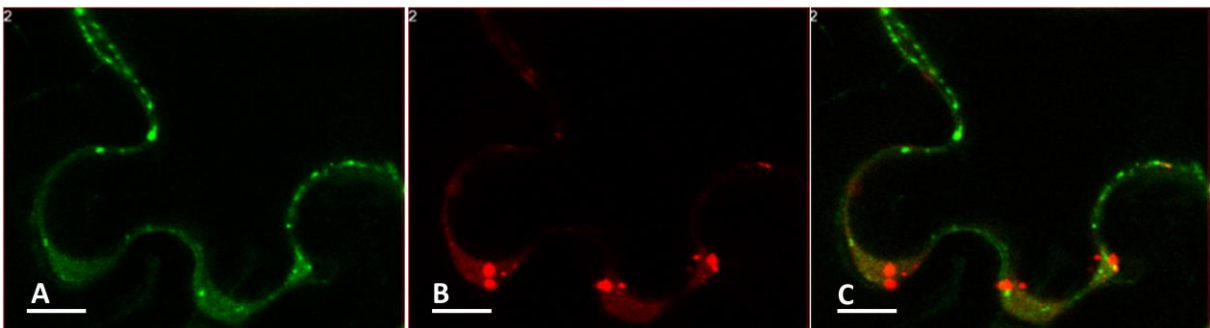
Figure 50: Subcellular distribution of AtMTM1-RFP co-expressed with RabA1e-YFP.

A-C: A part of cell showing RabA1e-YFP in (A); AtMTM1-RFP in (B) and a merge of the two in (C). Transient co-expression shows no co-localization.
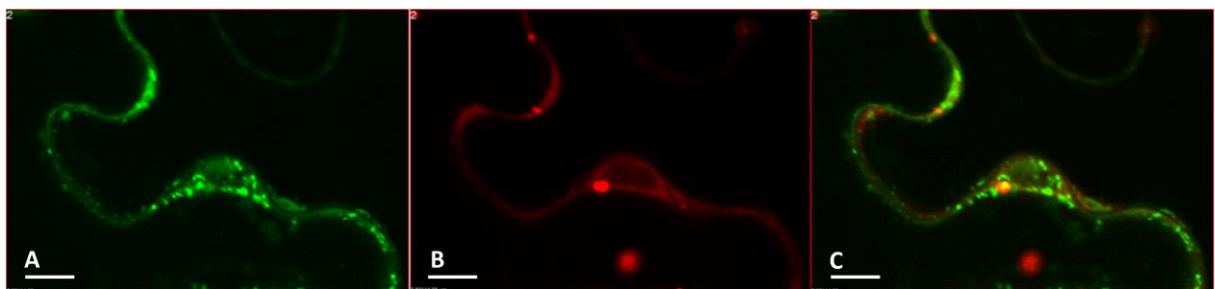
Figure 51: Subcellular distribution of AtMTM1-RFP co-expressed with ST-GFP.

A-C: A part of cell showing ST-GFP in (A); AtMTM1-RFP in (B) and a merge of the two in (C). Transient co-expression shows no co-localization.
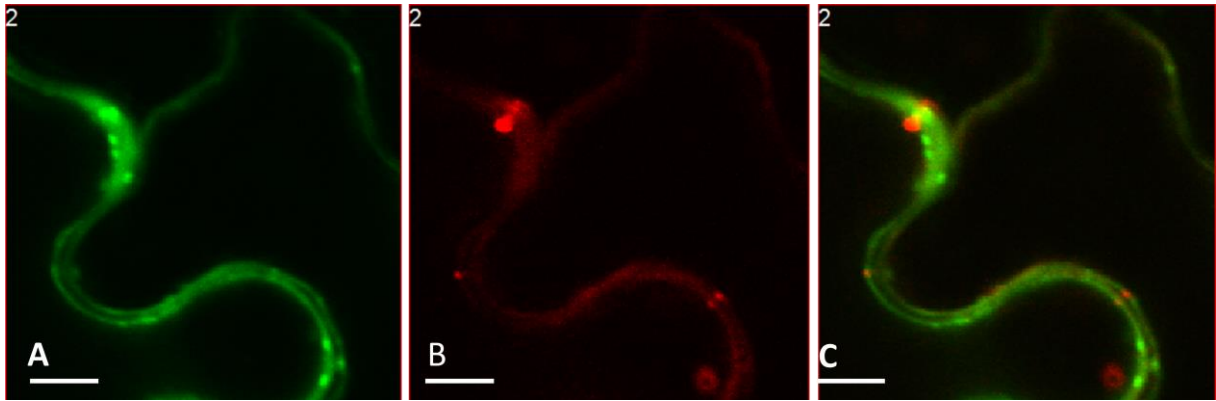

Figure 52: Subcellular distribution of AtMTM1-RFP co-expressed with SYP61-GFP.

A-C: A part of cell showing SYP61-GFP in (A); AtMTM1-RFP in (B) and a merge of the two in (C). Transient co-expression shows no co-localization.

Figure 53: Subcellular distribution of AtMTM1-RFP co-expressed with VTI12-GFP.

A-C: A part of cell showing VTI12-GFP in (A); AtMTM1-RFP in (B) and a merge of the two in (C). Transient co-expression shows no co-localization.

Figure 54: Subcellular distribution of AtMTM1-RFP co-expressed with RabA1d-GFP.

A-C: A part of cell showing RabA1d-GFP in (A); AtMTM1-RFP in (B) and a merge of the two in (C). Transient co-expression shows no co-localization.

ACKNOWLEDGEMENTS

PUBLICATIONS

Manuscripts in preparation:

Nagpal A, Baluska F, Avramova Z (2014) Subcellular localization of Myotubularins in *Arabidopsis thaliana*.

Nagpal A, Baluska F, Avramova Z (2014) Role of Serine-rich domain in regulating the activity of AtMTM1 (*Arabidopsis* Myotubularin 1).

Published abstract:

Nagpal A, Baluska F, Avramova Z (2012) Subcellular localization of Myotubularins in *Arabidopsis thaliana*, International Conference on Biotechnology BTBS – 2012

Nagpal A, Baluska F, Avramova Z (2014) Serine-rich domain regulates the activity of AtMTM1 towards ATX1, International Symposium on Plant Signalling and behavior – 2014.

ERKLÄRUNG

Ich versichere hiermit, dass ich die vorliegende Arbeit in allen Teilen selbst und ohne jede unerlaubte Hilfe angefertigt habe. Diese oder eine ähnliche Arbeit ist noch bei keiner anderen Stelle als Dissertation eingereicht worden.

Ich habe früher noch keinen Promotionsversuch unternommen.

Bonn, den